Dissertation

Submitted to the

Combined Faculties for the Natural Sciences and for Mathematics

of the Ruperto-Carola University of Heidelberg, Germany

for the degree of

Doctor of Natural Sciences

presented by

Diplom-Biologist Claudia Zenkert

born in: Friedrichroda, Germany

Oral examination: 20.12.2011

Molecular and Cellular Analysis of the *Nematostella vectensis* Cnidom

Referees: PD Dr. Suat Özbek

Prof. Dr. Thomas Holstein

For my family – blood and heart alike

„ Es kommt nicht darauf an, wie eine Geschichte anfängt. Auch nicht darauf wie sie aufhört. Sondern auf das, was dazwischen passiert.“

- Walter Moers

Declaration

I hereby declare that my contribution to the paper “A Non-sulfated Chondroitin Stabilizes Membrane Tubulation in Cnidarian Organelles” was ~ 5 %: I performed anti-chondroitin stainings in different developmental stages of *Nematostella vectensis* providing necessary data for the hypothesis arguing for a high conservation of the chondroitin function in developing nematocysts of cnidarians. The paper “Morphological and Molecular Analysis of the *Nematostella vectensis* Cnidom” was written independently by me. I performed all the experiments concerning the qualitative and quantitative analysis of nematocysts, the cloning and *in situ* hybridizations for minicollagen genes 1, 3 and 4 as well as the Westernblot analysis and the antibody stainings. Therefore my share was 80 %. My contribution to the paper “Neurotoxin localization to ectodermal gland cells uncovers an alternative mechanism of venom delivery in sea anemones” was ~ 5 %. I performed the co-stainings of neurotoxin 1 (Nv1) with Nematostella minicollagen 3 (NvNCol-3) and chondroitin. These results let to the conclusion that the neurotoxin is not synthesized in nematocytes and is never co-localized with capsules. The manuscript “Histology and Cell Cycle Kinetics in *Nematostella vectensis*” was written by me. The qualitative cell type analysis in macerated tissue and cryo-sections, the EdU-labeling experiments for cell cycle analysis as well as the anti-minicollagen 3 (NvNCol-3) stainings for the analysis of capsule synthesis were done be me. Hence, my contribution to the manuscript is ~80 %.

Heidelberg, 07.11.2011

(Claudia Zenkert) (PD Dr. Suat Özbek, 1st supervisor)

Table of Contents

Name: **Claudia Zenkert**

Title: **Molecular and Cellular Analysis of the Nematostella vectensis Cnidom**

1st Supervisor: **PD Dr. Suat Özbek**

Abstract

Cnidaria is the sister group of Bilateria and thus phylogenetically at the base of the Metazoa. The characteristic trait of the phylum is the presence of nematocysts or cnidae. These unique extrusive organelles are used for prey capture, feeding, defense and partly locomotion. Cnidae or nematocysts consist of a capsule wall, a tubule with or without spines, and an opercular structure. They are produced in specialized cells (nematocytes) as secretory products in a giant post-Golgi vesicle. These stinging organelles can resist extremely high pressure and their discharge is one of the fastest mechanisms in animal kingdom. In the last decade the sea anemone *Nematostella vectensis* (Anthozoa) became an emerging model organism alongside *Hydra* (Hydrozoa) for developmental and evolutionary biology. Nevertheless basic data on histology and the nematocyst repertoire (cnidom) of *Nematostella vectensis* are still missing. In my thesis, I characterized the *Nematostella vectensis* cnidom based on morphological classification. For that matter an isolation technique for intact capsules was established and the different nematocysts were analyzed using electron and light microscopy. The three capsule types (basitrichous haplonema, microbasic mastigophores and spirocysts) were quantitatively analyzed along the body axis and in the different developmental stages. Besides the morphological characterization, three molecular capsule components, minicollagen 1, 3 and 4 were isolated and in situ hybridization was performed to see their expression patterns. Antibody stainings revealed a partly abundant and partly nematocyst specific patterns of the minicollagens.

The second part of the work was focused on the cellular identification of nematocysts in *Nematostella vectensis*. Thus, all cell types were characterized qualitatively and a cell cycle analysis was performed. Nematocytes were identified to be cuboidal epithelial cells using antibody stainings on macerates. Hence, the nematocysts in Nematostella vectensis have an epithelial origin and not as in Hydra a neuronal.

Zusammenfassung

Die Cnidaria oder Nesseltiere sind die Schwestergruppe der Bilateria und stehen somit phylogenetisch an der Basis der Metazoen. Das bezeichnende Merkmal aller Cnidaria ist das Vorhandensein von Nesselkapseln oder Cniden, nesselnde Organellen, die zum Beutefang, der Verteidigung und teilweise auch zur Fortbewegung genutzt werden. Cniden oder Nematozysten bestehen aus einer zylindrischen Kapselwand, einem Schlauch mit oder ohne Dornen und einem Deckelapparat (Operculum). Spezialisierte Zellen (Nematozyten) produzieren die Organellen als Sekretionsprodukte in einem riesigen post-Golgi Vesikel. Nesselkapseln können immensem Druck standhalten und ihr Entladungsprozess ist eine der schnellsten biologischen Vorgänge im gesamten Tierreich. Die Seeanemone *Nematostella vectensis* (Anthozoa) ist in den letzten zehn Jahren neben dem Süßwasserpolypen *Hydra* (Hydrozoa) zu einem wichtigen Modellorganismus der Entwicklungs- und Evolutionsbiologie geworden. Trotz dieser Entwicklung fehlten bisher Daten zum Nematozystenrepertoire (Cnidom) und zur Identität der Nematozyten in diesem Organismus. In der vorliegenden Arbeit wurde zunächst das Cnidom von *Nematostella* morphologisch charakterisiert. Hierzu wurde ein Isolierungsverfahren für intakte Nematozysten aus Gewebe etabliert und lichtmikroskopische sowie elektronenmikroskopische Techniken zu deren Analyse eingesetzt. Die identifizierten drei Kapseltypen (basitriche Haplonemen, mikrobasische Mastigophoren und Spirocysten) wurden quantitativ entlang der Körperachse adulter Tiere und in verschiedenen Entwicklungsstadien erfasst. Neben der morphologischen Charakterisierung wurden Minikollagene als molekulare Komponenten der Nesselkapseln isoliert und deren Expressionsmuster durch ISH-Experimente (in *situ* Hybridisierung) beschrieben. Immunohistochemische Färbungen mit spezifischen Antikörpern zeigten teilweise abundante und zum Teil eine kapselspezifische Verteilung von Minikollagenen. Als schlauchspezifischer Marker wurde zudem ein nicht-sulfatiertes Chondroitin in Nematozyten nachgewiesen.

Der zweite Teil der Arbeit war auf die zelluläre Identifizierung von Nematozyten in *Nematostella* fokussiert. Hierzu wurden zunächst alle Zelltypen qualitativ charakterisiert und einer Zellzyklusanalyse unterworfen. Kapselsynthetisierende Zellen konnten dann mit Hilfe von Minikollagenfärbungen in Mazeraten als kuboidale Epithelzellen identifiziert werden. Im

Unterschied zu Hydra gehen Nematozysten demnach nicht aus einer speziellen Stammzellpopulation hervor und haben einen epithelialen und nicht neuronalen Ursprung.

1. Introduction

Cnidaria, which represent a sister group to Bilateria have proven to be an interesting model for evolutionary questions in developmental biology. The recent sequencing of several cnidarian genomes and the establishment of methods for manipulating gene expression inspired new perspectives in cnidarian research.

The phylum Cnidaria comprises ~9000 aquatic species, most of them living in marine environments. Cnidaria are divided into Anthozoa (corals, anemones and sea pens) and Medusozoa (jellyfish, box jellyfish, stalked jellyfish and hydrozoans) (Figure 1). Anthozoans live as sessile polyps, while Medusozoa basically have both a free-swimming state and a polyp state in their life-cycles.

Cnidarian diversification occurred over ~500 million years ago. Researchers found Cambrian fossils of four out of the five recent cnidarian classes (Cartwright et al., 2007). As a sister group of Bilateria, Cnidaria have proven to be an ideal model for evolutionary research.

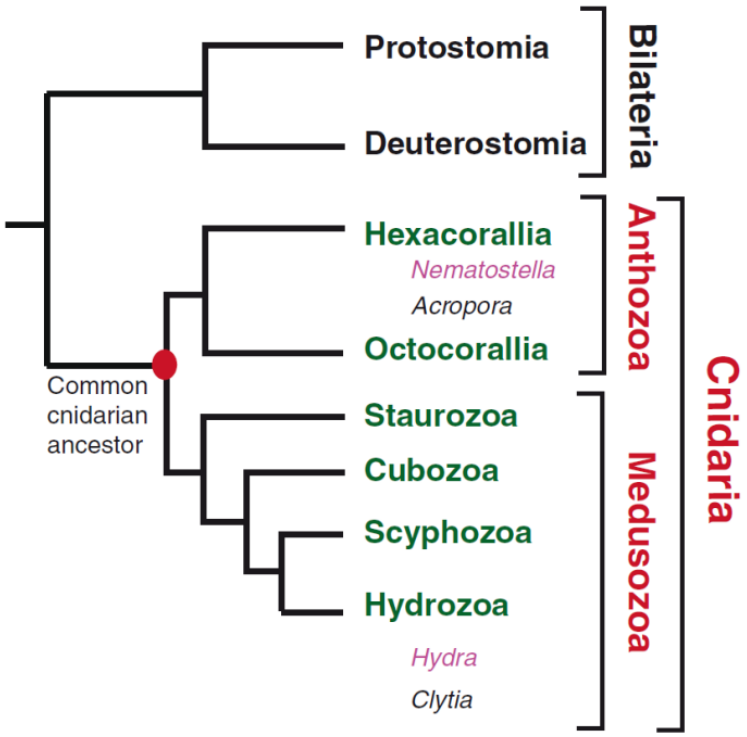

Figure 1. Phylogenetic relationships of classes in the phylum Cnidaria. A phylogenetic tree showing the relationships within the phylum Cnidaria. The two main divisions (Anthozoa and Medusozoa) are indicated in red. Anthozoa is a class that contains two subclasses (green), whereas medusozoa is a subphylum consisting of four classes (green). Sequenced genomes (pink) are available for *Nematostella* and *Hydra* (Chapman et al., 2010; Putnam et al., 2007), whereas the genomes of *Acropora* and *Clytia* are currently being sequenced (black). Technau et al., 2011.

Cnidarians consist of only two cell layers (ectoderm and endoderm), have an external radial symmetry (anthozoans may display an internal asymmetry) and have a gastro-vascular cavity functioning as both mouth and anus. Figure 2 shows the body plan of *Hydra* exemplaric for all cnidarians. Ectoderm and endoderm are separated by an acellular extracellular matrix (mesogloea). Hydrozoans have an interstitial stem cell lineage, basically multipotent cells that are able to differentiate into neurons, gland cells, nematocytes or gametes (David and Murphy, 1977) (Figure 2B). Many cnidarians can undergo both sexual and asexual reproduction. In the case of *Hydra* asexual reproduction is maintained by budding, *Nematostella* can fission off basal parts.

The defining trait of cnidarians is the nematocyst or cnidae, unique extrusive organelle used for feeding, defense and in some cases locomotion (Holstein, 1981; Tardent and Holstein, 1982).

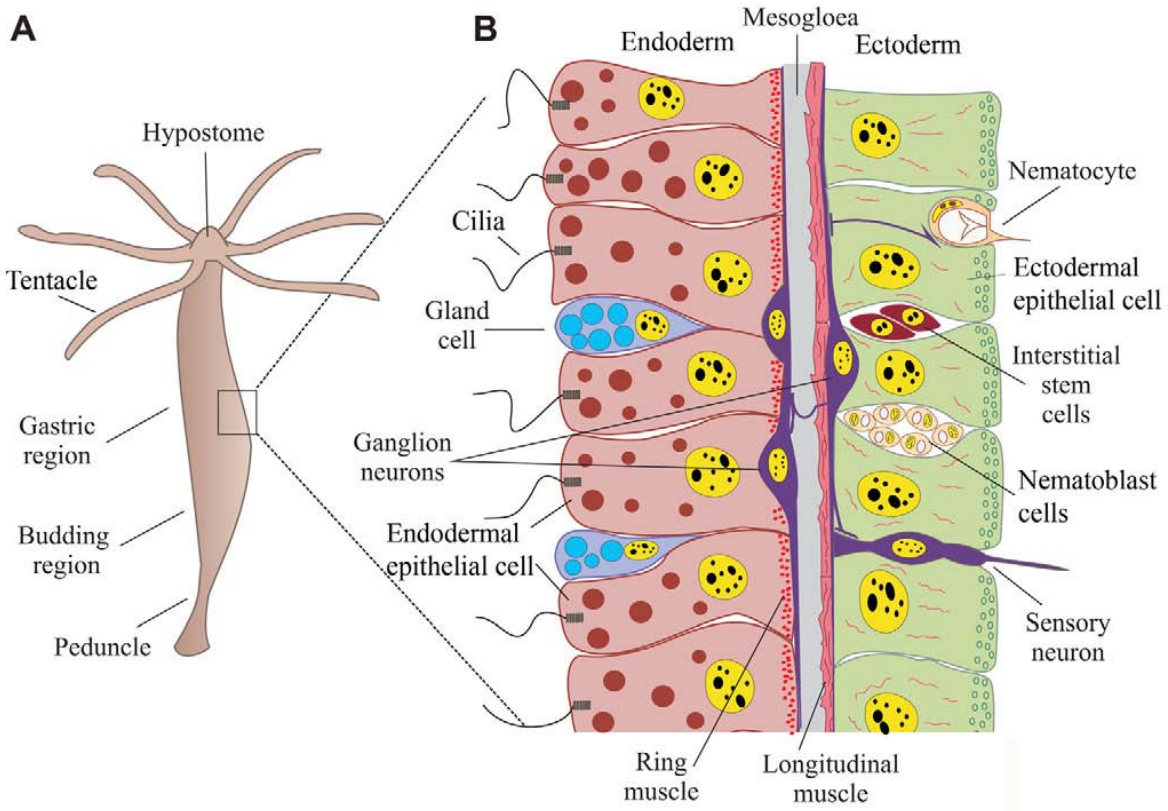

Figure2. Anatomy of a hydrozoan polyp. A A *Hydra* polyp is essentially a two-layered tube, with a ring of tentacles around the mouth opening at the tip of the hypostome. Asexual budding occurs on the lower half of the body column. Interstitial stem cells and nematoblasts are distributed evenly in the body column. B The bilayered cellular organization of a *Hydra* polyp. All epithelial cells in *Hydra* are myoepithelial, with myofibers on the basal side (red). Most interstitial cells and nematoblast clusters are located between ectodermal epithelial cells. Neurons are found in both the endoderm and ectoderm. Different types of gland cells, most of which are found in the endoderm, are intermingled between the epithelial cells. Technau et al., 2011.

1.1. *Nematostella vectensis* as an emerging model organism

Within the past ten years *Nematostella* has become one of the leading cnidarian model organisms. It is a small, widely distributed estuarine sea anemone, which inhabits soft sediments, salt marshes, permanent pools and tidal creeks all along the coastlines from England to Northern America. Its unsurpassed ease of culturing of all developmental stages under laboratory conditions raised the attention of researchers worldwide. Like all cnidarians it has a high regenerative capacity, the possibility of asexual reproduction and a short, anthozoan-typical sexual reproduction cycle (Figure 3). With its clear systematic position at the base of metazoan evolution, the fully sequenced genome and the availability of well-established genetic manipulation techniques, *Nematostella* quickly became an attractive model organism (Figure 4). Despite this fact, a full description of its nematocyst repertoire has remained elusive. The aim of the presented work was to fill this gap in *Nematostella* biology and to provide tools for further comparative studies in cnidarian research.

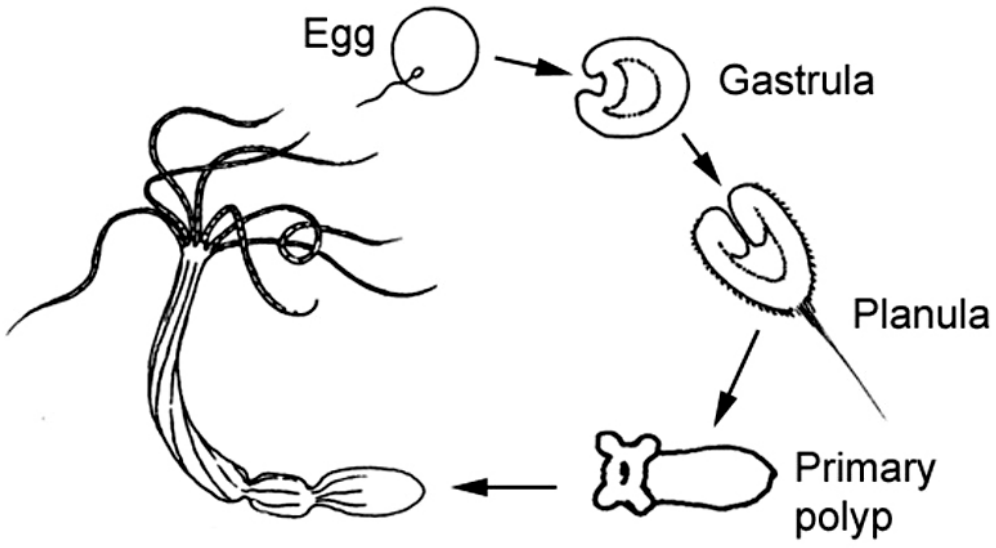

Figure 3. Life cycle of *Nematostella*. The female releases hundreds of jelly-coated eggs that, after gastrulation, turn into a planula larva. The animal undergoes metamorphosis to become a primary polyp, which elongates and outgrows into an adult polyp. Drawing by Hanna Kraus (Technau et al., 2011).

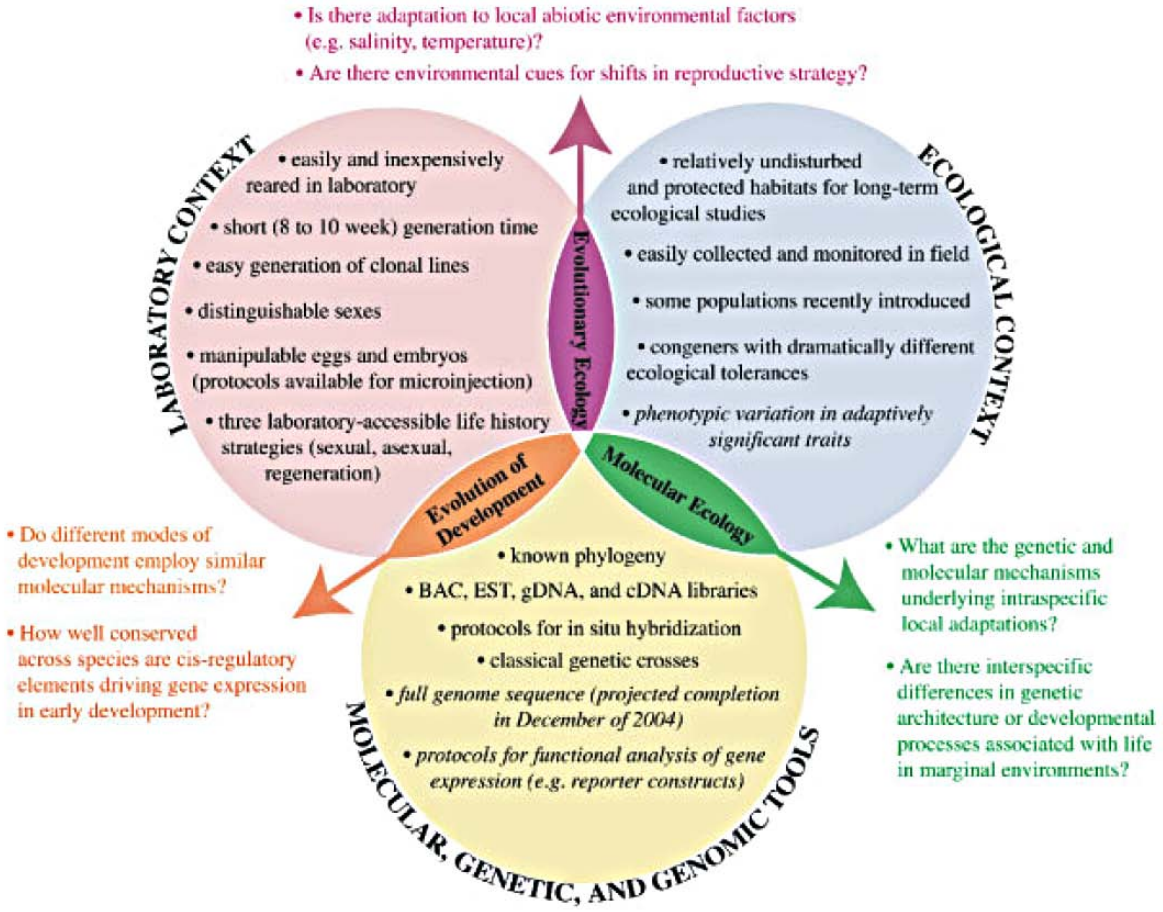

Figure 4. *Nematostella vectensis* as a model system. *Nematostella* possesses a number of characteristics that make it attractive as a model system for a variety of research questions, ranging from dissection of developmental pathways and comparative evolutionary genomics to investigation of ecologically relevant phenotypic traits. *Nematostella*'s physiology and life history make it particularly well suited for laboratory manipulation (violet circle), its ecological context makes it amenable to field monitoring and population-level studies (blue) and the growing availability of molecular and genomic tools (yellow) have encouraged a small but expanding research community. Darling et al., 2005.

1.2. Capsule types in Anthozoa

Eventhough hydrozoans have the greatest diversity of nematocysts, anthozoans are the only cnidarians possessing all three types of capsules – nematocysts, spirocysts and ptychocysts (exclusively in Ceriantharia) (Werner, 1965; Mariscal, 1974).The only cnidae able to inject venom are nematocysts. Based on the original classification (Weill,1934), 10 of the 30 types of nematocysts are present in anthozoans (Carlgren, 1940, 1945; Werner, 1965; Mariscal, 1974, 1977). Later Schmidt (1969, 1972 and 1974) developed an alternative classification

system specifically for anthozoans, though the following work is guided by the Weill classification (1934).All classification is based on morphology. The main characteristics are closed tubule tip (Astomocniden) and open tubule tip (Stomocniden), tubules of equal diameter and tubules with thicker bases or tips. The number and pattern of spines are also of relevance.

There is no historical record of the capsule types in *Nematostella* (Family: Edardsiidae). The closest relatives with an examined capsule repertoire are actinarian families like Actiniidae (*Tealia*), Sagartiidae (*Sagartia*) and Aiptasiidae (*Aiptasia*). The drawings below give examples of Weill's work, depicting spirocysts (Figure 5A) and several different nematocyst types (Figure 5B) found in Anthozoa.

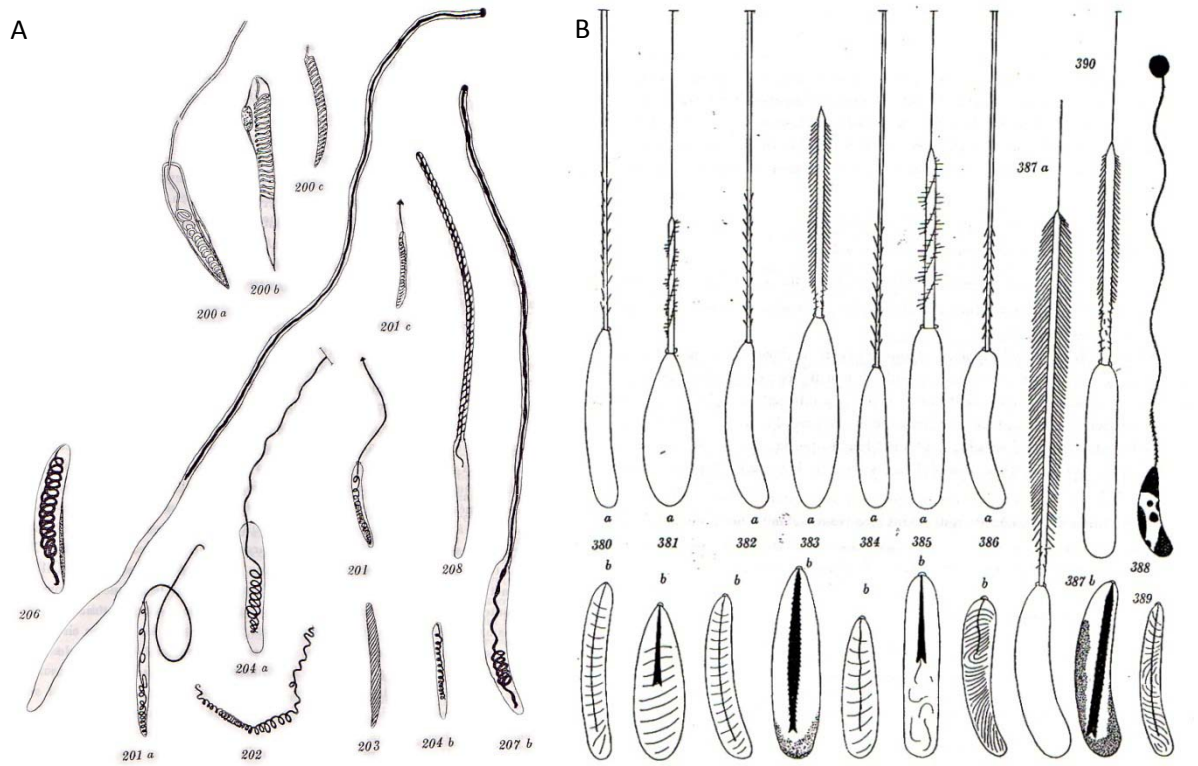

Figure 5. Different capsule types found in Anthozoa. A Spirocysts in charged and discharged conditions. B Nematocyst types in Actinaria. 380, 381 *Tealia crassicornis*. 382, 383 *Sagarita miniata*. 384, 385 *Actinoloba dianthus*. 386- 390 *Aiptasia annulata*. Weill (1934).

1.3. Nematocyst morphogenesis

Nematocyst development is a highly organized intracellular secretion process leading to the self-assembly of structural proteins at the inner surface of a vesicle membrane. In the nematocytes the nematocysts form within a giant post-Golgi vesicle (Slautterback et al., 1958; Skaer, 1973; Holstein, 1981). The pre-capsule forms and grows by addition of more vesicles from the trans-Golgi network (TGN). Also, the tubule grows externally by fusion of additional secretory vesicles before it invaginates into the capsule matrix (Holstein, 1981) (Figure 6).

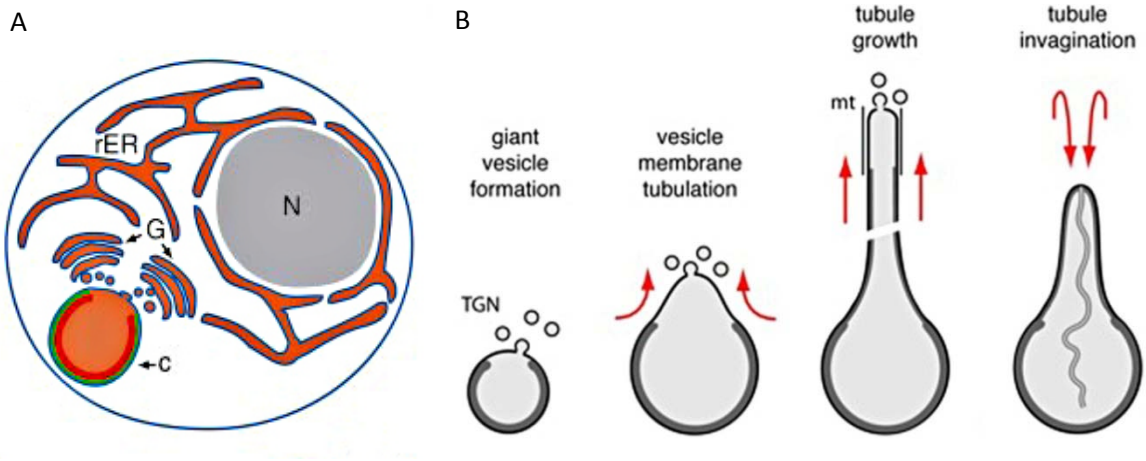

Figure 6. Schematic representation of nematocyst morphogenesis. A Nematocyte with nucleus (N), rough Endoplasmic Reticulum (rER), Golgi apparatus (G) and forming capsule (c). Engel et al., 2001. B The premature capsule wall is lining the inner surface of the nematocyst vesicle. The area of tubule outgrowth adjacent to the trans-Golgi network (TGN) is free of capsule wall material. The growing tubule is stabilized by microtubules (mt) at the cytoplasmic surface (Adamczyk et al., 2010).

When the tubule is completely inverted and coiled up inside the capsule body, the different capsule components start to cross-link. The future opening site is covered either by an operculum or (as in anthozoans) by opercular flaps (Godknecht and Tardent, 1988). The fully charged nematocyst capsule comprises a collagenous polymer, which is able to withstand 150 bar of osmotic pressure. The capsule matrix is pressurized by poly-γ-glutamate, which binds a 2 M concentration of cations (Özbek et al., 2009). The mature nematocysts are docked at the apical pole of the nematocytes, and each one is anchored by a tight basket of microtubules and intermediate filaments (Wood and Novak, 1983).

1.4. Nematocyst discharge in anthozoans

Cnidae are, according to Mariscal (1974), “among the largest and most complex intracellular secretion products known.” Reacting to a chemical and/or mechanical stimulus (reviewed by Anderson and Bouchard, 2009) the capsule opens and the tubule everts. This discharge mechanism is one of the fastest cellular processes. It has been most thoroughly studied in *Hydra* (Holstein and Tardent, 1984; Nüchter et al., 2006). Nematocytes contain a cnidocil (Figure 7), which triggers the discharge process upon excitation leading to a Ca^{2+} influx. Then the tubule is released and completely everted in 700 ns generating an acceleration of 5,400,000 g and a pressure of 7.7 GPa at the site of impact (Nüchter et al., 2006).

This process is accompanied by a volume increase of the capsule body. This kind of vesicle swelling is a well-known phenomenon in most exocytotic systems. In most cases, the matrix of the secretory organelle acts like a cationic ion exchanger through a high density of fixed negative charges (Parpura and Fernandez, 1996). After the fusion pore formation there is a high influx of counter ions, like N^+ or K^+ from the extracellular medium along with water causing the matrix to swell up (Fernandez et al., 1991). In some anthozoans the capsules swell by >50 % immediately prior to discharge and then return to their original dimensions (Robson, 1972). Özbek et al. (2009) postulated that in addition proteins located in the opercular flaps might change their supra-molecular architecture and so facilitate discharge.

The discharge itself can be divided into four stages: (i) the initial lag phase, (ii) the rapid phase of discharge, (iii) the temporary arrest phase and (iv) the toxin release phase (Özbek et al., 2009). The initial lag phase marks the delay between depolarization and opening of the opercular structure, and is strongly Ca^{2+}-dependent. The rapid phase of discharge is characterized by lid opening and tubule ejection, and it can be as short as 3 µs. In the temporary arrest phase the internal pressure has to rise again in order to inject venoms, enzymes etc. The release itself takes place with a velocity of 0.27 ± 0.21 m/s (Nüchter et al., 2006) in the final toxin release phase.

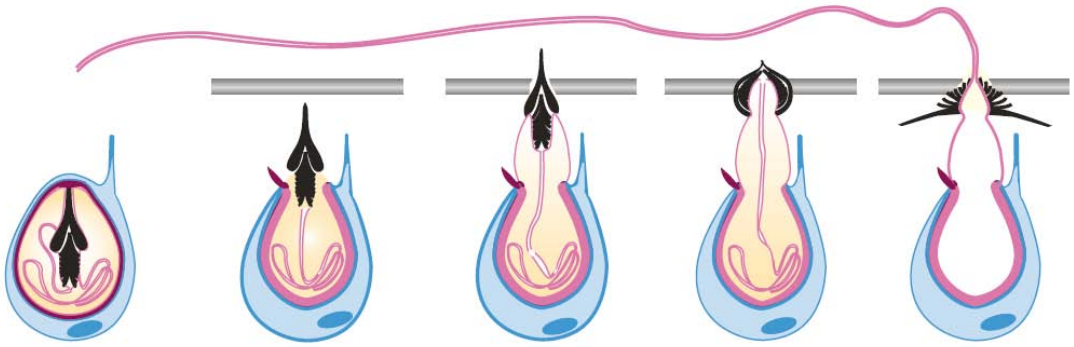

Figure 7. Discharge of a stenotele nematocyst shown schematically (Hydrozoa). A Nematocytes (blue; cell and vesicle membranes in dark blue) harbor one cyst (pink; minicollagen wall, tubule, and operculum) with styletts (black) punching a hole into prey. Nüchter et al., 2006.

1.5. Structural components of nematocysts

1.5.1. Minicollagens

Collagens are a major protein component of all animals, and were assumed to have appeared with metazoan multicellularity (Exposito et al., 2002). They are composed of repetitive glycine-X-Y units, where X is mostly proline and Y 4-hydroxyproline. Figure 8 shows the organization of these repetitive Gly-X-Y sequences in triple helical structures that establish the major fibrous element of animal tissues.

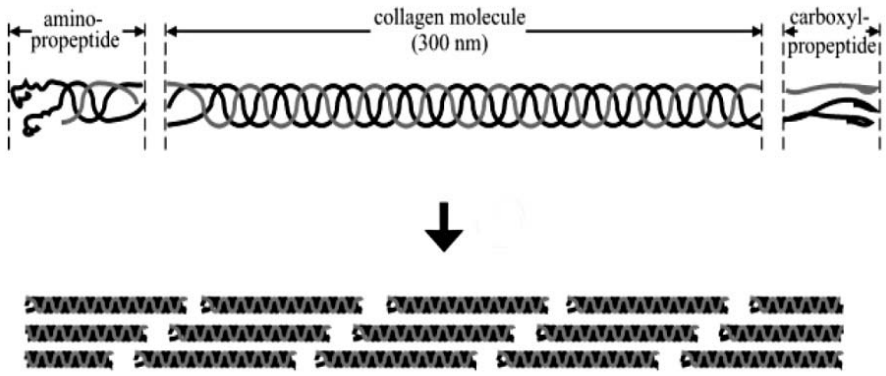

Figure 8. Fibrillar collagens. Type I collagen is used to illustrate the formation of fibrils from collagen chains. Collagen molecules are involved in the supramolecular organization of collagen fibrils. Exposito et al., 2002.

In Cnidaria, a family of uniquely short collagens with eight to 16 Gly-X-Y repeats (minicollagens) was identified (Kurz et al., 1991; Özbek et al., 2002). Minicollagens constitute

a major part of nematocysts. They are comprising a central triple helical domain flanked by variable poly-proline stretches and terminal cysteine-rich domains (CRDs) with a canonical $CX_3CX_3CX_3CX_3CC$ pattern (Figure 9A). These CRDs are involved in the capsule wall formation by facilitating disulfide-dependent intermolecular links (Figure 9B) (Özbek et al., 2002). The N-terminal CRD is structurally the same in all minicollagens, while the C-terminal CRD mostly adopts a novel fold, creating a molecular polarity, which may be involved in the macromolecular assembly of the capsule (Meier et al., 2007) or as it is the case in *Hydra* minicollagen-15 are composing the tubule structure specifically, thus limited to a certain area of the capsule. Those CRD domains constitute the variable element that are the basis for molecular phylogeny, resulting in three major groups (David et al., 2008). Group I comprises minicollagen with both conserved N- and C-terminal CRDs, while in group II, the C-terminal CRDs are duplicated, and the additional domain has a deviating cysteine pattern. Minicollagens of group III have altered patterns at both the N- and C-terminus and thus are not supposed to be able to interact with group I.

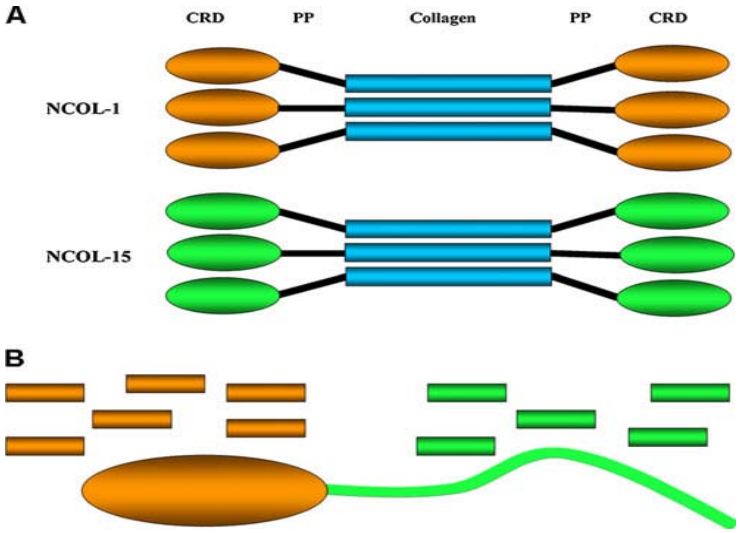

Figure 9. A Common domain organization of minicollagens; CRD cysteine-rich domain, PP polyproline stretch. B Incorporation of different minicollagens into the capsule architecture is controlled by a "CRD code". NCol-1 with conserved CRDs is part of the capsule wall; NCol-15, which shows derivated CRDs, is exclusively found in the tubule structure. Özbek, 2010.

Özbek (2011) suggests the short triple helix of the minicollagens to be a primordial state, which might have given rise to larger fibrillar minicollagens in the extracellular matrix.

1.5.2. Chondroitin a conserved tubule antigen in cnidarians

Proteoglycans (PGs) are major components of the extracellular matrix and consist of a core protein, to which chains of complex glycosaminoglycans (GAGs; large hydrophilic polysaccharide chains) are covalently attached (Figure 10). Chondroitin and chondroitin sulfate are typical GAGs (Yamada et al., 2007). They are involved in the regulation and maintenance of cell adhesion, motility, proliferation, differentiation, tissue morphogenesis and embryogenesis (Kjellén and Lindahl, 1991). Sugahara et al. (2003) found GAGs to play important roles in neural development by regulating neuronal adhesion and migration as well as the formation of neurites, and axonal guidance. This high extent of variability is acquired through extensive modifications involving sulfation and urinate epimerization (Fransson, 1985). Since GAGs were found in *Caenorhabditis elegans*, *Drosophila melanogaster* and *Hydra magnipapillata* they seem to be conserved through evolution, and play fundamental roles in animal development. The average molecular size of *Hydra* chondroitin sulfate was estimated to be 110 kDa, which is similar to that of mammals. The epitope of the anti-chondroitin antibody is present in developing nematocysts (Yamada et al., 2007). The morphogenesis of cnidae takes place in giant post-Golgi vesicles, which topologically represent extracellular space. A non-sulfated chondroitin appears as a scaffold in early morphogenesis of all nematocyst types in *Hydra* and *Nematostella*.

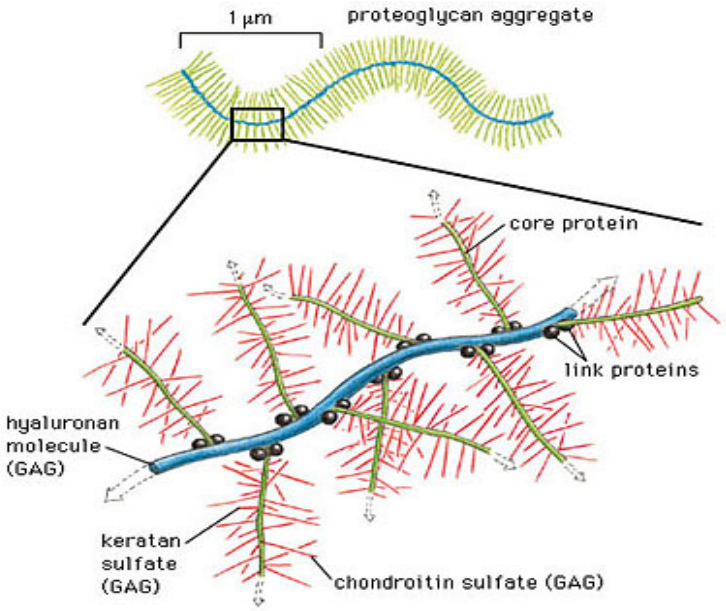

Figure 10. Organization of proteoglycans. http://www.indinine.biz/Misc%20Pics/cellular_organization_3.htm.

2. Aim of this work

Over the past six years *Nematostella vectensis* has become an important model organism in evolutionary and developmental biology. Its phylogenetic position at the base of the Metazoa and the early split between Anthozoa and Hydrozoa makes it particularly interesting for evolutionary research. Nevertheless, little is known about tissue distribution and kinetics, the nematocyst repertoire and capsule components of this anthozoan species. The aim of this work was to provide basic knowledge about the cell composition and organization as well as clarification of the cnidom and molecular components of nematocysts, using immunocytochemistry, and basic molecular and cell biological methods.

3. Results

3.1. Capsule types in *Nematostella vectensis*

Nematocysts were isolated by Percoll gradient centrifugation and characterized morphologically using light and scanning electron microscopy (SEM). Three different capsule types were distinguished, according to the classification of Weill (Weill et al., 1934): (i) the smallest and most common nematocyst type is the basitrichous haplonema (Figure 11A- E). It is about 12 µm long and 2 µm in width. The tubule has a diameter of 0.5 µm, with a total length of 90- 110 µm (Fig. 11B- C). Dense spines of 1- 2 µm in length are arranged in spirals along a stretch of 20- 25 µm at the base of the tubule (Figure 11D). SEM analysis revealed smaller spines (~0.1 µm) (Figure 11E) covering up to 2/3 of the total tubule length; (ii) the larger microbasic mastigophores (Figure 11F-J) are 17- 22 µm long and 3 µm in width. The clearly discernible tubule base (30- 40 µm) is about 1.5 µm in diameter and covered with dense spirals of spines (1- 4 µm each) (Figure 11G- I). The tubule has a total length of 180 µm with a narrower and smooth distal part (Figure 11H and J); (iii) spirocysts are the characteristic con-shaped nematocysts of anthozoans. In *Nematostella* they are about 25-30 µm long and thus represent the largest capsule type (Figure 11K- P). The spineless tubule (Figure 11P) is visible in typical large coils inside the capsule body and has an average diameter of 1 µm and a length of about 180 µm (Figure 11K- M). Most spirocysts are disrupted by the isolation procedure and quantification has to rely on careful maceration. SEM analysis revealed that they lack an opercular structure (Figure 11N, O). Capsule closure appears to be realized by folds at the base of the inverted tubule (Figure 11O) suggesting a continuous structure between tubule and capsule body for this nematocyst type.

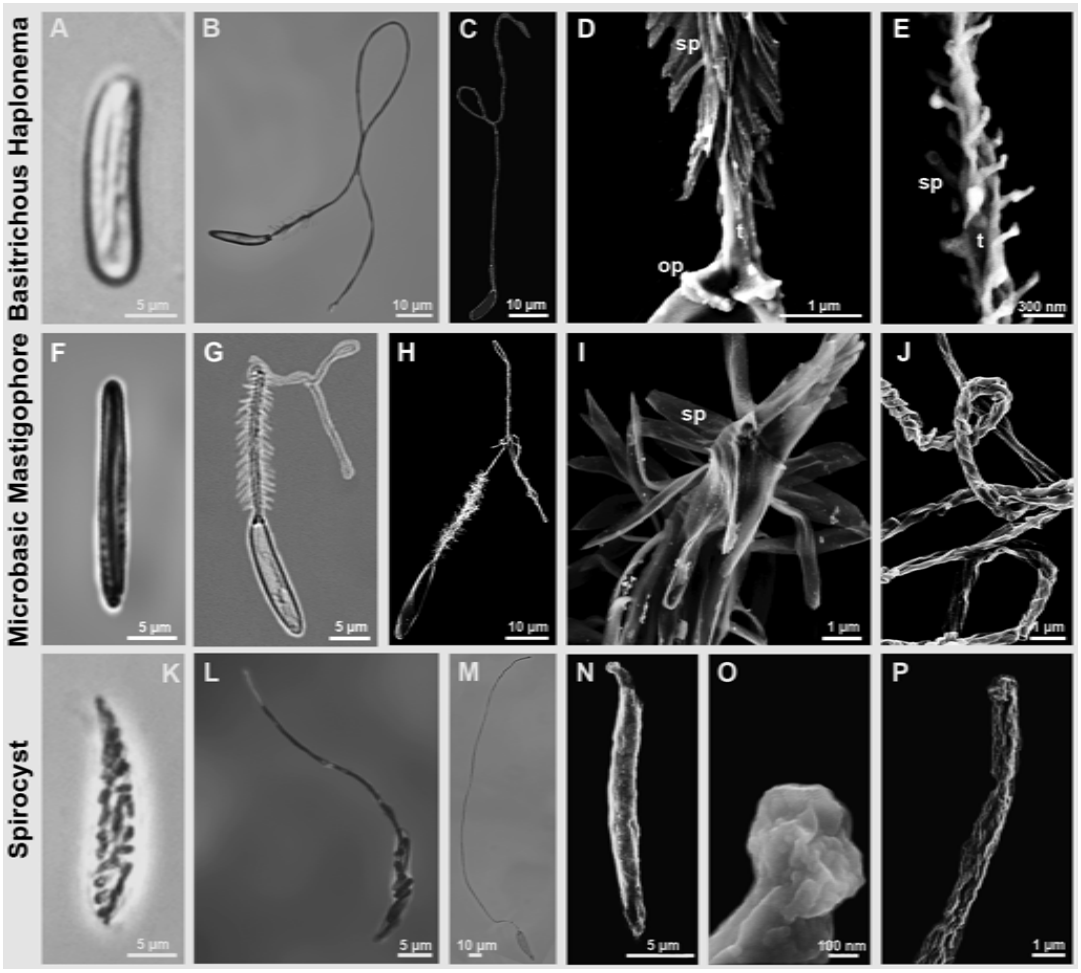

Figure 11. Capsule types in *Nematostella vectensis*. A- E. Basitrichous haplonema. F- J. Microbasic mastigophores. K- O. Spirocysts. A- B, F- G and K- M are light microscopic images. C- E, H- J, and N- P are SEM images. op operculum. sp spines. t tubule. Scale bars are 10 µm (B, C, H, M, N), 5 µm (A, F, G, K, L), 1 µm (D, I, J, O) and 300 nm (E).

3.2. Nematocyst distribution

In planula larvae basitrichous haplonema clearly dominated, constituting 91 % of all capsule types, while mastigophores and spirocysts were represented only to 5.3 % and 3.7 %, respectively (Figure 12A). The percentage of basitrichous haplonema was slightly reduced in primary (83.4 %) and adult polyps (69.2 %), whereas microbasic mastigophores were almost constant at 15 % and 16.5 %, respectively. Spirocysts stayed at a low level (1.6 %) in primary polyps but were increased to 14.3 % in adult animals. Considering the total tissue of the animal, nematocytes made up 4- 5 % of all cells at each developmental stage.

Mature nematocysts are distributed all along the body axis, the highest density of capsules is found in the tentacles, the tentacle base and the hypostomal area (Figure 12B). In the head region, the majority of nematocysts (45.3 %) are spirocysts, followed by basitrichous haplonema (41.1 %) and microbasic mastigophores (13.6 %). Nematocysts in the body column and foot region are mainly basitrichous haplonema (77 % and 89.9 %) and microbasic mastigophores (22.4 % and 9.9 %), suggesting that spirocysts and microbasic nematocysts are offensive capsule types used for prey capture, while basitrichous haplonema mainly have a defensive function against predators.

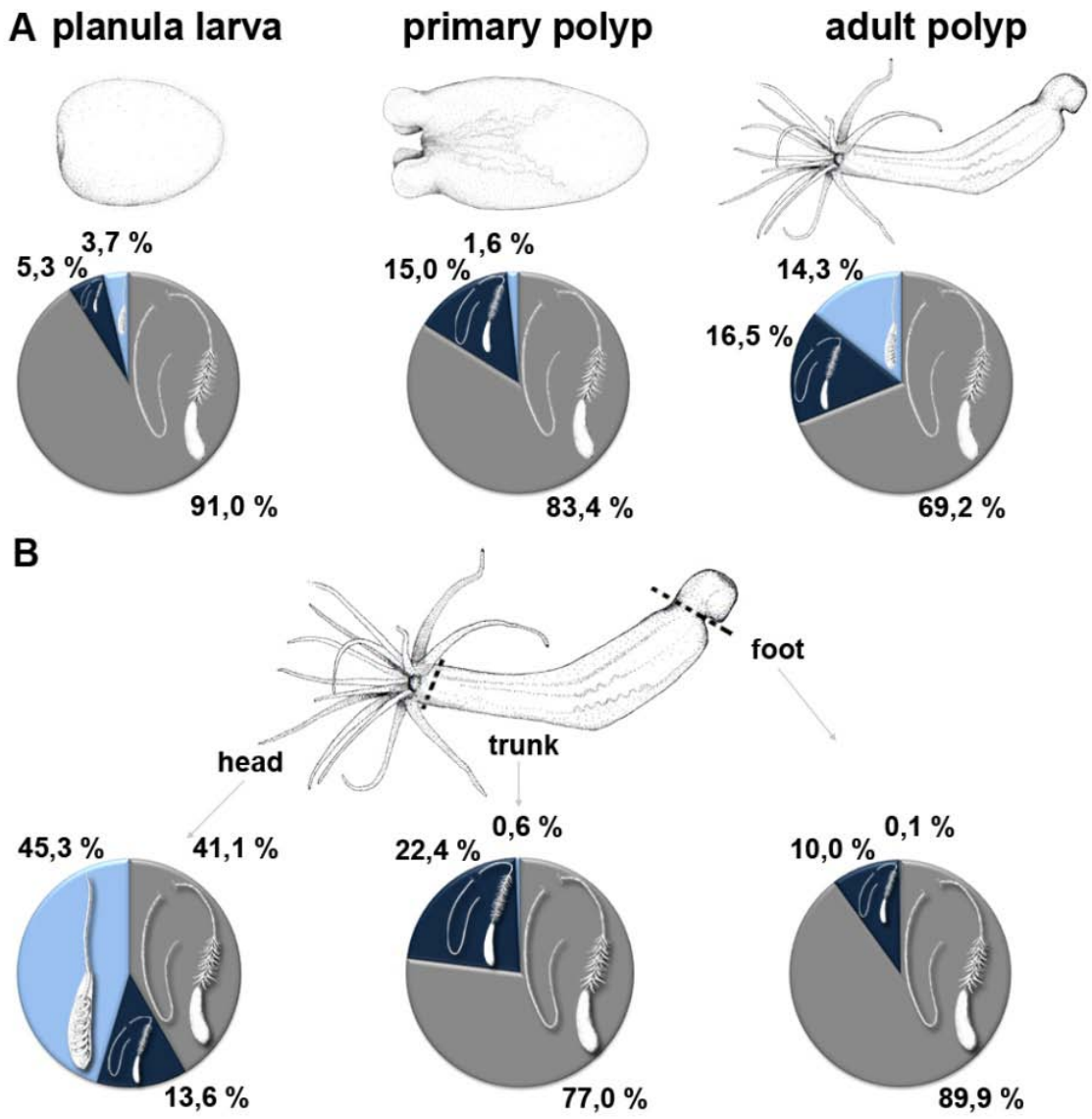

Figure 12. Quantitative distribution of nematocysts in *Nematostella* polyps. A. Distribution of nematocyst types in different developmental stages. B. Distribution of nematocyst types in different body parts of *Nematostella vectensis*.

3.3. *Nematostella* minicollagens 1, 3 and 4

Five different minicollagen genes were identified in the genome database, in contrast to the 17 minicollagens in *Hydra*, reflecting the lower complexity of anthozoan nematocysts (David et al., 2008).As minicollagens are important markers of nematocyst morphogenesis, the *Nematostella* minicollagen genes were isolated by cloning from cDNA. While minicollagens 1, 3 and 4 (NvNCol-1, NvNCol-3 and NvNCol-4) were successfully cloned, the predicted gene sequences of NvNCol-5 and NvNCol-6) could not be amplified. This is probably due to highly homologous sequences between minicollagens and a lower abundance in the respective cDNAs.

The full-length minicollagen sequences are shown in Figure 13. NvNCol-1 has an open reading frame (ORF) of 516 nucleotides, coding for 172 amino acids. NvNCol-3 is slightly shorter with 429 nucleotides (143 amino acids) and NvNCol-4 comprises 570 nucleotides coding for 190 amino acids. All three identified NvNCols have individual signal peptides with 19- 21 amino acids followed by a propeptide sequence terminating with the characteristic lysine-arginine (KR) cleavage site. Their domain composition includes a central collagen sequence comprising between 14- 27 Gly-X-Y repeats flanked by variable polyproline stretches and terminal CRDs. NvNCol-3 and NvNCol-4 possess single canonical CRDs while NvNCol-1 shows a CRD duplication at the C terminus with the second one lacking the first two cysteines of the conserved pattern as in *Hydra* NCol-15 (Adamczyk et al., 2008). In contrast to Hydra, the minicollagen genes are positioned on different scaffolds and do not occur in clusters of tandemly repeated genes sharing a common signal peptide (David et al., 2008).

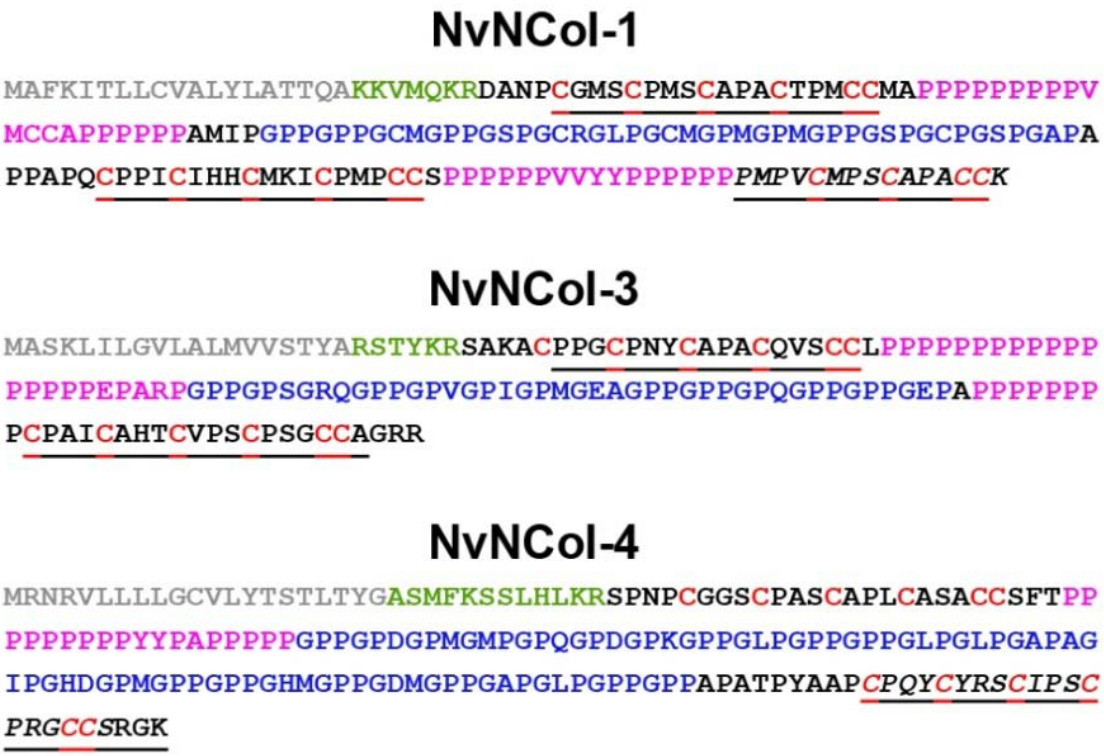

Figure 13. Amino acid sequences of Nematostella minicollagens. Protein sequences of minicollagens NvNCol-1, NvNCol-3, and NvNCol-4. Signal peptides in grey; propeptide in green; poly-proline stretches in pink; cysteine-rich domains (CRDs) are indicated in underlines, cysteine residues are in red. The C-terminal CRDs printed in italics were chosen for raising the polyclonal antibodies.

The expression patterns of the isolated minicollagen genes were assayed by *in situ* hybridization (ISH) of whole mounts from different developmental stages (Figure 14). All assayed *Nematostella* minicollagens showed a comparable temporal and local expression. Initial signals in the late gastrula stage appeared spot-like and were evenly distributed (Figure 14A, E and I). In planula larvae the expression is significantly increased at the hypostomal area (Figure 14B, F and J). In primary polyps and adult animals minicollagen expression is mainly restricted to the tentacles and the hypostome (Figure 14C, G and K). NvNCol-3 showed additional weaker signals throughout the body column, which were not detectable for the other assayed minicollagens (Figure 14G).

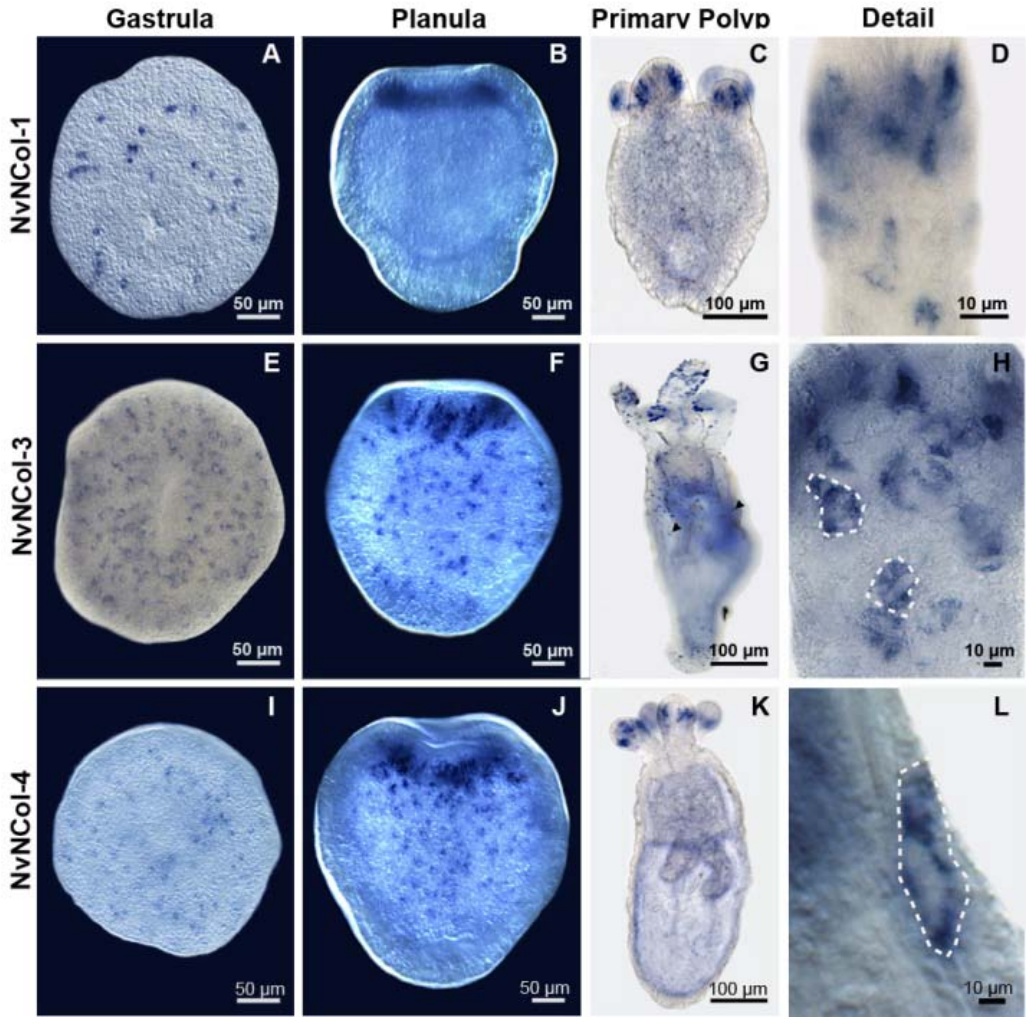

Figure 14. Whole mount in situ hybridization for minicollagen genes at different developmental stages of *Nematostella vectensis*. Gene expression patterns for NvNCol-1 (A- D), NvNCol-3 (E- H) and NvNCol-4 (I- L). Arrows in G denote NvNCol-3 positive signals along the body column. Dotted lines in H and L mark the borders of nematocytes. Scale bars are 100 µm (C, G and K), 50 µm (A, B, E, F, I and J) and 10 µm (D, H and L).

To analyze the distribution of the different minicollagens on protein level, polyclonal antibodies were raised against their respective C-terminal CRD domains (Figure 13). It was shown that the CRD domains in *Hydra* minicollagens can be used as discriminating antigens for antibody production and do not show cross-reactions with other minicollagen proteins (Adamczyk et al., 2008).

All minicollagen antibodies used in our study specifically recognized developing nematocysts throughout the animal in adult polyps (Figure 15A, E, and I). In contrast to *Hydra*, nematocytes in *Nematostella* do not migrate or form nests of multiple cells producing one capsule type. Interestingly, the distribution of the different minicollagens among the various

capsule types was inhomogeneous. NvNCol-1 could be detected in basitrichous haplonema and microbasic mastigophores (Figure 15B and C), but was absent in spirocysts (Figure 15D). NvNCol-3 and NvNCol-4 were detected in all three capsule types with slight variations in their intensity (Figure 15E- L). All signals detected by the minicollagen antibodies were restricted to the capsule body and did not show any tubule structures. A tubule staining had been expected for NvNCol-1 due to the homology of the cysteine pattern in its truncated C-terminal CRD to the one in Hydra NCol-15 (Adamczyk et al., 2008).

In summary, NvNCol-3 appeared to be a basic component of all capsule types, whereas the other minicollagens showed variations in their distribution among different capsule types.

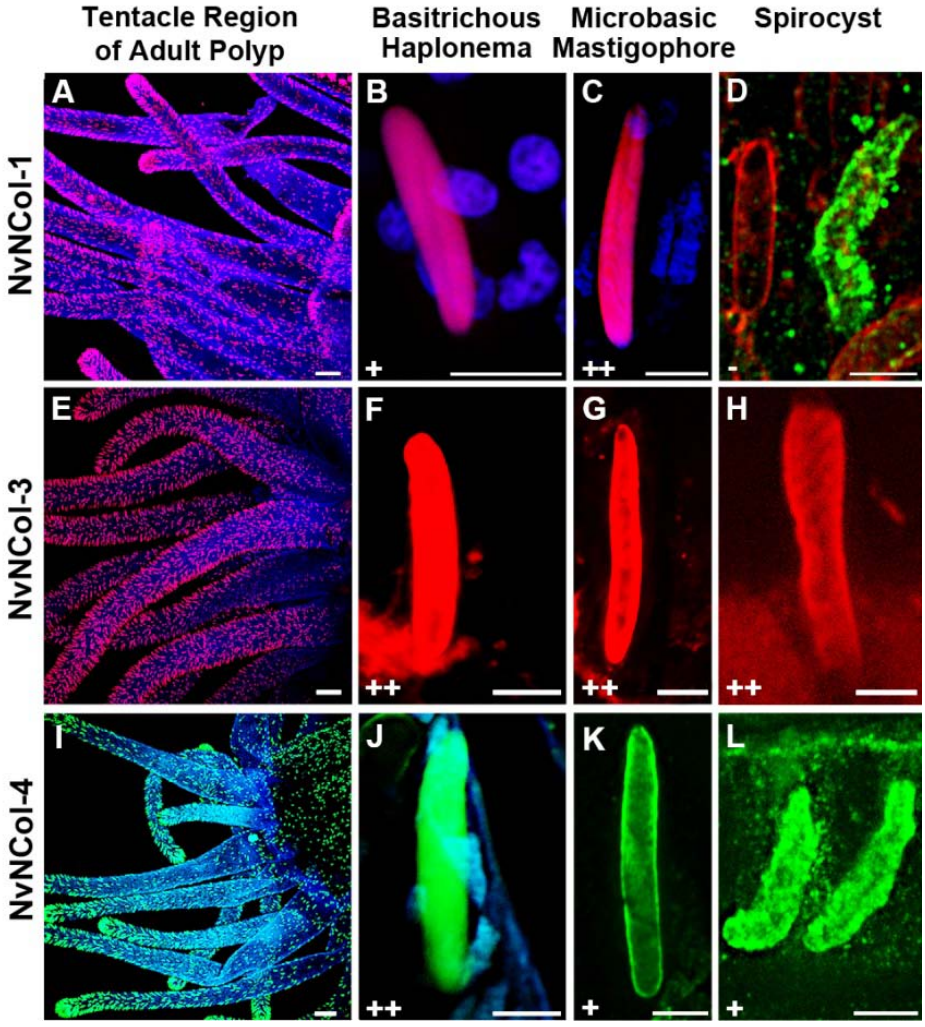

Figure 15. Detection of *Nematostella* minicollagens by immunocytochemistry. Adult polyps were stained with polyclonal minicollagen antibodies and DAPI. A- D. NvNCol-1 staining for different capsule types. D shows a co-staining with NvNCol-4 antibody (green) to demonstrate a lack of NvCol-1 staining in developing spirocysts. E- H staining for nematocysts using anti-NvNCol-3 antibody. I-L NvNCol-4 staining of different nematocysts. In A- C and E- H minicollagens were stained with Alexa-568 (red) and in I-L with Alexa-488 (green). + positive signal. ++ strong signal. – no signal. Scale bars are 100 µm (A, E and I), 10 µm (L), and 5 µm (B, C, D, F, G, H, J and K).

3.4. A Nematocyst-specific Chondroitin in *Nematostella*

Chondroitin forms the outer layer of the developing nematocyst tubule, both in *Hydra* and the sea anemone *Nematostella vectensis* (Yamada et al., 2007). Co-stainings performed with the *Hydra* minicollagen-1 (NCol-1) antibody demonstrated a clear restriction of the chondroitin signal to the tubule of the growing vesicle (Figure 16). NCol-1 is deposited into the capsule wall and therefore marks the capsule body inside the vesicle. The chondroitin signal initially appears as a vesicular structure around the tip of the outer growing tubule in early morphogenetic stages, therefore correlating with the onset of tubule growth (Figure 16C). During morphogenesis the staining pattern follows the growing tubule thereby covering it like a sheath of scaffold (Figure 16F). After invagination of the tubule and maturation of the nematocyst the signal remains at the operculum (Figure 16D). The tubule-specific Minicollagen-15 is incorporated only after the pre-tubule structure is invaginated (Adamczyk et al., 2008). These findings suggest that the nematocyst-specific chondroitin is involved in the formation of a pre-tubule structure that accompanies membrane protrusion and serves as a scaffold for minicollagen assembly after invagination.

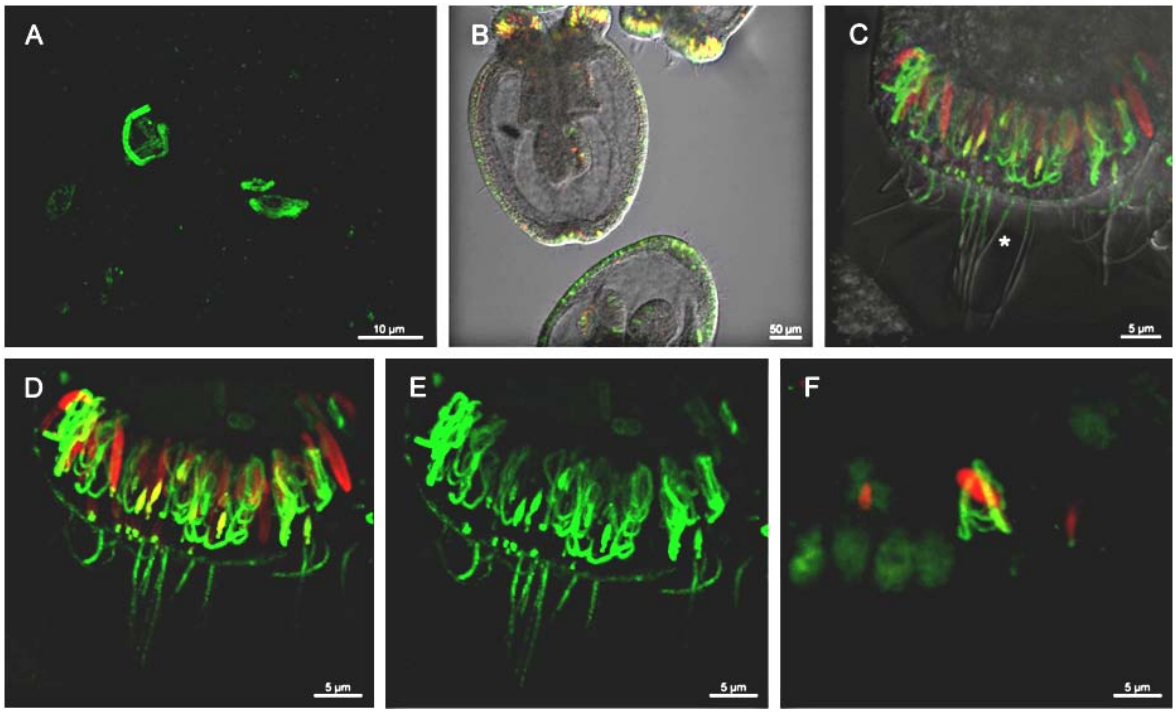

Figure 16. Co-staining of anti-chondroitin and *Hydra* minicollagen-1 (NCol-1) in *Nematostella vectensis*. Chondroitin signals in green and NCol1 in red. A Confocal image of everted tubules in planula larvae. B Primary polyps. C- E Developing tentacle. C Confocal image underplayed with DIC. Asterisk marks the tubules of discharged nematocysts. D Detail of different stages of nematocyst synthesis. E Only anti-chondroitin. F Detail of basitrichous haplonema. Scale bars are 50 µm (B), 10 µm (A) and 5 µm (C- F).

3.5. Spirocysts are of less molecular complexity than nematocysts

Using Percoll gradient centrifugation procedure to isolate nematocysts, spirocysts could not be acquired. Even in light microscopy spirocysts seem more fragile and less dense (Figure 11M) and the fixation for SEM analysis proved difficult. As shown above, spirocysts, in contrast to the other capsule types, did not contain all minicollagens identified. Recent experiments using second harmonic generation image analysis (SHG) showed that basitrichous haplonema and microbasic mastigophores have dense capsule wall structures emitting SHG light (Figure 17) (Strompen et al., unpublished). Spirocysts at all developmental stages were only visible in auto-fluorescent spectrum (Figure 17B and C). These results point to the conclusion, that the anthozoan specific spirocyst has a less dense capsule wall structure and might therefore represent an ancient capsule type.

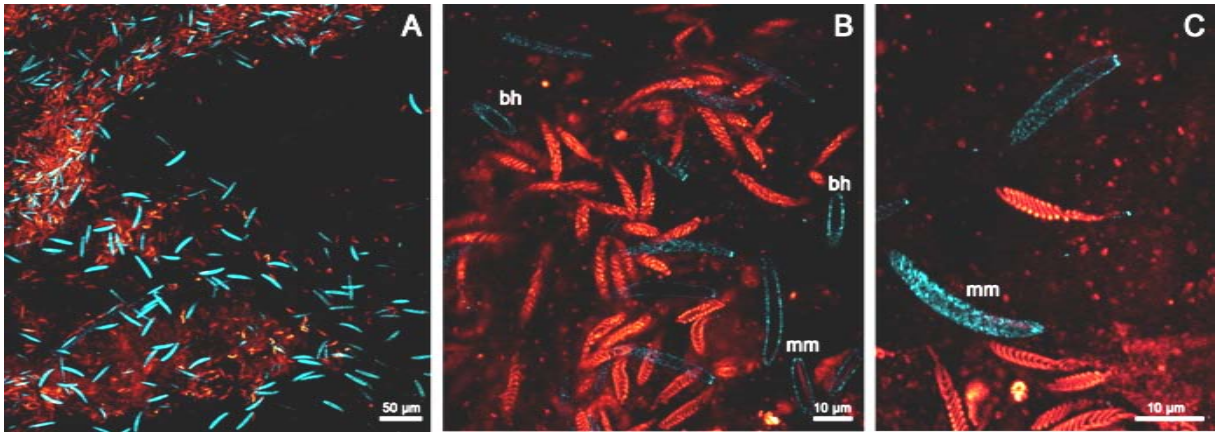

Figure 17. Second harmonic generation image analysis of *Nematostella* mesogloea. Only dense structures are capable of emitting SHG light. A Nematocysts cover the surface of the isolated mesogloea. B Microbasic mastigophores (mm) and basitrichous haplonema (bh) are dense enough to be emitting SHG light (blue), while spirocyst can only be seen for their auto-fluorescence. C Detail of spirocysts and microbasic mastigophores. Scale bars are 50 µm (A) and 10 µm (B and C). Experiments done by J. Strompen and M.-O. Diesner (unpublished).

3.6. Cell type analysis in *Nematostella vectensis*

To identify the cellular origin of nematocysts in *Nematostella* a qualitative cell type analysis was performed using primary polyps. The animals were macerated and cell nuclei were visualized by DAPI staining. Seven cell types could be distinguished by light microscopy

(Figure 18). Epithelial cells range from cuboidal to columnar in shape. They generally contain a few vacuoles and a visible nucleolus or densely dotted chromatin. Considering the variation in morphological appearance three types of epithelial cells were classified (Figure 18A- C): (i) the columnar epithelial cell with a length of 20- 25 µm and a width ranging from 2- 9 µm. The nucleus is round to elliptic and occupies up to 45 % of the cell body (Figure 18A). (ii) Cuboidal epithelial cells vary from 18- 25 µm in length and 15- 25 µm in width. The nucleus is centered, less dense than the ones in columnar epithelial cells, but with a visible nucleolus (Figure 18B). (iii) Endodermal epithelial cells, which are 12- 15 µm in length and 10- 14 µm in width and vary greatly in shape, ranging from columnar to elliptical. The nucleus is generally located at base of the cell (Figure 18C). The *Nematostella* tissue also contains numerous gland cells that are cylindrical in shape, 20- 25 µm long and 5- 10 µm wide, and densely packed with granules (Figure 18E). Two types of neurons could be distinguished: sensory neurons (Figure 16F) and multipolar (mainly tripolar) ganglions (Figure 18G). Their nuclei range from 8- 10 µm, the chromatin is dense and granular, and lacks a nucleolus. There is no interstitial stem cell lineage reported for *Nematostella vectensis*. Nevertheless, two types of small and seemingly undifferentiated cells were identified. Figure 18I shows an undifferentiated cell with elliptic shape ranging from 5- 7 µm in size. The second type ranged from 10- 14 µm in length and is characterized by an elongated, bent shape of the nucleus taking up most of the cell body (Figure 18H).

Nematocyte-containing cells were found frequently in macerates and represented cuboidal epithelial cells (Figure 18D and J). Mature nematocysts take up most of the cell body, the nucleus being tightly set against the capsule body.

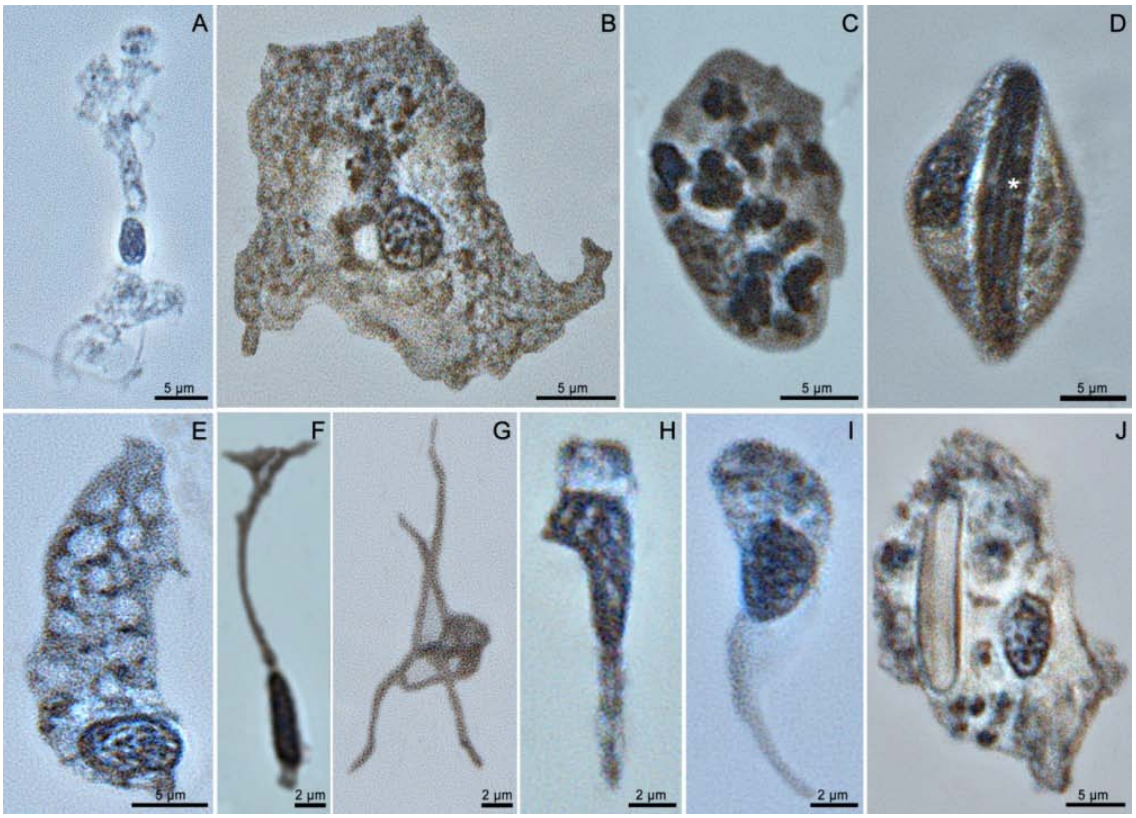

Figure 18. Cell types in *Nematostella vectensis*. A Columnar epithelial cell. B Cuboid epithelial cell. C Endodermal epithelial cell. D Nematocyte. Asterisk points at the stilette apparatus. E Gland cell with granules. F- G Neurons. F Sensory neuron. G Tripolar neuron. H Pinnochio. I Undifferentiated cells. J Cuboidal epithelial cell with nematocyte. Scale bars 5 µm (A, B, C, D, E and J) and 2 µm (F, G, H and I).

To analyze whether the composition of tissue changed during development, the different cell types were quantified (Figure 19). Like all cnidarians, *Nematostella* has an epithelial character (85.4 % in planula, 74.9 % in primary polyps and 86.5 % in adult animals). In planula larvae columnar epithelial cells clearly dominated, constituting 72.5 % of all epithelial cells, while cuboidal and endodermal epithelial cell were represented only by 15.6 % and 11.9 %, respectively. Gland cells make up 10.6 % of the planula tissue. Neurons are only represented by 1.0 %, same as pinnochio cells. The undifferentiated cells make up 2.0 % of the tissue. The composition of epithelial cells changes in primary polyps, for columnar cells now provide 40.1 % while the cuboidal type makes up 49.2 % of the tissue. The percentage of entodermal epithelial cells is the same as in planula larvae (10.7 %). Gland cells make up 8.6 %, while undifferentiated cells (6.1 %) and pinnochios (6.0 %) are equally contributed. The level of neurons is increased to 4.4 %. In adult polyps the columnar epithelial cells are most common with 45.4 %, followed by the cuboidal type with 34.1 % and

endodermal cells with 20.5 %. Gland cells make up 6.7 % of the adult *Nematostella* tissue, slightly lower than in primary polyps. Neurons keep level with 4.5 %. Undifferentiated cells make up 0.9 % of the tissue, while pinnochios provide 1.4 %.

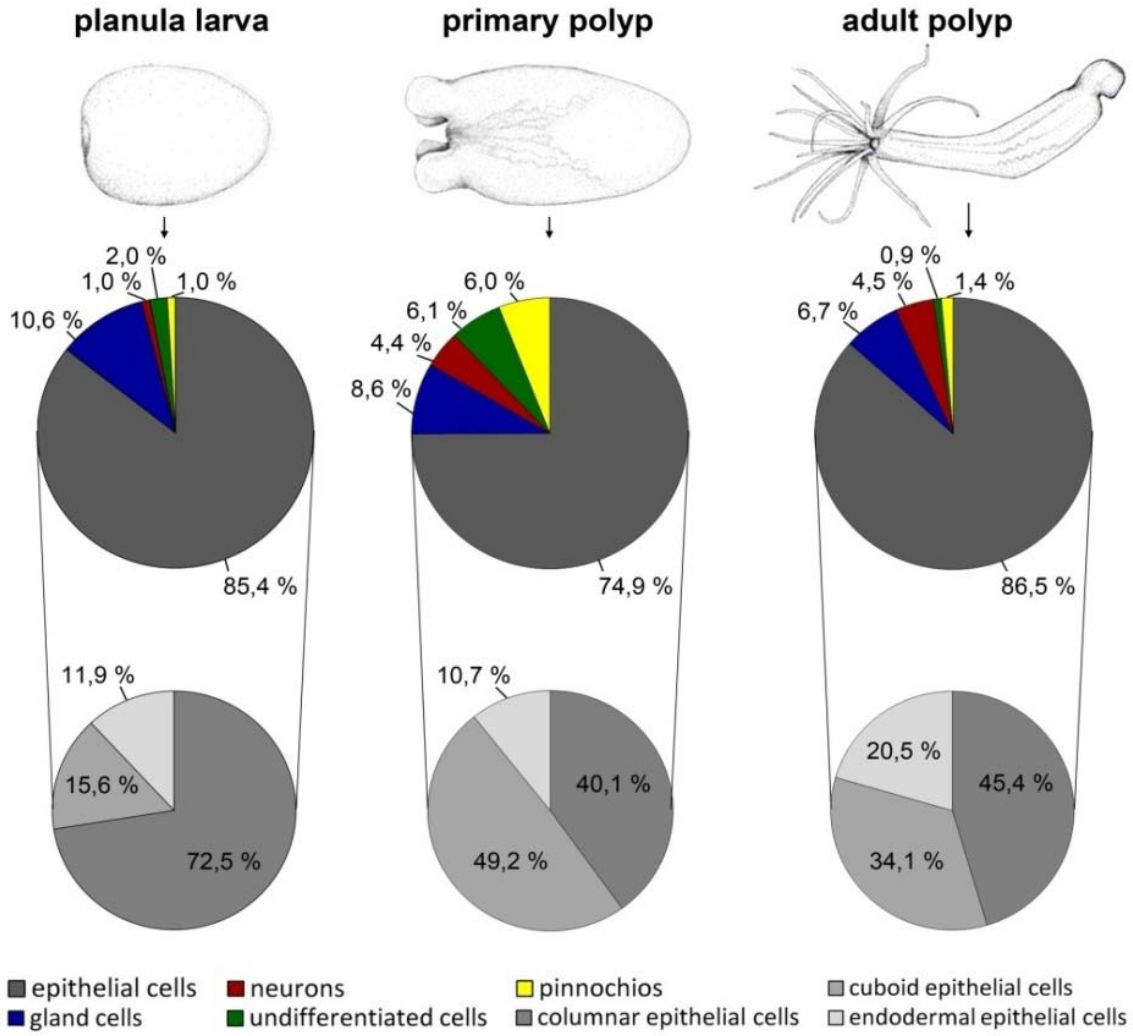

Figure 19. Quantitative distribution of cell types in *Nematostella* polyps at different developmental stages.

To analyze the nematocyst distribution in the endoderm, cryo-sections of *Nematostella* polyps were stained with minicollagen3 (NvNCol-3) antibody and analyzed using confocal and phase contrast microscopy (Figure 20). The cross section revealed that the tissue lining the distal parts of the mesenteries contains plenty of nematocysts (Figure20A, B). Of the three different types of nematocysts two could be located in the endoderm, microbasic mastigophores and basitrichous haplonema (Figure 20C, D), both in mature and immature states.

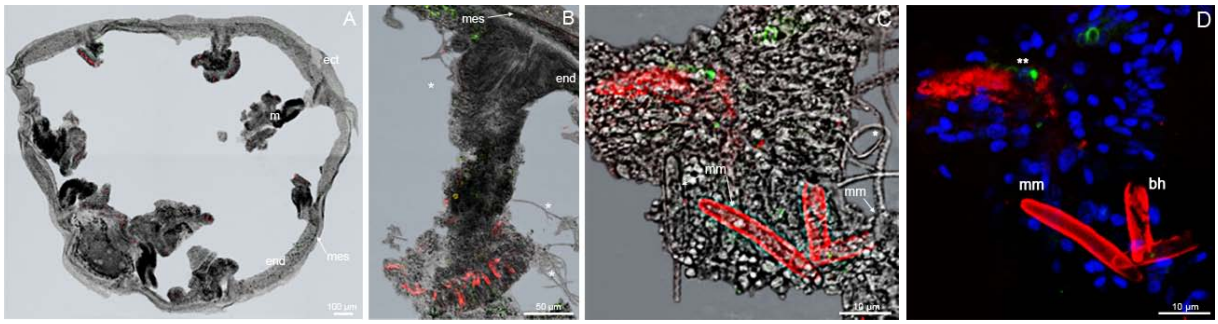

Figure 20. Nematocyst distribution in the endoderm, visualized through anti-minicollagen 3 (NvNCol-3; red) and anti-chondroitin (green) stainings in cryo-sections of adult *Nematostella*. A Cryo-section through body column. B Close up on mesentery. Asterisks point at discharged tubules. C- D Detail of a mesentery region. mm microbasic mastigophores. bh basitrichous haplonema. Opercular chondroitin signals marked by two asterisks. ect ectoderm. end endoderm. mes mesogloea. m mesentery. Scale bars are 100 µm (A), 50 µm (B) and 10 µm (C, D).

3.7. Nematocyst synthesis in cuboidal epithelial cells

To verify the cellular identity of nematocyst-synthesizing cells we stained macerates with a minicollagen-3 antibody (NvNCol-3). Minicollagen signals could be detected already at early stages of nematocyst morphogenesis in the form of vesicles that bud off from the Golgi apparatus to generate the capsule primordium (Figure21).Nematocyst synthesis was visible in all the different stages, until final maturation begins.

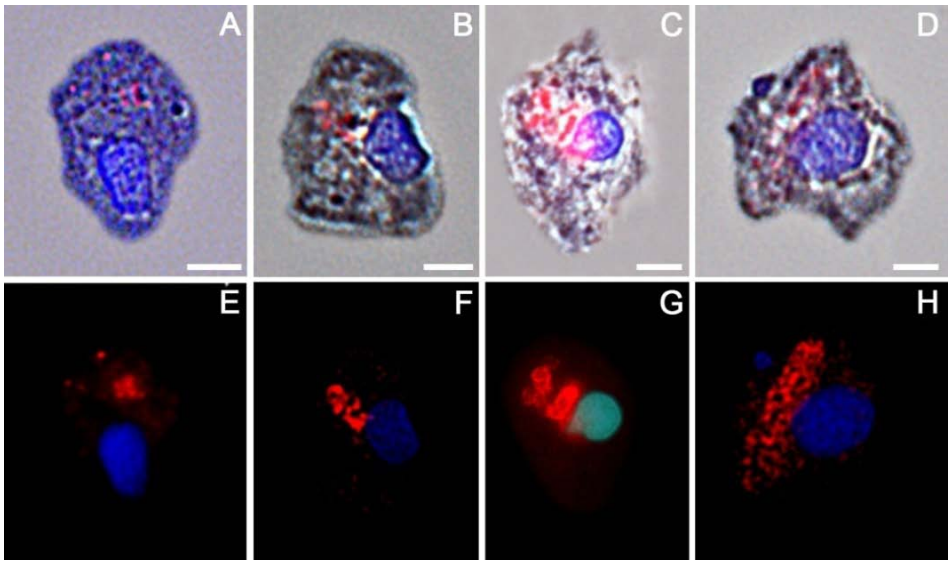

Figure 21. Capsule morphogenesis in macerated cuboidal epithelial cells. Minicollagen 3 (NvNCol-3) staining in red and nuclei visualized with DAPI. A-D Overlays of light and confocal images. Scale bars 5 µm.

Structural components of the nematocysts such as minicollagen genes are expressed in very early stages of embryogenesis (Figure 14). Nevertheless, in a time course through the development of juvenile *Nematostella*, the first functional capsules appeared 60 h post fertilization (pf) (Figure 22). The first minicollagen-positive protein vesicles appear in the nematocytes 30 h pf (Figure 22A). After 42 h the protein filled vesicles are more prominent (Figure 22B). The capsule body is filled completely with NvNCol-3 protein by 48 h pf (Figure 22C). At 54 h pf the tubule starts to elongate (Figure 22D). The final maturation and cross-linking of capsule components starts at 60 h pf (Figure 22E- F). After that, the signal is lost and the nematocyst is ready for discharge.

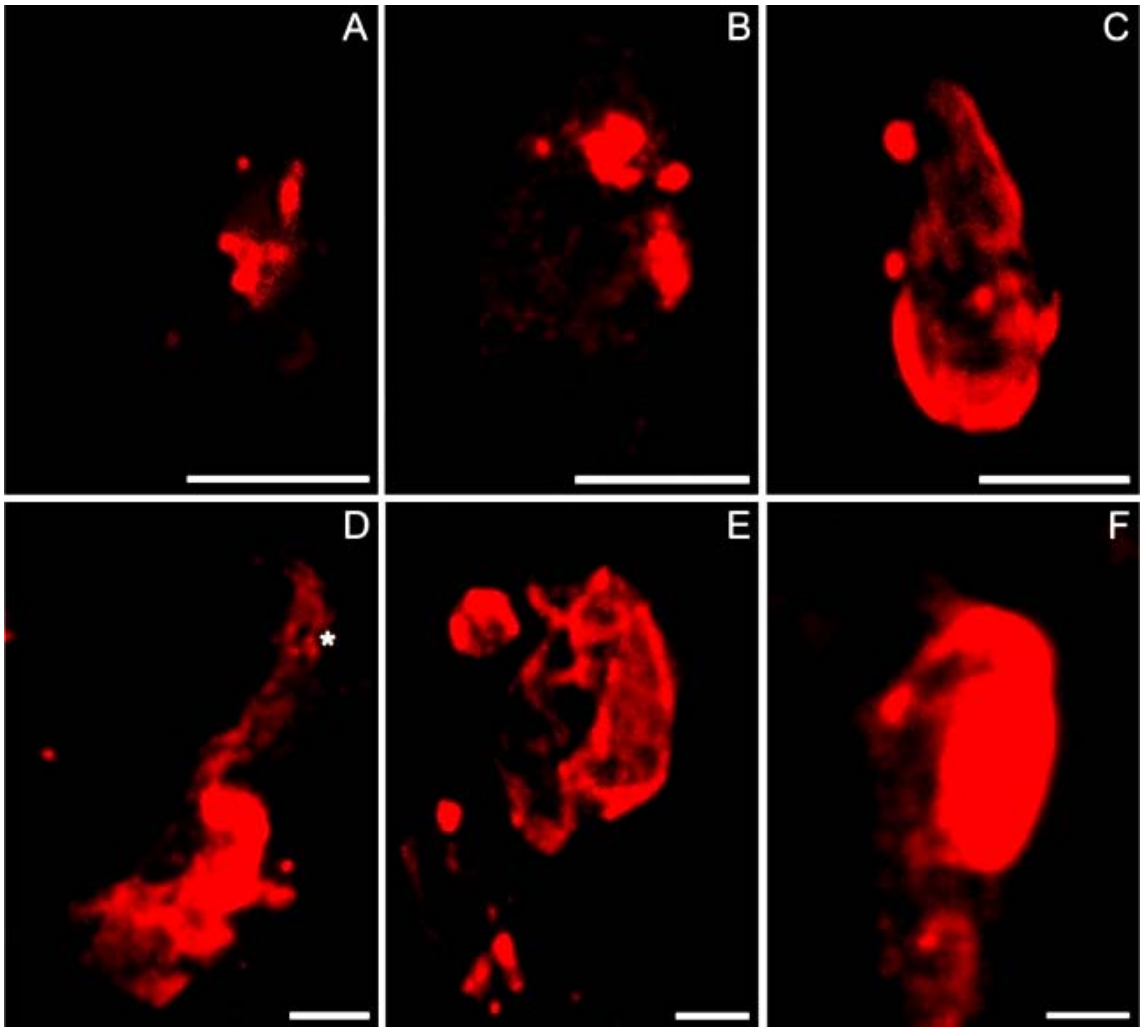

Figure 22. Antibody staining (NvNCol-3) showing nematocyst synthesis in the course of development. A 30 h post fertilization (pf): appearance of first protein vesicles. B 42 h pf: vesicles organize. C 48 h pf: vesicles produce the capsule body. D 54 h pf: once the capsule body takes shape the tubule (asterisk) starts to elongate. E- F 60 h pf: the tubule invaginates and the wall structure matures. Scale bars 5 µm.

3.8. Cell cycle kinetics of the different cell types

To evaluate the cell cycle kinetics of *Nematostella vectensis*, proliferating cells were labelled with 1 µM EdU (5 ethynyl-2' deoxyuridine) and stained with Alexa 488. EdU is a thymidine analogue and used to label cells in their S-phase (DNA replication) of the cell cycle. Afterwards the macerated tissue was analyzed using light and confocal microscopy (Nikon 80i). A labelling index was determined after one hour of EdU incubation (t0). For cuboidal epithelial cells the labelling index was 18 % (Figure 23A). Within 48 h the percentage of proliferating cells went up to 39.9 %. After 72 h of EdU incubation, 61.0 % were EdU positive. At t120, 77.2% and after 240 h, 93.6 % of all cuboidal epithelial cells were Alexa 488 positive (Figure 23A). Mature nematocysts had a labelling index of 26.9%. After 48 h of EdU incubation 35.6% of the nematocysts were EdU positive. The proliferation rate was up to 68.7% after 72 h respectively. 120 h of labelling resulted 76.6% and 240 h in 96.7% stained nuclei.

Figure 23B depicts the cell cycle kinetics of columnar and entodermal cells including their precursor cells, pinnochios and undifferentiated cells. The columnar epithelial cells and the pinnochios both have labelling indices of 13.1 %. Within 48 h the proliferation rates rise to 33.2 % (columnar) and 33.4 % (pinnochios), respectively. At 72 h 55.4 % (columnar) and 48.3 % (pinnochios), and after 120 h 70.0 % of all columnar epithelial cells and 62.5 % of all pinnochios are labelled. 240 h of EdU labelling led to 95.7 % proliferating columnar epithelial and 90.1 % pinnochio cells. Entodermal epithelial cells have a higher labelling index of 32. 1 % and the undifferentiated cells did not show any labelling after 1 h. After 48 h the entodermal cells were up to 46 % while the undifferentiated cells had a proliferation rate of 15.9 %. 72 h of EdU labelling resulted in 50.1 % entodermal and 17.4 % undifferentiated proliferating cells. After 120 h, 81.7 % of the entodermal cells and 50.5 % of the undifferentiated cells were labelled. 98.3 % of all entodermal epithelial cells and 79.4 % of all undifferentiated cells were proliferating after 240 h. Compared to *Hydra attenuata* (3 d) (David and Campbell, 1972) the cell cycle kinetics of epithelial cells in *Nematostella* take almost double the time with ~95 % labelling after 7 days.

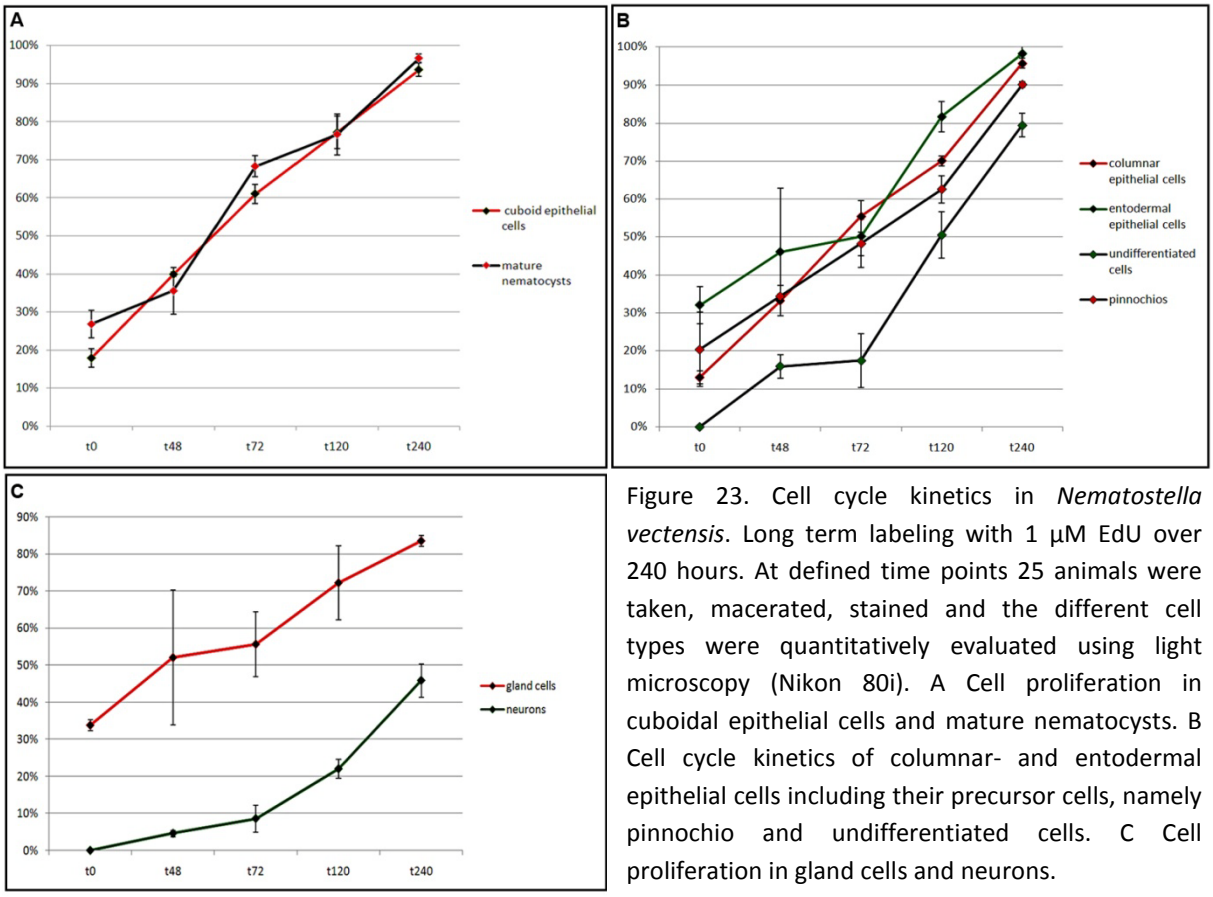

Figure 23. Cell cycle kinetics in *Nematostella vectensis*. Long term labeling with 1 µM EdU over 240 hours. At defined time points 25 animals were taken, macerated, stained and the different cell types were quantitatively evaluated using light microscopy (Nikon 80i). A Cell proliferation in cuboidal epithelial cells and mature nematocysts. B Cell cycle kinetics of columnar- and entodermal epithelial cells including their precursor cells, namely pinnochio and undifferentiated cells. C Cell proliferation in gland cells and neurons.

The cell cycle kinetics of gland cells and neurons are shown in Figure 23C. The labelling index of gland cells is 33.9 %. After 48 h and 72 h the proliferation rates are 52.1 % and 55.7 %, respectively. After 120 h 72.2 % of the gland cells are labelled. With a proliferation rate of 83.5 % after 240 h the cell cycle of gland cells is slightly slower than that of epithelial cells.

Neurons are in general very steady cells with a slower turnover rate. It is known for *Hydra attenuata* that neurons survive at least several times of tissue doubling (David and Gierer, 1974). In *Nematostella vectensis* the labelling index is 0.0 %. After 48 h 4.7 % and after 72 h 8.6 % of the neurons are proliferating. At 120 h of EdU labelling 22.1 % and finally at 240 h 45.9 % of all neurons are labelled.

Zusammenfassung

Die Cnidaria oder Nesseltiere sind die Schwestergruppe der Bilateria und stehen somit phylogenetisch an der Basis der Metazoen. Das bezeichnende Merkmal aller Cnidaria ist das Vorhandensein von Nesselkapseln oder Cniden, nesselnde Organellen, die zum Beutefang, der Verteidigung und teilweise auch zur Fortbewegung genutzt werden. Cniden oder Nematozysten bestehen aus einer zylindrischen Kapselwand, einem Schlauch mit oder ohne Dornen und einem Deckelapparat (Operculum). Spezialisierte Zellen (Nematozyten) produzieren die Organellen als Sekretionsprodukte in einem riesigen post-Golgi Vesikel. Nesselkapseln können immensem Druck standhalten und ihr Entladungsprozess ist eine der schnellsten biologischen Vorgänge im gesamten Tierreich. Die Seeanemone *Nematostella vectensis* (Anthozoa) ist in den letzten zehn Jahren neben dem Süßwasserpolypen *Hydra* (Hydrozoa) zu einem wichtigen Modellorganismus der Entwicklungs- und Evolutionsbiologie geworden. Trotz dieser Entwicklung fehlten bisher Daten zum Nematozystenrepertoire (Cnidom) und zur Identität der Nematozyten in diesem Organismus. In der vorliegenden Arbeit wurde zunächst das Cnidom von *Nematostella* morphologisch charakterisiert. Hierzu wurde ein Isolierungsverfahren für intakte Nematozysten aus Gewebe etabliert und lichtmikroskopische sowie elektronenmikroskopische Techniken zu deren Analyse eingesetzt. Die identifizierten drei Kapseltypen (basitriche Haplonemen, mikrobasische Mastigophoren und Spirocysten) wurden quantitativ entlang der Körperachse adulter Tiere und in verschiedenen Entwicklungsstadien erfasst. Neben der morphologischen Charakterisierung wurden Minikollagene als molekulare Komponenten der Nesselkapseln isoliert und deren Expressionsmuster durch ISH-Experimente (in *situ* Hybridisierung) beschrieben. Immunohistochemische Färbungen mit spezifischen Antikörpern zeigten teilweise abundante und zum Teil eine kapselspezifische Verteilung von Minikollagenen. Als schlauchspezifischer Marker wurde zudem ein nicht-sulfatiertes Chondroitin in Nematozyten nachgewiesen.

Der zweite Teil der Arbeit war auf die zelluläre Identifizierung von Nematozyten in *Nematostella* fokussiert. Hierzu wurden zunächst alle Zelltypen qualitativ charakterisiert und einer Zellzyklusanalyse unterworfen. Kapselsynthetisierende Zellen konnten dann mit Hilfe von Minikollagenfärbungen in Mazeraten als kuboidale Epithelzellen identifiziert werden. Im

Unterschied zu Hydra gehen Nematozysten demnach nicht aus einer speziellen Stammzellpopulation hervor und haben einen epithelialen und nicht neuronalen Ursprung.

5. References

Adamczyk P, Meier S, Gross T, Hobmayer B, Grzesiek S (2008): Minicollagen-15, a novel minicollagen isolated from *Hydra*, forms tubule structures in nematocysts. *J Mol Biol 376: 1008- 1020*.

Anderson PAV, Bouchard C (2009): Regulation of cnidocyte discharge. *Toxicon 54, 1046-1053*.

Chapman JA, Kirkness EF, Simakov O, Hampson SE, Mitros T, Weinmaler T, Rattel T, Balasubramanian PG, Borman J, Busam D et al. (2010): The dynamic genome of *Hydra*. *Nature 464, 592-596*.

Carlgren O (1940): A contribution to the knowledge of the structure and distribution of the cnidae in Anthozoa. *Lunds. Univ.'s Årskrift, 36: 1- 62*.

Carlgren O (1940): Further contributions to the knowledge of the cnidom of the cnidae in the Anthozoa especially in the Actinaria. *Lunds. Univ.'s Årskrift, 41 (9): 1- 24*.

Cartwright P, Halgedahl SL, Hendricks JR, Jarrard RD, Marques AC, Collins AG and Lieberman BS (2007): Exceptionally preserved jellyfishes from the Middle Cambrian. *PLoS One 2, e1121*.

Darling JA, Reitzel AR, Burton PM, Mazza ME, Ryan JF, Sullivan JC, Finnerty JR (2005): Rising starlet: the starlet sea anemone, *Nematostella vectensis*. *BioEssays 27:211- 221*.

David CN, Campbell RD (1972): Cell cycle kinetics and development of *Hydra attenuata*: I. Epithelial Cells. *J Cell Sci 11(2): 557-568*.

David CN, Gierer A (1974): Cell cycle kinetics and development of *Hydra attenuata*: II. Nerve cell and nematocyst differentiation. *J. Cell Sci 16(2): 349- 358*.

David CN, Murphy S (1977): Characterization of interstitial stem cells in hydra by cloning. *Dev. Biol. 58, 372- 383*.

David CN, Özbek S, Adamczyk P, Meier S, Pauly B (2008): Evolution of complex structures: minicollagens shape the cnidarian nematocyst. *Trends Genet 24: 431- 438*.

Exposito JY, Cluzel C, Garrone R, Lethias C (2002): Evolution of Collagens. *Anat Rec 268(3): 302- 316*.

Fernandez JM et al. (1991): Reversible condensation of mast cell secretory products in vitro. *Biophys. J. 59, 1022- 1027*.

Fransson LA (1985): Mammalian glycosaminoglycans. *Aspinall GO Editor. The Polysaccharides (NY). Academic Press Vol. 3 pp. 337- 415*.

Godknecht A, Tardent P (1988): Discharge and mode of action of the tentacular nematocysts of *Anemonia sulcata* (Anthozoa: Cnidaria). *Mar. Biol. (Berlin) 100, 83- 92*.

Holstein T (1981): The morphogenesis of nematocytes in Hydra and Forskålia: an ultrastructural study. *J. Ultrastruct. Res. 75, 276- 290*.

Holstein T, Tardent P (1984): An ultrahigh-speed analysis of exocytosis: nematocyst discharge. *Science 223, 830- 833*.

Kass-Simon G, Scappaticci JAA (2002): The behavioral and developmental physiology of nematocysts. *Can J Zool 80: 1772- 1794*.

Kjellén L, Lindahl U. (1991): Proteoglycans: structures and interactions. *Annu Rev Biochem. 60: 443- 475*.

Kurz EM, Holstein TW, Petri BM, Engel J, David CN (1991): Mini-collagens in *Hydra* nematocytes. *J Cell Biol. 115(4): 1159- 1169*.

Mariscal RN (1974): Scanning electron microscopy of the sensory surface of the tentacles of sea anemones and corals. *Zellforsch Mikrosk Anat, 147 (2): 149- 56*.

Mariscal RN, McLean RB, Hand C (1977): The form and function of cnidarian spirocysts. 3. Ultrastructure of the thread and the function of spirocysts. *Cell Tissue Res 178(4): 427- 33*.

Meier S, Jensen PR, David CN, Chapman J, Holstein TW, et al. (2007): Continuous molecular evolution of protein-domain structures by single amino acid changes. *Curr Biol 17: 173- 178*.

Nüchter T, Benoit M, Engel U, Özbek S, Holstein T (2006): Nanosecond-scale kinetics of nematocysts discharge. *Curr Biol. 16(9): R316- 8*.

Özbek S, Pertz O, Schwagert M, Lustig A, Holstein T (2002): Structure/function relationships in the minicollagen of *Hydra* nematocysts. *J Biol Chem 277(51): 49200- 49204*.

Özbek S, Balasubramanian PG, Holstein TW (2009): Cnidocyst structure and the biomechanics of discharge. *Toxicon 54, 1038- 1045*.

Özbek S (2010): The cnidarian nematocyst: a miniature extracellular matrix within a secretory vesicle. *Protoplasma*.

Parpura V, Fernandez JM (1996): Atomic force microscopy study of the secretory granule lumen. *Biophys. J. 71, 2356-2366*.

Putnam NH, Srivastava M, Hellsten U, Dirks B, Chapman J, Salamov A, Terry A, Shapiro H, Lindquist E, Kapitonov VV et al. (2007): Sea anemone genome reveals ancestral eumetazoan gene repertoire an genomic organization. *Science 317, 86- 94*.

Robson EA (1972): The discharge of nematocysts in relation to properties of the capsule. *Publ. Seto Mar. Biol. Lab, 653- 673*.

Schmidt H (1969): Die Nesselkapseln der Aktinien und ihre differentialdiagnostische Bedeutung. *Helgoländer wiss. Meeresunters., 19: 284- 317*.

Schmidt H (1972): Die Nesselkapseln der Anthozoa und ihre Bedeutung für die phylogenetische Systematik. *Helgoländer wiss. Meeresunters., 23: 422- 458*.

Skaer RJ (1973): The Secretion and Development of Nematocysts in a Siphonophore. *J. Cell. Sci. 13, 371-393*.

Slautterback DB, Fawcett DW (1958): The development of the cnidoblasts of Hydra; an electron microscope study of cell differentiation. *J. Biophys. Biochem. Cytol. 5, 441- 452*.

Sugahara K, Mikami T, Uyama T, Mizuguchi S, Nomura K, Kitagawa H (2003): Recent advances in the structural biology of chondroitin sulfate and dermatan sulfate. *Curr Opin Struct Biol. 13:612- 620*.

Tardent P, Holstein T (1982): Morphology and morphodynamics of the stenotele nematocyst of *Hydra attenuata* Pall. *Cell Tissue Res 224 (2): 269- 90*.

Technau U, Steele RE (2011): Evolutionary crossroads in developmental biology: Cnidaria. *Development 138, 1447- 1458.*

Weill R (1934): Contribution a l'etude des cnidaires et de leurs nematocystes. I. Recherches sur les nematocystes (Morphologie, Physiologie Developpement). *Trav. Pp 1-347.*

Werner B (1965): Die Nesselkapseln der Cnidaria, mit besonderer Berücksichtigung der Hydroida. I. Klassifikation und Bedeutung für die Systematik und Evolution. *Helgoland Marine Research Volume 12, Numbers 1- 2: 1- 39*.

Wood RL, Novak PL (1982): The anchoring of nematocysts and nematocytes in the tentacles of Hydra. *J. Ultrastruct. Res. 81, 104- 116*.

Yamada S, Morimoto H, Fujisawa T, Sugahara K (2007): Glycosaminoglycans in *Hydra magnipapillata* (Hydrozoa, Cnidaria): demonstration of chondroitin in the developing nematocyst, the sting organelle, and structural characterization of glycosaminoglycans. *Glycobiology, 17(8), 886- 94*.

THE JOURNAL OF BIOLOGICAL CHEMISTRY VOL. 285, NO. 33, pp. 25613–25623, August 13, 2010

A Non-sulfated Chondroitin Stabilizes Membrane Tubulation in Cnidarian Organelles*

Received for publication, January 26, 2010, and in revised form, May 27, 2010 Published, JBC Papers in Press, June 9, 2010, DOI 10.1074/jbc.M110.107904

Patrizia Adamczyk[‡], Claudia Zenkert[‡], Prakash G. Balasubramanian[‡], Shuhei Yamada[§], Saori Murakoshi[§], Kazuyuki Sugahara[§1], Jung Shan Hwang[¶], Takashi Gojobori[¶], Thomas W. Holstein[‡], and Suat Özbek[‡2]

From the [‡]Institute of Zoology, Department of Molecular Evolution and Genomics, Heidelberg University, Im Neuenheimer Feld 230, 69120 Heidelberg, Germany, the [§]Laboratory of Proteoglycan Signaling and Therapeutics, Faculty of Advanced Life Science, Graduate School of Life Science, Hokkaido University, Sapporo 001-0021, Japan, and the [¶]Center for Information Biology and DNA Data Bank of Japan, National Institute of Genetics, Mishima, Shizuoka 411-8540, Japan

Membrane tubulation is generally associated with rearrangements of the cytoskeleton and other cytoplasmic factors. Little is known about the contribution of extracellular matrix components to this process. Here, we demonstrate an essential role of proteoglycans in the tubulation of the cnidarian nematocyst vesicle. The morphogenesis of this extrusive organelle takes place inside a giant post-Golgi vesicle, which topologically represents extracellular space. This process includes the formation of a complex collagenous capsule structure that elongates into a long tubule, which invaginates after its completion. We show that a non-sulfated chondroitin appears as a scaffold in early morphogenesis of all nematocyst types in *Hydra* and *Nematostella*. It accompanies the tubulation of the vesicle membrane forming a provisional tubule structure, which after invagination matures by collagen incorporation. Inhibition of chondroitin synthesis by β-xylosides arrests nematocyst morphogenesis at different stages of tubule outgrowth resulting in retention of tubule material and a depletion of mature capsules in the tentacles of hydra. Our data suggest a conserved role of proteoglycans in the stabilization of a membrane protrusion as an essential step in organelle morphogenesis.

A key step in the dynamic remodeling of plasma membranes during tubulation processes are localized invaginations. These are controlled mostly by cytoskeletal rearrangements and specific intracellular proteins like BAR domain proteins able to impose membrane curvature through direct surface interactions (1). Such membrane protrusions are reversible in most cases, and there are only few examples in which these structures are fixed by a molecular scaffold of extracellular matrix (ECM)[3] components. Here, we present the contribution of a chondroitin-rich structure to the formation of a tubular membrane structure during organelle morphogenesis in a basal metazoan. Nematocysts (cnidocysts) are the characteristic stinging organelles of the phylum Cnidaria, involved in prey capture, defense, and locomotion. They are produced as a secretory product in specialized neuronal cells named nematocytes (cnidocytes) (2–4). In the fresh water polyp *Hydra* four types of nematocytes can be distinguished based on the distinct morphology of their capsules: stenoteles, desmonemes, holotrichous, and atrichous isorhizas (5–7). During differentiation, which occurs exclusively in the body column, the nematocytes undergo several rounds of synchronous cell divisions (8, 9) and remain connected to each other by cytoplasmic bridges to form clusters or nests (10, 11) (Fig. 1*B*). After differentiation, these nests break up and the single cells migrate to the tentacles, where they become mounted in specialized epithelial cells, the battery cells. The nematocysts are produced inside a giant post-Golgi vesicle of the nematocyte (11–13) (Fig. 1, *A–C*). The pre-capsule forms and grows by addition of more vesicles from the trans-Golgi network (TGN). Also, the tubule grows externally by fusion of additional secretory vesicles before it invaginates into the capsule matrix (11) (Fig. 1, *D* and *E*).

Proteoglycans (PGs) are major components of the extracellular matrix and consist of core proteins, to which chains of complex glycosaminoglycans (GAGs) are covalently attached. GAGs are known to participate in many biological processes like signaling, cell adhesion, infection of pathogens, brain development, modulation of enzymes, cytokines, and growth factors (14, 15). In a recent publication, Yamada *et al.* (16) characterized GAGs in *Hydra magnipapillata* and demonstrated by immunostainings that the epitope of the anti-chondroitin antibody 473A12 is present in developing nematocysts, though the precise role of this nematocyst-specific chondroitin remained unclear. Here, we demonstrate that this chondroitin forms the outer layer of the developing nematocyst tubule, both in *Hydra* and the sea anemone *Nematostella vectensis*. Inhibition of GAG synthesis leads to a disordered development of all four nematocyst types in *Hydra* emphasizing the essential role of chondroitin in this

* This work was supported by a grant from the German Science Foundation (Deutsche Forschungsgemeinschaft) (to S. Ö. and T. W. H.) and in part by Grants-in-aid for Scientific Research (B) (20390019) from the Ministry of Education, Culture, Sports, Science, and Technology of Japan (MEXT) (to K. S.).

[1] To whom correspondence may be addressed: Faculty of Advanced Life Science, Hokkaido University, Nishi 11-choume, Kita 21-jo, Kita-ku, Sapporo, Hokkaido 001-0021, Japan. Tel.: 81-11-706-9054; Fax: 81-11-706-9056; E-mail: k-sugar@sci.hokudai.ac.jp.

[2] To whom correspondence may be addressed. Tel.: 496221545638; Fax: 496221545678; E-mail: soezbek@zoo.uni-heidelberg.de.

[3] The abbreviations used are: ECM, extracellular matrix; TGN, trans-Golgi network; GAG, glycosaminoglycan; PNN, perineuronal net; TEM, transmission electron microscopy; CS, chondroitin sulfate; PG, proteoglycan; BSA, bovine serum albumin; PBS, phosphate-buffered saline; 2AB, 2-aminobenzamide.

process. Our data on this unusual cnidarian neuronal cell type have also implications on the evolution of the neuronal extracellular matrix, in particular the perineuronal net (PNN), which is of neuronal origin. In the PNN chondroitin PGs form together with polymeric hyaluronic acid a meshwork required for synapse development and function (17).

EXPERIMENTAL PROCEDURES

Animals—*H. magnipapillata* or *N. vectensis* were used for all experiments. Hydra animals were cultured in *Hydra* medium (18) at 18 °C and fed three to five times a week with *Artemia nauplii*. Animals used for experiments were starved for 24 h. *Nematostella* were cultured in 1/3 artificial seawater (Tropic Marin) pH 7.5–8.0 at 18 °C in the dark and fed 1–2 times a week with *A. nauplii*.

Preparation of GAGs from Isolated Hydra Nematocysts—GAGs were prepared as described previously (16). Isolated capsules were dried and digested with actinase E at 60 °C for 2 days. The samples were treated with 5% trichloroacetic acid (TCA) to remove proteins and peptides, and then the TCA was removed from the supernatant by extraction with diethylether, followed by a treatment with 80% ethanol to precipitate polysaccharides, which were reconstituted in H_2O. To remove salt and low molecular weight contaminants, the sample was subjected to gel filtration on a Superdex peptide column (Amersham Biosciences), and the flow-through fraction was collected.

Gel Filtration Chromatography of the GAG Preparation—To determine the molecular size of the components in the GAG preparation, gel filtration chromatography was performed on a Superdex 200 column (Amersham Biosciences) (flow rate, 0.3 ml/min), and fractions were collected at 4-min intervals (16). The samples were digested with a mixture of chondroitinases AC-I, AC-II, and ABC, and derivatized with a fluorophore 2-aminobenzamide (2AB), followed by the removal of the excess derivatization reagents by chloroform extraction and anion-exchange HPLC analysis on an amine-bound silica column (19).

Analysis of the Reducing Terminal Structure of the Hydra Chondroitin Chains—To examine whether the chondroitin chains are assembled on a core protein through the common linkage structure, the reducing terminal sugar residue of the GAG preparation was labeled with 2AB before or after LiOH treatment (20), which liberates GAG chains from core proteins. The 2AB-derivative of the *Hydra* GAG preparation was digested with a mixture of chondroitinases AC-I, AC-II, and ABC, and analyzed by anion-exchange HPLC on an amine-bound silica column (19).

Investigation of the Reactivity of 473A12 toward Various GAG Variants—Biotinylated GAG (0.5 μg each) were immobilized on a streptavidin-coated plate in phosphate-buffered saline (PBS) at room temperature overnight. Blocking reaction was performed using 3% BSA/PBS for 1 h at 37 °C. The antibody 473A12 was diluted 1000-fold with 0.1% BSA/PBS and then added to the plate. After incubation for 2 h at 37 °C, the plate was washed with Tris-buffered saline (TBS) containing 0.05% Tween 20 three times. The reactivity of the antibody was evaluated by incubation with the secondary antibody, alkaline phosphatase-conjugated goat-anti mouse IgA (3000-fold dilution with 0.1% BSA/TBS), followed by plate development with disodium *p*-nitrophenyl phosphate.

β-D-Xyloside Treatment—Animals were cultured in *Hydra* medium in the presence of 2 mM *p*-nitrophenyl-β-D-xylopyranoside, for at least 17 days. The concentration applied was chosen to have a maximal effect on nematocyst morphogenesis without affecting tissue integrity as deduced in preliminary experiments. Animals were fed during the first days of treatment until tentacles lacked of mature nematocysts and were not able to catch artemias anymore. The β-D-xylopyranoside was renewed periodically every 3 days with each *Hydra* medium change.

Immunofluorescence—For immunostainings with polyclonal rabbit antibodies NCol-15 (21), NCol-1 (22) and polyclonal rat nematogalectin antibody[4] as well as with the monoclonal chondroitin antibody (Seikagaku Corp.) hydra animals were relaxed in 2% urethane in *Hydra* medium for 1 min and fixed in Lavdovsky's fixative for at least 12 h (23). For co-immunostainings with the polyclonal guinea pig anti-NCol-1 propeptide antibody animals were fixed in 4% PFA in *Hydra* medium. After several washing steps using PBS/0.1% Triton X-100, the polyps were incubated overnight at 4 °C with primary antibody (diluted in PBS/0.1% BSA). Animals were washed several times with PBS and incubated for 1–2 h with adequate secondary antibody coupled to ALEXA fluorochrome (Molecular Probes) at 1:400 in PBS/0.1% BSA. Animals were washed again several times in PBS before mounting on object slides in PBS/glycerol (1:9).

Microscopy—Fluorescence images were captured with the Nikon Eclipse 80i, confocal images with the Nikon A1R laser scanning microscope. Conventional transmission electron microscopy (TEM) of *Hydra vulgaris* was performed as described (11).

Image Processing—Image deconvolution was performed using Huygens Software (Scientific Volume Imaging) at the Nikon Imaging Center at the University of Heidelberg. Image processing was performed by using ImageJ and Adobe Photoshop CS3.

RESULTS

Localization of Chondroitin during Nematocyst Development—To visualize the steps of membrane tubulation, tubule outgrowth and invagination during nematocyst morphogenesis we performed TEM of nematocyst vesicle and tubule cross-sections (Fig. 1, *C–E*). Fig. 1*B* shows a light microscopic overview of a nematocyte nest at an early stage in which the nematocyst vesicle is visible in the cytoplasm of the nematocyte. Membrane tubulation is later initiated at a position where the pre-formed capsule wall structure is recessed (Fig. 1*C*). During outgrowth, the tubule membrane is lined with a thin electron-dense layer on the inside surface, which reaches up to the tip region supported by microtubules (Fig. 1*D*, *inset* in *E*). The lumen of the tubule is filled with granular material delivered by TGN vesicles. The invagination process is marked by a twisted and very condensed structure reaching into the capsule lumen (Fig. 1*E*). To demonstrate a detailed localization of chondroitin during

[4] J. S. Hwang, unpublished data.

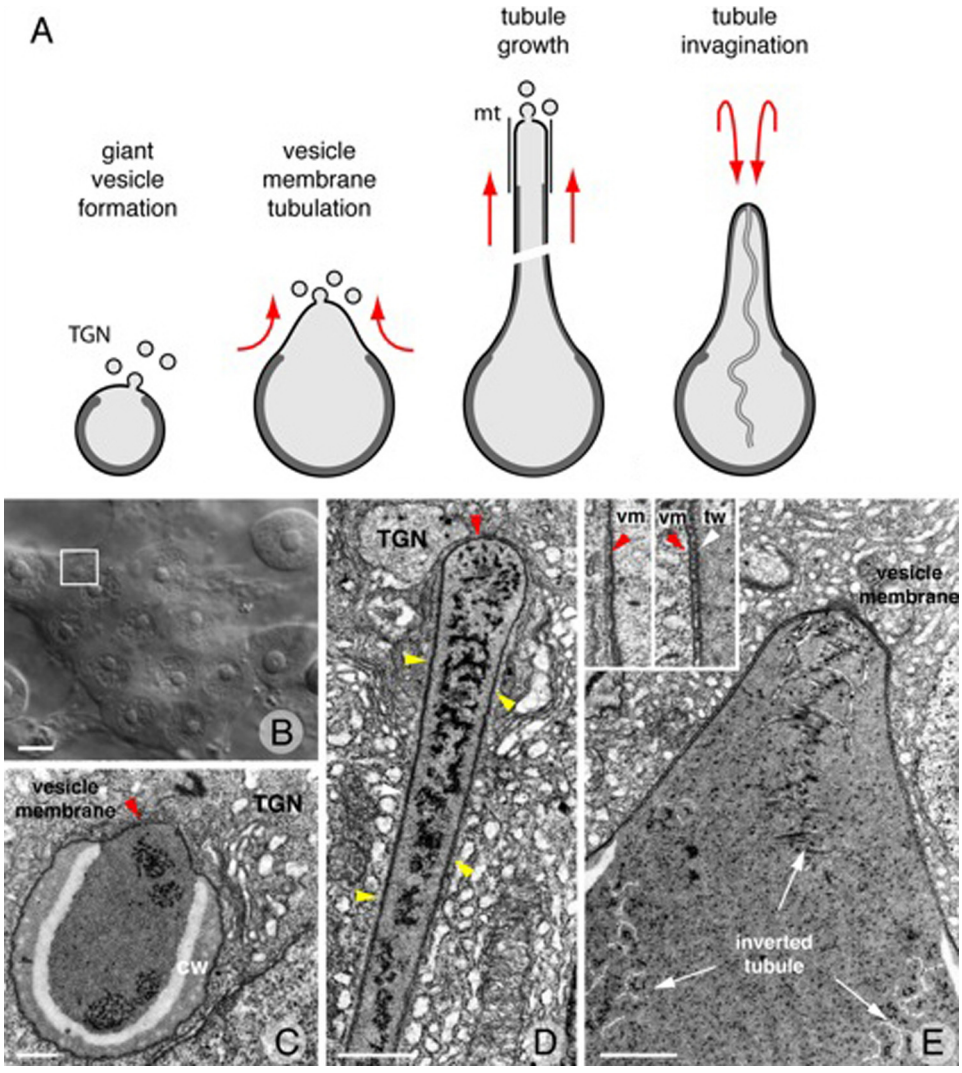

FIGURE 1. **Tubulation during nematocyst morphogenesis illustrated by thin sections.** *A*, schematic representation of nematocyst morphogenesis. *B*, differential interference contrast image of nematocyst nest at early stage. The nematocyst vesicle is visible as a rounded vesicle (*box*) in the cytoplasm of the nematocyte. *Scale bar*, 2 mm. *C*, onset of vesicle membrane tubulation (*arrow*). A premature capsule wall (*cw*) is lining the inner surface of the nematocyst vesicle. The area of tubule outgrowth adjacent to the TGN is free of capsule wall material. *D*, growing tubule is stabilized by microtubules at the cytoplasmic surface (*yellow arrows*). The tubule tip is closed by the vesicle membrane only (*red arrow*) whereas the tubule wall shows an additional inner layer (see also *inset* in *E*). *E*, tubule invagination. Cross sections of the invaginated and coiled tubule inside the vesicle matrix are marked by *arrows*. The *inset* shows the vesicle membrane at the tubule tip and the double-layered tubule with an inner tubule wall (*tw*) along the shaft. *TGN*, trans-Golgi network, *mt*, microtubules. *Scale bars*, 1 μm.

nematocyst development, immunostaining of *H. magnipapillata* was carried out using the commercial anti-chondroitin antibody 473A12 (16). In whole mount immunostainings, the chondroitin signal was detected in nests of all differentiating nematocyte types in the body column of *Hydra* (Fig. 2, *A* and *B*). Costainings performed with the *Hydra* minicollagen-1 (NCol-1) antibody demonstrated a clear restriction of the chondroitin signal to the tubule structures of the growing vesicles (Fig. 2*B*′). NCol-1 is deposited into the capsule wall of the developing nematocyst and therefore marks the capsule body inside the vesicle. The chondroitin signal initially appears as a vesicular structure around the tip of the outer growing tubule in early morphogenetic stages arguing for a close correlation with the onset of tubule growth (Fig. 2, *C* and *D*). During morphogenesis the staining pattern follows the growing tubule structure thereby covering it like a sheath or scaffold (Fig. 2, *E–H*). In the large stenoteles the tubule appears to be untensioned and large in diameter at the beginning of growth (Fig. 2, *E* and *F*) before it compacts to a more narrow structure, whereas in isorhizas the tubule keeps a constant diameter (Fig. 2, *G* and *H*). At later stages the chondroitin staining marks the invagination process of the tubule with a thin thread-like structure coiling inside the capsule matrix while the rest of the tubule is still outside showing an increased signal due to the doubled tubule wall (Fig. 2, *I* and *J*). After invagination the tubule is coiled completely inside the capsule matrix in a highly ordered configuration (Fig. 2, *K* and *L*). At this developmental stage chondroitin is also present at the emerging operculum (see *arrows* in Fig. 2*L*), and while the tubule signal disappears after maturation and wall hardening, the operculum staining persists in mature stenoteles in the tentacle region (data not shown). In anti-chondroitin stainings performed with the anthozoan *N. vectensis* also developing tubule structures were detected in the tentacle bulb (Fig. 2, *M* and *N*) arguing for a high conservation of the chondroitin function in developing nematocysts of cnidarians.

Analysis of GAGs in Hydra Nematocysts—To analyze the molecular composition of the GAG structure, nematocyst capsules were isolated from *Hydra* tissue and after solubilization the sample was treated with chondroitinase ABC. The obtained fragments were subjected to HPLC. Non-sulfated chondroitin was the major component of the isolated capsules (data not shown). Neither sulfated disaccharide units derived from chondroitin sulfate (CS) nor heparan sulfate disaccharides, if any, were detected due to their limited amounts. The molecular size of the chondroitin chains in nematocysts of *Hydra* was analyzed by gel filtration chromatography (Fig. 3*A*). Two major peaks were observed, and the average molecular sizes of these peaks were estimated to be ~90 and 40 kDa, respectively.

The chondroitin chains were subjected to derivatization with 2AB before and after treatment with mild alkali, which liberates GAG chains from core proteins. After removal of the excess 2AB reagent, the samples were digested with a mixture of chon-

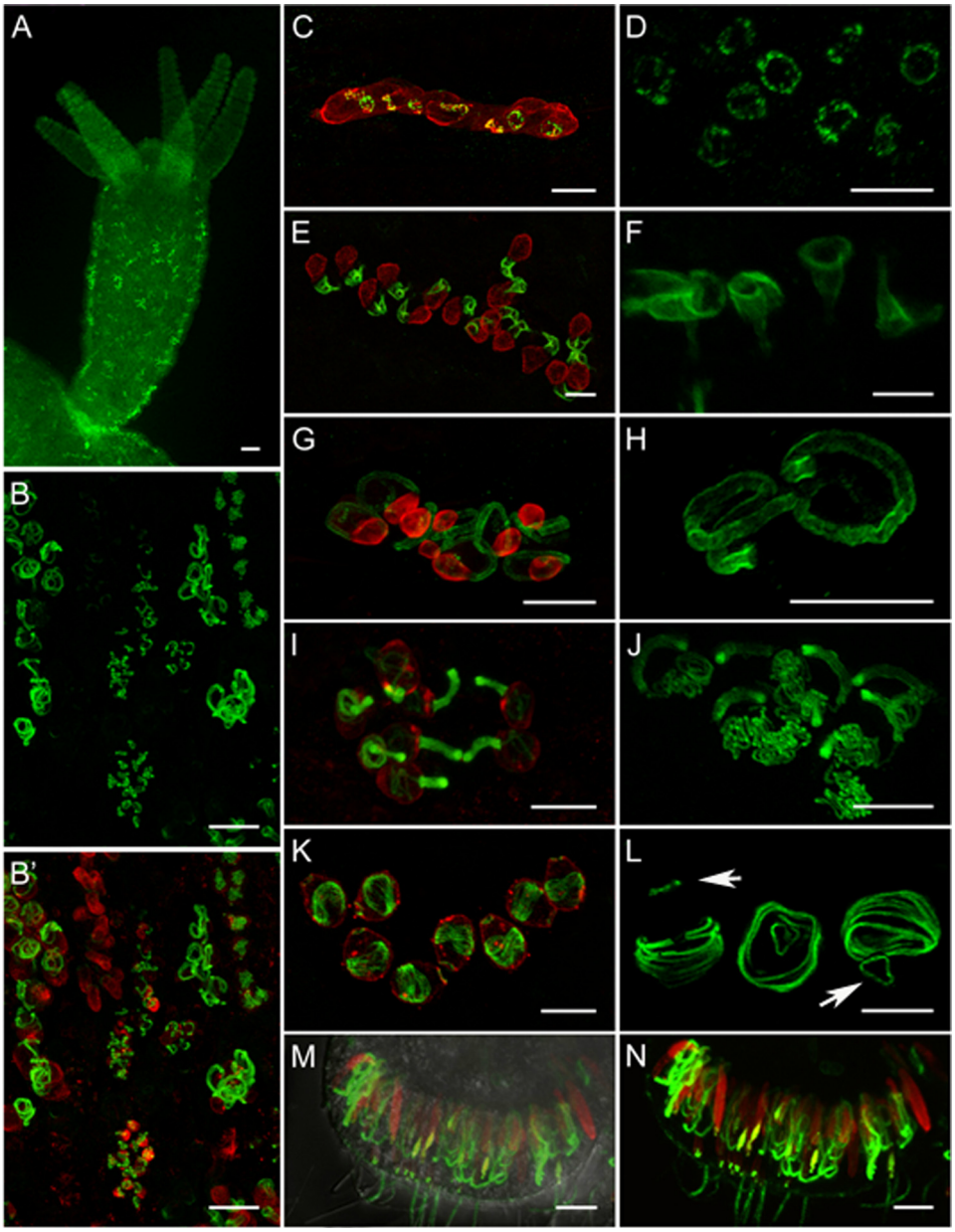

FIGURE 2. **Immunocytochemical detection of chondroitin in *Hydra* and *Nematostella* whole mounts.** To present a more comprehensible view, some images show co-immunostainings with anti-NCol-1, which stains the capsule body (*red signals*). *A–N*, whole mounts of *H. magnipapillata* (*A–L*) or primary polyps of *N. vectensis* (*M–N*) were incubated with anti-chondroitin antibody and Alexa 488 as secondary antibody (*A*, *D*, *F*, *H*, *J*, *L*), followed by incubation with anti-NCol-1 antibody and Alexa 568 as second secondary antibody (*B*, *C*, *E*, *G*, *I*, *K*, *M*, *N*). *A*, whole mount of *Hydra*. *Scale bar*, 50 μm. *B-B'*, nests of differentiating nematocytes in the gastric region of *Hydra*. *Scale bar*, 20 μm. *C–L*, close-up view of differentiating *Hydra* nematocytes at different morphological stages stained with anti-chondroitin antibody. *C*, *E*, *G*, *I*, and *K* show co-immunostainings of developing nests with anti-NCol-1. *D*, *F*, *H*, *J*, and *L* show enlarged chondroitin immunostainings at similar developmental stages. Each *scale bar* represents 10 μm. *M* and *N*, co-immunostained (anti-NCol-1 and anti-chondroitin) nematocytes in *Nematostella* in the tentacle bulb of a primary polyp with (*M*) and without (*N*) differential interference contrast DIC image overlay. *Scale bars*, 5 μm.

droitinases ABC, AC-I, and AC-II, resulting in the 2AB-oligosaccharides derived from the reducing terminus of the chondroitin chains. Each digest was analyzed by HPLC on an amine-bound silica PA-03 column. As shown in the *upper panel* of Fig. 3*B*, 2AB-labeled oligosaccharides were detected without alkali treatment, suggesting that the reducing terminal sugar residues of the chondroitin chains had a free aldehyde group even before treatment with alkali and that free chondroitin chains are present in nematocysts. Although peaks were detected at the positions of authentic unsaturated disaccharide standards, ΔHexUA-GalNAc(6-sulfate) and ΔHexUA-GalNAc(4-sulfate), the structure of the 2AB-oligosaccharides derived from the reducing end could not be determined due to the limited amount, as a single GAG chain consisting of ~100 or 225 disaccharide units contains only one mole of the reducing terminus per mole. Because additional peaks were detected after treatment with LiOH (*lower panel* in Fig. 3*B*), chondroitin chains in nematocysts may be present as chondroitin PGs as well as free GAG chains. To characterize the core protein of the chondroitin PG, *Hydra* nematocysts were treated with 4 M guanidine-HCl, and the purified PG fraction was subjected to Western blotting after digestion with chondroitinases using anti-unsaturated hexuronic acid antibody (chondroitin stub antibody), which recognizes the chondroitin stubs generated by digestion with bacterial chondroitinases. However, specific bands could not be detected (results not shown). We concluded that the amount of the core protein (PG) in the nematocyst sample might be too little to be detected by Western blotting under the conditions used. Alternatively, the chondroitin chains in the sample might be resistant to chondroitinase ABC because of its tight binding to some other components such as minicollagen. To investigate the reactivity of the applied chondroitin antibody, we performed an ELISA experiment using different GAGs as antigens. As shown in Fig. 3*C*, the 473A12 antibody recognized in this assay exclusively chondroitin and not chondroitin sulfate or other GAGs, confirming the GAG analysis for isolated nematocysts.

Chondroitin and Minicollagen-1 Take Separate Secretory Routes in the trans-Golgi Network—To mark the TGN at the tip of the growing tubule we produced a polyclonal antibody against the NCol-1 propeptide, which is cleaved shortly before the mature protein enters the nematocyst vesicle (Fig. 4*A*). Because of the high concentration of immature minicollagen molecules and cleaved propeptides in vesicles of the TGN the

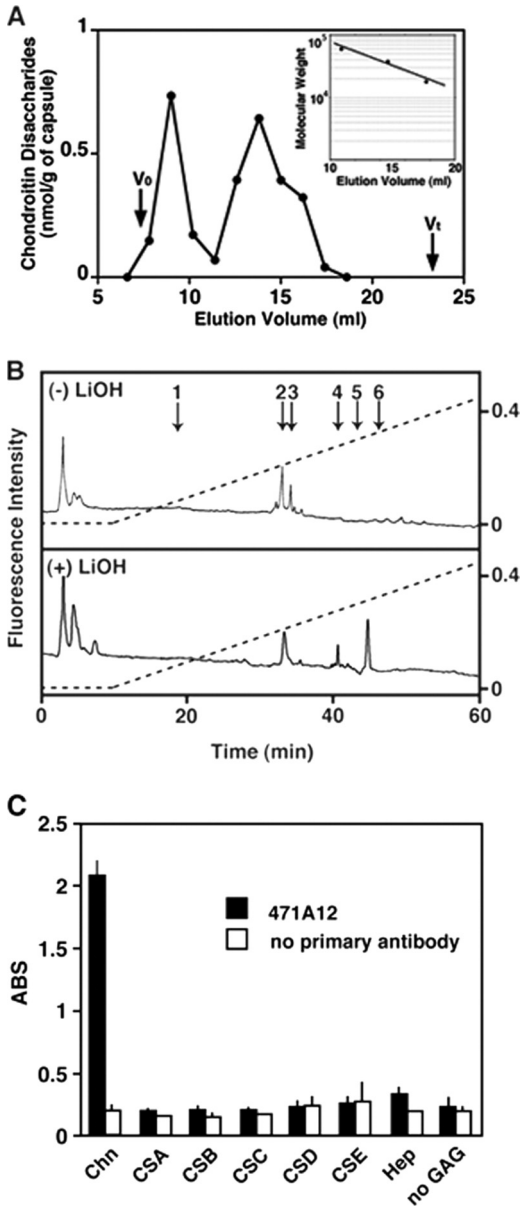

FIGURE 3. **GAG analysis of isolated nematocysts and determination of antibody specificity.** *A*, gel-filtration chromatography of the *Hydra* GAG fraction on a Superdex 200 column. 1.2-ml fractions were collected, digested individually with chondroitinases, derivatized with 2AB, and then analyzed by anion-exchange HPLC on an amine-bound silica column. The amount of the 2AB-derivative of unsaturated disaccharides from chondroitin of *Hydra* nematocysts was calculated based on the fluorescence intensity of the peaks. V_0 and V_t were determined using hyaluronan from human umbilical cord and NaCl, respectively. The *inset* shows the calibration curve giving a linear relationship between log M_r and elution volume, which was generated using size-defined commercial dextran preparations (average M_r: 60,000, 37,500, and 18,100). *B*, analysis of the reducing terminal structure of the *Hydra* chondroitin chains. The *Hydra* GAG fraction was subjected to derivatization with 2AB before (*upper panel*) or after (*lower panel*) treatment with mild alkali (LiOH). After removal of the excess 2AB reagent, the 2AB-derivative was digested with chondroitinases. Each digest was analyzed by HPLC on an amine-bound silica column with a linear NaH_2PO_4 gradient as indicated by *dashed lines*. The positions of authentic 2AB-disaccharides are indicated by *numbered arrows*: 1, ΔHexUA-GalNAc; 2, ΔHexUA-GalNAc(6-sulfate); 3, ΔHexUA-GalNAc(4-sulfate); 4, ΔHexUA(2-sulfate)-GalNAc(6-sulfate); 5, ΔHexUA(2-sulfate)-GalNAc(4-sulfate); 6, ΔHexUA-GalNAc(4,6-disulfate), where ΔHexUA represents 4,5-unsaturated hexuronic acid. *C*, reactivity of the antibody 473A12 to immobilized biotinylated GAG variants. Experiments were performed in duplicate. Values are expressed as means ± ranges. *Chn*, chondroitin; *Hep*, heparin. The antibody specifically recognized chondroitin.

anti-NCol-1 propeptide staining is exclusively restricted to this vesicular structure (Fig. 4, *B* and *C*). As shown in Fig. 4*C* the TGN as detected by the anti-NCol-1 propeptide antibody forms a corona of vesicles around the tip of the growing tubule, while anti-NCol-1, which detects exclusively the mature protein, only stains the capsule wall. Co-stainings with the anti-chondroitin antibody demonstrate that chondroitin shows a similar spiral pattern with TGN vesicles marking early tubule stages (Fig. 4*D*), giving evidence that chondroitin, like NCol-1, is secreted intracellularly. Interestingly, the vesicles for chondroitin and minicollagen are clearly distinguished arguing for separated secretory routes to the nematocyst vesicle (Fig. 4*D*).

Chondroitin Production Precedes That of NCol-15 in Tubule Morphogenesis of Stenoteles and Isorhizas—The recently characterized minicollagen-15 (NCol-15) can be localized exclusively at tubule structures of *Hydra* nematocysts (21). To compare the distribution of the nematocyst chondroitin and NCol-15 during tubule morphogenesis, co-immunostainings with anti-chondroitin and anti-NCol-15 were performed in Hydra whole mounts (Fig. 5*A*). In differentiation stages where the tubule is still outside of the capsule matrix, NCol-15 is detected as aggregated protein material migrating from the tubule tip toward the matrix. Only after invagination it is incorporated into the tubule structure. As shown in Fig. 5, *B* and *C*, chondroitin marks the outer growing tubule in differentiating stenoteles and is broader at the tubule base (Fig. 5*B*) but narrows toward the tubule growth zone (Fig. 5*C*). In isorhizas (Fig. 5, *E* and *F*), the growing tubule is constant in diameter. In the early stages of both capsule types, NCol-15 passes through the tubule in dense globular particles (Fig. 5, *B*, and *E*), which accumulate in the capsule matrix (Fig. 5, *C* and *F*). After tubule invagination, the NCol-15 signal appears at the inverted tubule covered by a strong chondroitin staining at the tubule base and operculum (Fig. 5, *D* and *G*). Nematocysts stained with anti-NCol-15 only, reveal the whole length of the inverted tubule (21).

Nematocyst Chondroitin Is Closely Associated with a Newly Isolated Collectin-like Protein—Collectin molecules are part of the innate immune system of vertebrates where they bind to complex carbohydrates on the microbial surface. In *Hydra*, the hm_2450 gene encodes a protein with minicollagen-like Gly-X-Y repeats and a C-terminal galactose lectin domain, which was termed nematogalectin.[4] A polyclonal antibody was raised against this protein and showed its expression in developing nematocysts in the body column of *Hydra*. Interestingly, nematogalectin shows a similar distribution pattern as chondroitin and is also restricted to the tubules of differentiating nematocysts (Fig. 6*A*). We therefore tested the hypothesis that *Hydra* nematogalectin might serve as a linker molecule connecting the collagenous tubule structure to the chondroitin network. Co-immunostainings with anti-nematogalectin and anti-chondroitin antibodies revealed that both molecules are not colocalized but rather represent different parts of the tubule structure at different morphological stages of all capsule types: desmonemes (Fig. 6, *B–D*), isorhizas (Fig. 6, *E–G*), and stenoteles (Fig. 6, *H–J*).

In isorhizas or stenoteles, the chondroitin staining apparently covers the nematogalectin structure along the whole

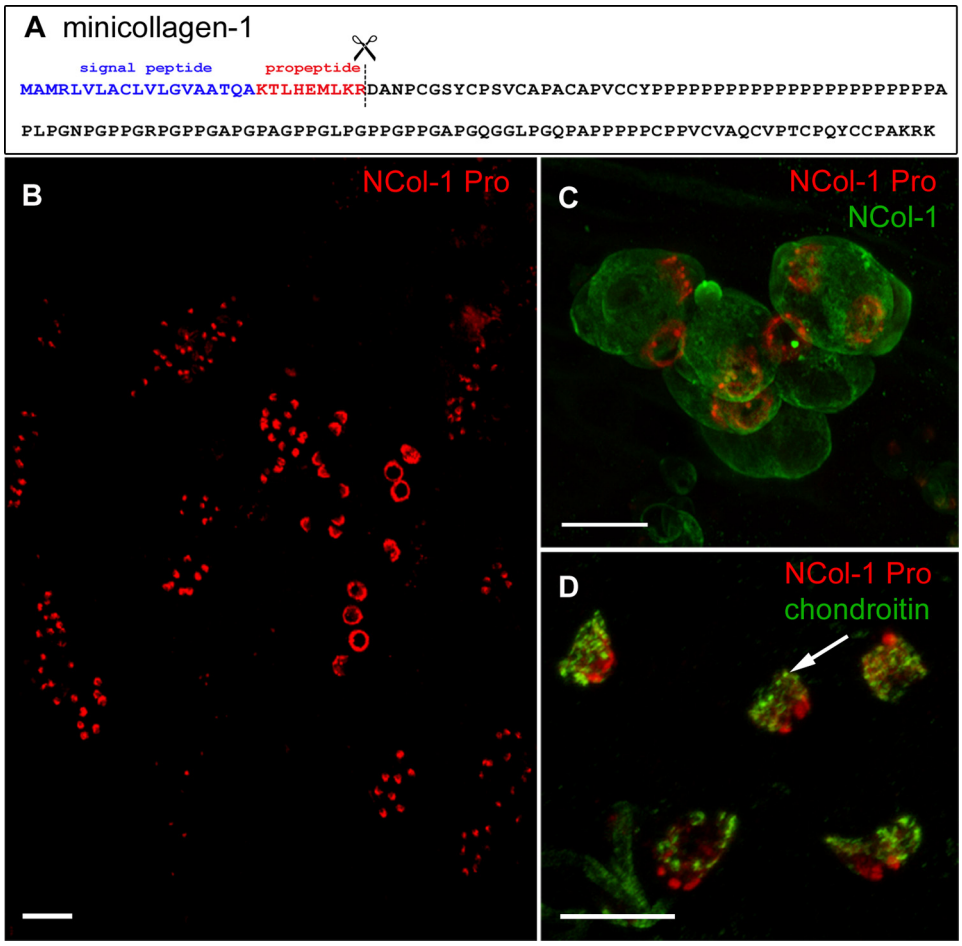

FIGURE 4. **Immunostaining with anti-NCol-1 propeptide and anti-chondroitin antibodies.** *A*, sequence of NCol-1 with the signal peptide in *blue* and the propeptide in *red*. The propeptide is cleaved in trans-Golgi vesicles after the conserved KR dipeptide. *B–D*, whole mounts of *H. magnipapillata* were treated with anti-NCol-1 propeptide antibody (*red*), followed by anti-chondroitin antibody (*D*, *green*), or anti-NCol-1 antibody (*C*, *green*). *B*, nests of differentiating nematocytes in the gastric region of hydra. *Scale bar*, 10 μm. *C*, arriving vesicles from the Golgi apparatus are stained with anti-NCol-1 propeptide antibody (*red*) at the onset of tubule development, while the capsule body is marked by anti-NCol-1 antibody (*green*). *Scale bar*, 10 μm. *D*, vesicles stained with anti-chondroitin antibody (*green*) and anti-NCol-1 propeptide (*red*) antibodies are clearly separated in the trans-Golgi network surrounding the growing tubule. *Scale bar*, 10 μm.

tubule (Fig. 6*E*). During invagination this pattern is reversed with the new external surface showing a strong nematogalectin signal (Fig. 6*F*). This circumstance for the first time allows a detailed imaging of the tubule invagination process in nematocysts as the outer and inner surfaces exhibit clearly distinguishable signals with the chondroitin composing the external layer while nematogalectin represents the inner tubule layer. Because of the invagination process the thread turns inside out and the inner layer gets exposed to the surface now showing a dominant nematogalectin staining. Isorhizas in particular clearly demonstrate that the invaginating tubule is in close contact with the inner surface of the still evaginated tubule only at the onset of the 180° bend.

During its further movement toward the capsule matrix the invaginating tubule structure is extremely condensed and partly recessed from the outer tubule (Figs. 1*E* and 6*F*, *blow-up*) arguing against a sliding mechanism by adhesive surface-to-surface contacts. Rather, invagination appears to be kinetically driven by the tension of the tubule structure at the bending area or a molecular zipper mechanism joining the chondroitin-covered surfaces. Shortly before final maturation the whole tubule is coiled inside the capsule matrix showing a residual chondroitin signal at the base of tubule and operculum structures (Fig. 6*G*). The same observations could be made in stenoteles indicating a common molecular process for all capsule types (Fig. 6, *H–J*).

In desmonemes, early morphogenetic stages also show a nematogalectin signal over the whole length of the tubule, whereas the chondroitin is still restricted to TGN vesicles at the tubule tip (Fig. 6*B*). During tubule growth, the chondroitin signal gets distributed over the whole tubule length, too (Fig. 6*C*). Interestingly, chondroitin seems to be located mainly at the concave tubule face, which later serves as the attachment site for spines.

Nematocyst Development Is Arrested at the Onset of Tubule Growth by GAG Inhibition—GAG synthesis is initiated by the xylosylation of a serine residue on the core protein. Exogenous β-xylosides also prime GAG synthesis and compete with endogenous core protein acceptor sites for the assembly of GAG chains at xylosylated core proteins. To investigate the dependence of nematocyst development on chondroitin synthesis, animals were cultured in media containing 2 mM *p*-nitrophenyl-β-D-xylopyranoside. After fixation of animals at different time points immunostainings were performed using nematocyst-specific antibodies to demonstrate inhibition of nematocyst development. Anti-NCol-15 and anti-NCol-1 antibodies stain the tubule and the capsule wall exclusively in developing nests of the body column, respectively. Hydra tentacles harbor only mature nematocysts where no immunostaining can be obtained with minicollagen-specific antibodies due to the compaction of the capsule wall, which impedes the access to epitopes (Fig. 7, *A* and *B*; *A′* and *B′*). After 2 weeks of β-xyloside incubation tentacles of Hydra were mostly devoid of mature capsules (Fig. 7, *C* and *D*). Interestingly, immature or defective nematocysts could be detected occasionally in the tentacle region using the tubule-specific NCol-15 antibody (Fig. 7, *C′* and *D′*) that in untreated animals does not stain nematocysts in the tentacle region. This finding suggests that nematocyte migration into the tentacles is not necessarily dependent on the maturation process of the capsule. Immature nests in the body column of treated animals mainly showed very early developmental stages, indicating that tubule formation was impeded by xyloside treatment. In

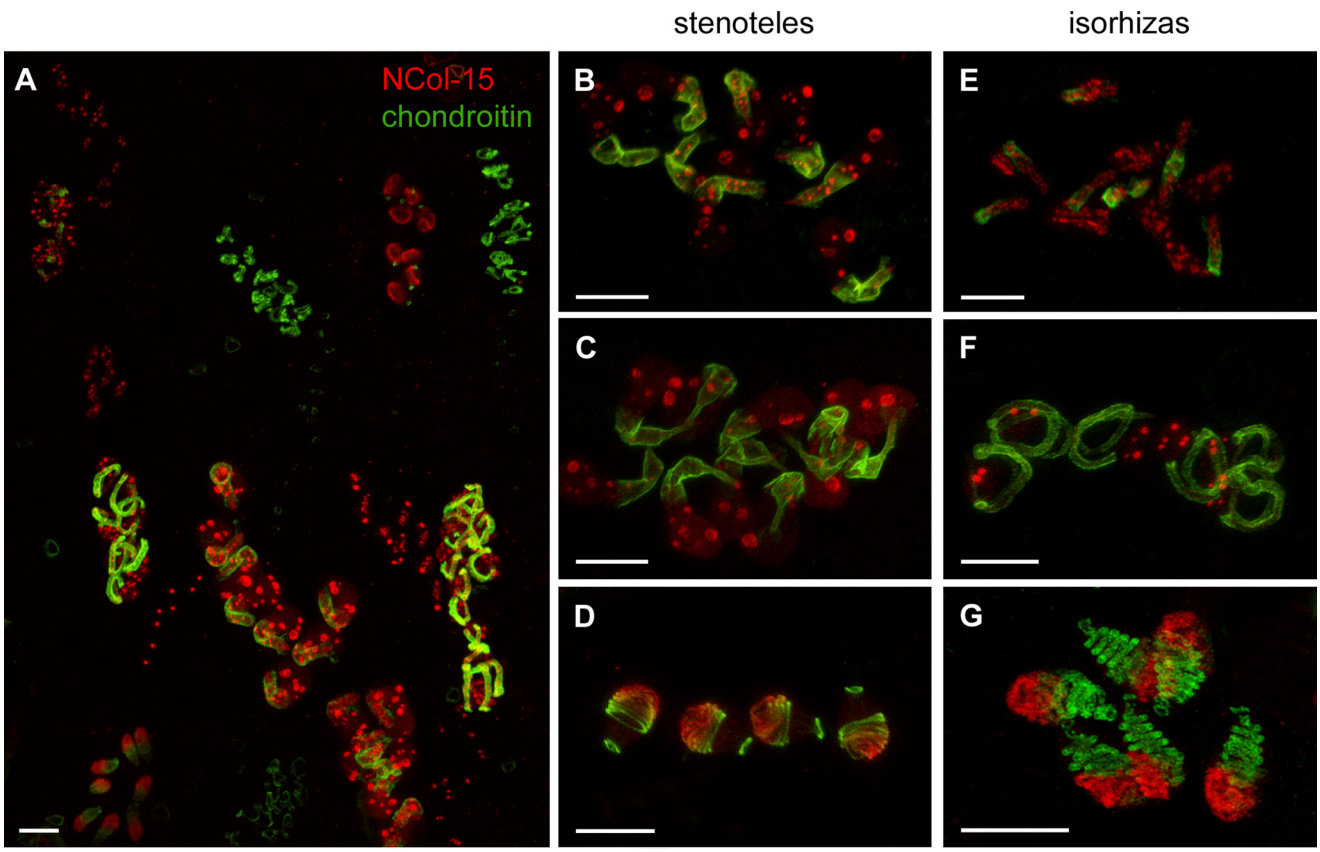

FIGURE 5. **Co-immunostaining with anti-chondroitin and anti-NCol-15 antibodies.** *A–G*, whole mounts of *H. magnipapillata* stained with anti-chondroitin antibody (*green*) and anti-NCol-15 antibody (*red*). *Scale bars*, 10 μm. *A*, nests of differentiating nematocytes in the gastric region. *B–D*, differentiating stenoteles at different morphological stages. *E–G*, differentiating isorhizas at different morphological stages. *D* and *G* show stages after tubule invagination.

untreated animals, NCol-15 migrates in the form of protein aggregates through the externally growing tubule to accumulate in the capsule matrix before it is dissipated and finally incorporated into the invaginated tubule structure (Fig. 8*A*). A similar picture can be seen in developing nematocysts after xyloside treatment with the difference that the particles are generally small and reduced in number, indicating that the secretion of capsule material into the nematocyst vesicle is constrained (Fig. 8*B*). In contrast to untreated animals (Fig. 8, *C* and *E*) the number of late-stage nests exhibiting tubule structures is reduced upon prolonged xyloside treatment. Staining for chondroitin still reveals residual tubule signals indicating that the effect of β-xyloside is not quantitative. Interestingly, in treated animals some nests show aggregated material positive for NCol-15 and chondroitin, which is never detected in untreated animals (Fig. 8*D*, *inset*). This suggests that chondroitin might accumulate predominantly in the form of free chains in these nests. The rarely detectable late-stage nests under these conditions revealed maturation defects with a disordered inverted tubule or unusually large protein accumulations inside the capsule matrix (Fig. 8, *F* and *G*).

DISCUSSION

Membrane tubulation is a dynamic process involving rearrangements of the actin and tubulin cytoskeleton and the interaction with intracellular coating proteins. The contribution of extracellular matrix components to this process is hitherto not well characterized. Here we report that membrane tubulation has an important function in the morphogenesis of a sophisticated secretory organelle, the nematocyst. Nematocyst development is a highly organized intracellular secretion process leading to the self-assembly of structural ECM type proteins at the inner surface of a vesicle membrane. Capsule wall formation precedes tubule morphogenesis, which initially results in an external structure that gets invaginated after having reached its full size. Previously we have demonstrated NCol-15 to be a specific molecular component of the nematocyst tubule, which is incorporated after invagination (21). In the present analysis we could detect the antigen of a chondroitin antibody lining the external tubules of developing nematocysts. This finding suggests that the chondroitin molecule is involved in the formation of a pre-tubule structure that accompanies membrane protrusion and serves as a scaffold for minicollagen assembly after invagination.

The Evolutionary Origin of GAGs in Metazoans—Chondroitin molecules are an essential component of the extracellular matrix and in a previous report by Yamada *et al.* (16) chondroitin isolated from whole *Hydra* tissue was analyzed and found to contain non-sulfated as well as 4-*O*-sulfated and 6-*O*-sulfated GalNAc residues. Our present analysis was restricted to nematocysts as these were the sites of chondroitin synthesis recognized by the applied antibody. Here, only an unusual non-sulfated form of chondroitin could be detected indicating that

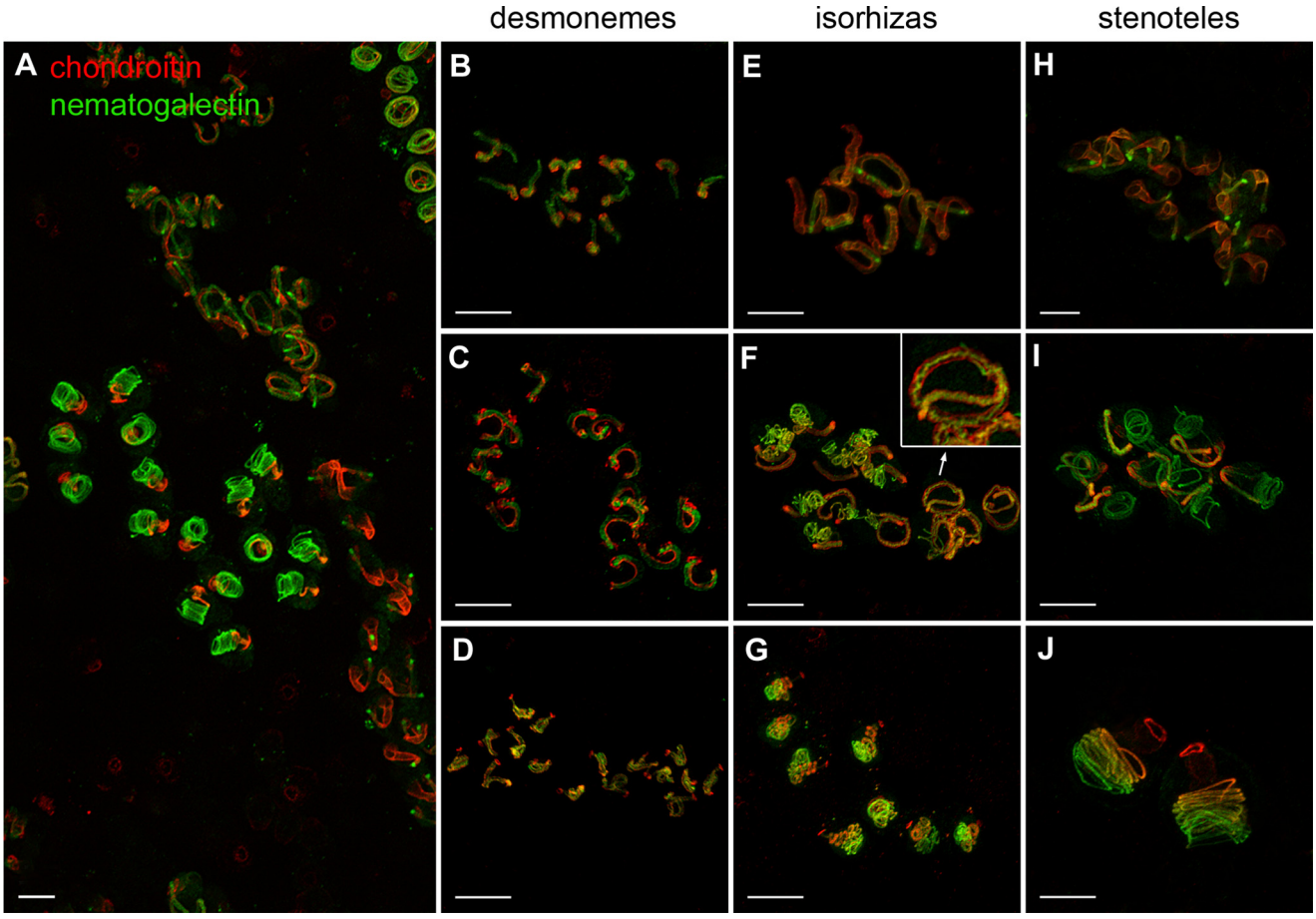

FIGURE 6. **Co-immunostaining with anti-chondroitin and anti-nematogalectin antibodies.** *A*, whole mount of *H. magnipapillata* stained with anti-nematogalectin antibody (*green*) and anti-chondroitin antibody (*red*). *B–J*, close views of differentiating nests of desmonemes (*B–D*), isorhizas (*E–G*), and stenoteles (*H–J*) at different morphological stages. *Scale bars* represent 10 μm.

sulfated forms are present in the cellular tissue but not in nematocysts. An ELISA screen against different GAG variants clearly demonstrated that the antibody exclusively recognizes non-sulfated chondroitin (Fig. 3*C*).

GAGs have diverse biological functions in animals as in collagen fibirillogenesis, regulation of protease activity, maintenance of cell-cell and cell-matrix interactions and the storage of soluble growth factors. So far, *Hydra* is the phylogenetically lowest organism that has been demonstrated to produce GAGs. Some bacterial strains can also synthesize GAG-like polysaccharides when they form extracellular polysaccharide capsules. For example, *Escherichia coli* strain K4 produces a capsule polysaccharide consisting of a chondroitin backbone, to which β-fructose residues are linked to position C-3 of the GlcA residues (24). However, these GAG-like polysaccharides are not attached to core proteins, which appears to be an animal innovation.

Chondroitins are generally sulfated. Reports on the existence of non-sulfated chondroitin are limited to extracellular matrices of the nematode *Caenorhabditis elegans* (25, 26), squid skin (27), and the dried regurgitated saliva of male *Collocalia* swiftlets (28). Non-sulfated chondroitin in *C. elegans* is involved in cell division during early development, since removal of chondroitin from fertilized eggs results in lethality after an oscillation of cell division and reversion of cytokinesis (29, 30). In addition chondroitin PGs in *C. elegans* are involved in the vulval morphogenesis, which requires epithelial invagination (30). The fact that the *Hydra* nematocyst chondroitin is non-sulfated might represent a mechanism to prevent a premature interaction with the positively charged minicollagen molecules.

GAGs in Nematocyst Membrane Tubulation—Chondroitin synthesis in nematocysts sets in with the beginning of tubule formation, which is dramatically impaired when chondroitin production is inhibited by xyloside treatment. As shown schematically in Fig. 9, our data demonstrate that the chondroitin matrix at the inner side of the tubule membrane is formed independently of the collagenous structure in both of the capsule wall and the tubule itself. This is emphasized by the detection of clearly separated routes for NCol-1 and chondroitin in the secretory pathway (Fig. 9*B*). A premature incorporation of NCol-15 during tubule growth appears to be inhibited by the storage of the minicollagen in dense protein bodies, which accumulate in the matrix (Fig. 9, *B–D*). We have observed a similar behavior for spinalin, which has to pass the invaginated tubule wall to form spines on its outer surface (data not shown). The primary role of the chondroitin-based matrix therefore seems to be in the outgrowth and stabilization of the initial tubule structure, probably by a close membrane attachment.

The delay of minicollagen and spinalin incorporation is most probably a prerequisite for the invagination process, which

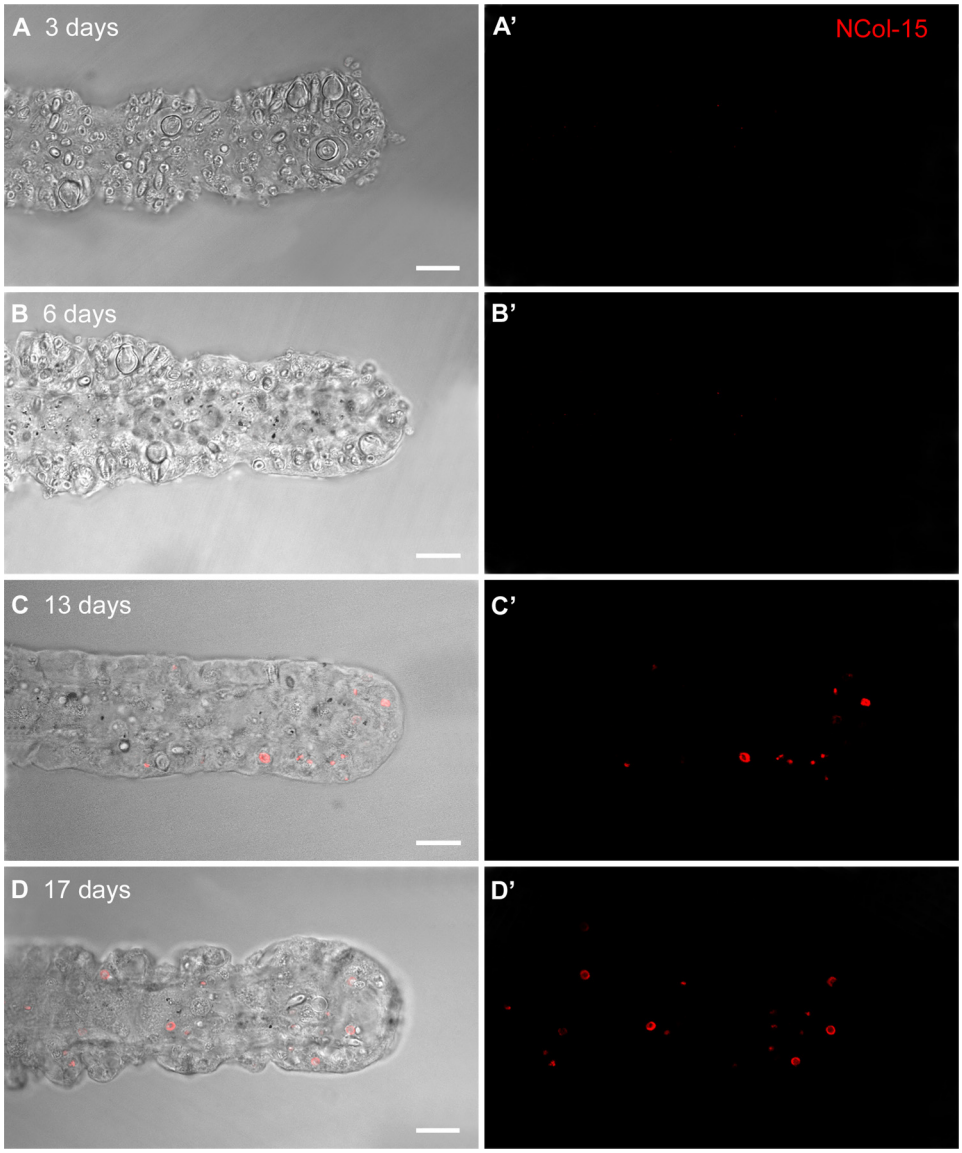

FIGURE 7. **Effect of xyloside treatment on nematocyst morphogenesis.** Animals were cultured in *Hydra* medium containing 2 mM *p*-nitrophenyl-β-D-xylopyranoside and fixed after different timepoints, followed by immunostaining with anti-NCol-15 antibody. *Scale bars* represent 20 μm. *A–D*, tentacles after 3 (*A*), 6 (*B*), 13 (*C*), and 17 (*D*) days of incubation with xyloside. *Left*: DIC images; *right*: corresponding fluorescence microscopy.

would be hampered by a fully matured tubule structure. The newly identified nematogalectin molecule appears to have a similar function in pre-tubule formation as chondroitin without being directly associated with it. It covers the membrane-distal inner surface of the tubule, which gets exposed to the matrix lumen during invagination (Fig. 9, *C–E*). As the nematocyst nematogalectin lacks a minicollagen cysteine-rich domain it is unlikely that it gets covalently linked to the collagenous network during nematocyst maturation. We therefore speculated that it might control the recruitment of minicollagens to the invaginated tubule by interacting with sugar residues. Minicollagens have been shown to be highly *N*-glycosylated (22).

Chondroitin chains in *C. elegans* and *H. magnipapillata* are attached to core proteins through the common linkage region tetrasaccharide, -4GlcAβ1–3Galβ1–3Galβ1–4Xylβ1- (16, 31). Although core proteins of *C. elegans* chondroitin PGs have been identified, no homologues have been found in vertebrates or in *Hydra* vulgaris (32). *Hydra* chondroitin PGs likely contain novel core proteins. In this study, β-xyloside treatment disrupted the formation of mature capsules. This is most likely caused by the impediment of the GAG biosynthesis, since exogenous β-xyloside inhibits the assembly of GAG chains to the Ser residues of core proteins, suggesting that *Hydra* chondroitin chains are synthesized on core proteins through the common linkage tetrasaccharide structure rather than as free chains. This is supported by the finding that in β-xyloside-treated animals chondroitin is sometimes found in large aggregates (Fig. 8*D*). However, in isolated nematocysts also free chondroitin chains were detected, as the reducing terminal sugar residues of the chondroitin chains were labeled with 2AB without alkali treatment (Fig. 3*B*). Recently we have identified and characterized a chondroitin-specific endoglycosidase in *C. elegans* (33) as well as CS-specific endoglycosidase in humans (34). Because the homologue of these genes exists in the *Hydra* nematocyst proteome, such an endohydrolase might be involved in the release of chondroitin chains from the putative core proteins.[5]

Our nematocyst proteome analysis also revealed several candidate enzymes, which are supposed to be involved in chondroitin synthesis.[5] They possess predicted β-1,4-*N*-acetylgalactosaminyltransferase or β-1,3-galactosyltransferase activities. Interestingly several of them are supposed to be products of horizontal gene transfer from bacteria. Thus, the possibility cannot be excluded that the free chondroitin chains in nematocysts might be assembled in a similar fashion to bacterial GAG-like polysaccharides. The presence of an ECM component in the nematocyst structure is not unusual, as we have detected in a proteome analysis of isolated nematocysts, beside the minicollagen family, a large number of further ECM proteins.[5] The capsule structure may therefore be seen as a specialized ECM inside a highly derived secretory vesicle. Interestingly, many of the capsular ECM proteins have lectin-type domains, suggesting a promi-

[5] P. G. Balasubramanian, A. Beckmann, C. Zenkert, U. Warnken, M. Schnölzer, E. Bornberg-Bauer, T. W. Holstein, and S. P. Özbek, submitted manuscript.

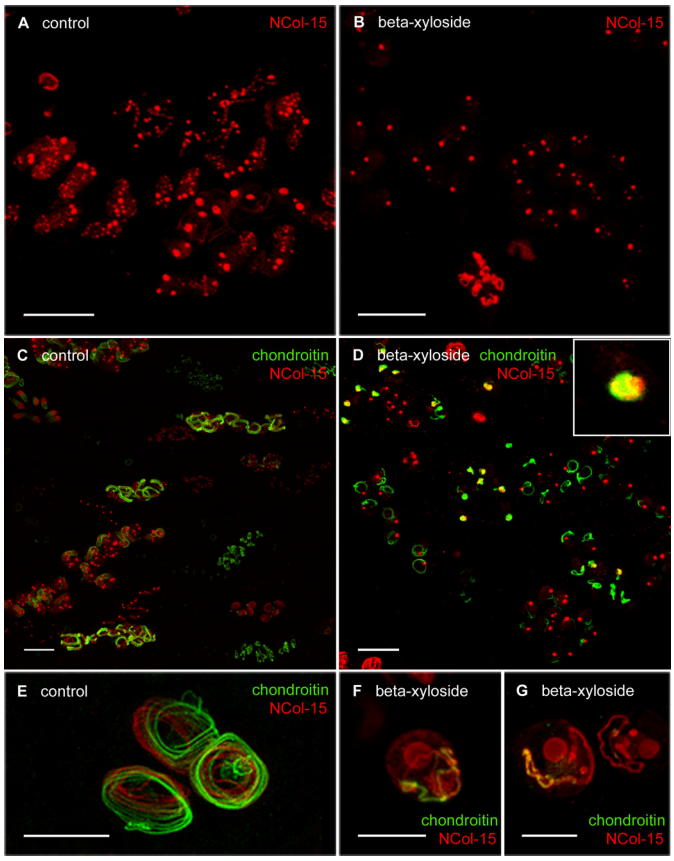

FIGURE 8. **Effect of xyloside treatment on differentiating nematocytes in the body column.** Animals were cultured in *Hydra* medium containing 2 mM *p*-nitrophenyl-β-D-xylopyranoside and fixed after different time points, followed by immunostaining with anti-NCol-15 antibody (*red*) and anti-chondroitin antibody (*green*). *A*, normal differentiating nests stained with anti-NCol-15 antibody after 3 days of xyloside treatment. *Bar*, 20 μm. *B*, disordered differentiating nests stained with anti-NCol-15 antibody after 17 days of xyloside treatment. *Bar*, 20 μm. *C*, normal differentiating late stage nest stained with anti-chondroitin and anti-NCol-15 antibodies without xyloside treatment. *Bar*, 10 μm. *D*, disordered late-stage nematocysts after 17 days of xyloside treatment. Inset shows magnification of aggregated material positive for both antigens. *E*, late-stage stenotele nest with invaginated tubules stained with anti-chondroitin and anti-NCol-15 antibodies. *F* and *G*, mature stenoteles after 17 days of xyloside treatment showing reduced and disordered tubules. *Bars*, 10 μm.

nent role for protein-carbohydrate interactions in the assembly of the nematocyst suprastructure.

Chondroitin PGs have also been characterized as matrix constituents in the nervous system forming perineuronal nets. These PNNs are specialized forms of the nerve cell matrix in the central nervous system (17). They form lattice structures around the nerve cell bodies, proximal dendrites and axon initial segments (35). The PNN has been found to have an inhibitory function on neuronal plasticity and regeneration, which is regained by digestion of CS-PGs with chondroitinase (36). Its primary role is believed to be in synaptic stabilization and neuroprotection. Because nematocytes represent a specialized neuronal cell type, which in *Hydra* arise from the same stem cell population as other nerve cells (for review see Ref. 37, 38) one might speculate that the nonsulfated chondroitin in cnidarian nematocysts represents a primordial PNN-like structure. Accordingly the ability to secrete chondroitin PGs might represent a primordial function in neuronal cell types that gave rise

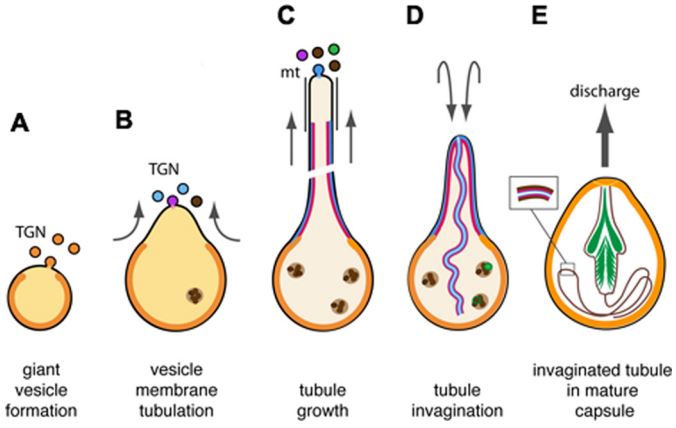

FIGURE 9. **Schematic drawing of chondroitin, nematogalectin, NCol-15, NCol-1, and spinalin antigen distribution during nematocyst morphogenesis (stenotele).** *A*, early tubule development at the apical side of the nematocyst. The capsule grows inside a giant post-Golgi vesicle by addition of NCol-1-filled vesicles from the TGN. The capsule wall shows NCol-1 immunostaining (*yellow*) at this stage. *B*, onset of membrane tubulation is accompanied by the secretion of chondroitin and nematogalectin into the nematocyst vesicle. *C*, during tubule growth the outer layer is formed by chondroitin (*blue*) and the tubule inner layer by nematogalectin (*red*). Dense globular NCol-15 particles (*brown*) migrate through the tubule into the vesicle matrix. *D*, during tubule invagination the inner tubule layer turns inside out and now nematogalectin (*red*) is present at the surface and obscures the subjacent chondroitin (*blue*). NCol-15 (*brown*) appears in this stage in few large protein agglomerates together with the spine protein spinalin (*green*). *E*, shortly before final maturation the tubule is completely coiled up inside the capsule matrix, and NCol-15 is then incorporated into the tubule structure.

to complex extracellular GAG-coated structures as in PNNs of vertebrates.

Acknowledgment—We thank the Nikon Imaging Center Heidelberg for technical assistance and for making it possible for us to perform confocal microscopy.

REFERENCES

1. Frost, A., Unger, V. M., and De Camilli, P. (2009) *Cell* **137,** 191–196
2. Watanabe, H., Fujisawa, T., and Holstein, T. W. (2009) *Dev. Growth Differ.* **51,** 167–183
3. David, C. N., Ozbek, S., Adamczyk, P., Meier, S., Pauly, B., Chapman, J., Hwang, J. S., Gojobori, T., and Holstein, T. W. (2008) *Trends Genet.* **24,** 431–438
4. Ozbek, S., Balasubramanian, P. G., and Holstein, T. W. (2009) *Toxicon.* **54,** 1038–1045
5. Chapman, G. B., and Tilney, L. G. (1959) *J. Biophys. Biochem. Cytol.* **5,** 79–84
6. Chapman, G. B., and Tilney, L. G. (1959) *J. Biophys. Biochem. Cytol.* **5,** 69–78
7. Holstein, T. W., and David, C. N. (1990) *Dev. Biol.* **142,** 392–400
8. Rich, F., and Tardent, P. (1969) *Rev. Suisse Zool.* **76,** 779–787
9. David, C. N., and Gierer, A. (1974) *J. Cell Sci.* **16,** 359–375
10. Fawcett, D. W., Ito, S., and Slautterback, D. (1959) *J. Biophys. Biochem. Cytol.* **5,** 453–460
11. Holstein, T. (1981) *J. Ultrastruct. Res.* **75,** 276–290
12. Slautterback, D. B., and Fawcett, D. W. (1959) *J. Biophys. Biochem. Cytol.* **5,** 441–452
13. Skaer, R. J. (1973) *J. Cell Sci.* **13,** 371–393
14. Jackson, R. L., Busch, S. J., and Cardin, A. D. (1991) *Physiol. Rev.* **71,** 481–539
15. Sugahara, K., Mikami, T., Uyama, T., Mizuguchi, S., Nomura, K., and Kitagawa, H. (2003) *Curr. Opin. Struct. Biol.* **13,** 612–620
16. Yamada, S., Morimoto, H., Fujisawa, T., and Sugahara, K. (2007) *Glycobiology* **17,** 886–894

17. Celio, M. R., Spreafico, R., De Biasi, S., and Vitellaro-Zuccarello, L. (1998) *Trends Neurosci.* **21,** 510–515
18. Loomis, W. F. (1953) *Science* **117,** 565–566
19. Kinoshita, A., and Sugahara, K. (1999) *Anal. Biochem.* **269,** 367–378
20. Sakaguchi, H., Watanabe, M., Ueoka, C., Sugiyama, E., Taketomi, T., Yamada, S., and Sugahara, K. (2001) *J. Biochem.* **129,** 107–118
21. Adamczyk, P., Meier, S., Gross, T., Hobmayer, B., Grzesiek, S., Bächinger, H. P., Holstein, T. W., and Ozbek, S. (2008) *J. Mol. Biol.* **376,** 1008–1020
22. Engel, U., Pertz, O., Fauser, C., Engel, J., David, C. N., and Holstein, T. W. (2001) *EMBO J.* **20,** 3063–3073
23. Technau, U., and Holstein, T. W. (1996) *Dev. Biol.* **177,** 599–615
24. Rodriguez, M. L., Jann, B., and Jann, K. (1988) *Eur. J. Biochem.* **177,** 117–124
25. Yamada, S., Sakamoto, K., Tsuda, H., Yoshida, K., Sugiura, M., and Sugahara, K. (1999) *Biochemistry* **38,** 838–847
26. Hwang, H. Y., and Horvitz, H. R. (2002) *Proc. Natl. Acad. Sci. U.S.A.* **99,** 14224–14229
27. Karamanos, N. K., Aletras, A. J., Antonopoulos, C. A., Tsegenidis, T., Tsiganos, C. P., and Vynios, D. H. (1988) *Biochim. Biophys. Acta.* **966,** 36–43
28. Nakagawa, H., Hama, Y., Sumi, T., Li, S. C., Maskos, K., Kalayanamitra, K., Mizumoto, S., Sugahara, K., and Li, Y. T. (2007) *Glycobiology* **17,** 157–164
29. Mizuguchi, S., Uyama, T., Kitagawa, H., Nomura, K. H., Dejima, K., Gengyo-Ando, K., Mitani, S., Sugahara, K., and Nomura, K. (2003) *Nature* **423,** 443–448
30. Hwang, H. Y., Olson, S. K., Esko, J. D., and Horvitz, H. R. (2003) *Nature* **423,** 439–443
31. Yamada, S., Okada, Y., Ueno, M., Iwata, S., Deepa, S. S., Nishimura, S., Fujita, M., Van Die, I., Hirabayashi, Y., and Sugahara, K. (2002) *J. Biol. Chem.* **277,** 31877–31886
32. Olson, S. K., Bishop, J. R., Yates, J. R., Oegema, K., and Esko, J. D. (2006) *J. Cell Biol.* **173,** 985–994
33. Kaneiwa, T., Yamada, S., Mizumoto, S., Montaño, A. M., Mitani, S., and Sugahara, K. (2008) *J. Biol. Chem.* **283,** 14971–14979
34. Kaneiwa, T., Mizumoto, S., Sugahara, K., and Yamada, S. (2010) *Glycobiology* **20,** 300–309
35. Zimmermann, D. R., and Dours-Zimmermann, M. T. (2008) *Histochem. Cell Biol.* **130,** 635–653
36. Galtrey, C. M., and Fawcett, J. W. (2007) *Brain Res. Rev.* **54,** 1–18
37. Watanabe, H., Hoang, V. T., Mättner, R., and Holstein, T. W. (2009) *Semin. Cell Dev. Biol.* **20,** 1114–1125
38. Bosch, T. C., Anton-Erxleben, F., Hemmrich, G., and Khalturin, K. (2010) *Dev Growth Differ* **52,** 15–25

OPEN ACCESS Freely available online

PLoS one

Morphological and Molecular Analysis of the *Nematostella vectensis* Cnidom

Claudia Zenkert[1], Toshio Takahashi[2], Mark-Oliver Diesner[1], Suat Özbek[1]*

1 Department for Molecular Evolution and Genomics, Centre for Organismal Studies, University of Heidelberg, Heidelberg, Germany, **2** Suntory Foundation for Life Sciences, Bioorganic Research Institute, Osaka, Japan

Abstract

The starlet sea anemone *Nematostella vectensis* is an emerging model organism for developmental and evolutionary biology. Due to the availability of genome data and its amenability to genetic manipulation *Nematostella* serves as a source for comparative molecular and phylogenetic studies. Despite this fact, the characterization of the nematocyst inventory and of nematocyst-specific genes is still fragmentary and sometimes misleading in this cnidarian species. Here, we present a thorough qualitative and quantitative analysis of nematocysts in *Nematostella vectensis*. In addition, we have cloned major nematocyst components, *Nematostella* minicollagens 1, 3 and 4, and show their expression patterns by in situ hybridization and immunocytochemistry using specific antibodies. Our data provides tools and insights for further studies on nematocyst morphogenesis in *Nematostella* and comparative evolution in cnidarians.

Citation: Zenkert C, Takahashi T, Diesner M-O, Özbek S (2011) Morphological and Molecular Analysis of the *Nematostella vectensis* Cnidom. PLoS ONE 6(7): e22725. doi:10.1371/journal.pone.0022725

Editor: Peter K. Dearden, University of Otago, New Zealand

Received May 10, 2011; **Accepted** July 4, 2011; **Published** July 28, 2011

Funding: This work was supported by the German Science Foundation (OE416/4-1). The funders had no role in study design, data collection and analysis, decision to publish, or preparation of the manuscript.

Competing Interests: The authors have declared that no competing interests exist.

* E-mail: suat.oezbek@cos.uni-heidelberg.de

Introduction

Due to their phylogenetic position as a sister group to bilatarians cnidarians have been of interest for the exploration of animal body patterning and embryonic development [1]. The genomes of *Hydra* [2] and *Nematostella* [3] have been sequenced and provide a basis for extensive comparative studies. The establishment of transgenesis in both species has opened additional experimental possibilities for functional genetic approaches [4,5]. Despite this progress there is only limited information on nematocysts in *Nematostella* compared to the extensive studies performed in *Hydra* [6]. Nematocysts are the defining predatory organelles of the phylum cnidaria and represent a complex secretory product of the Golgi apparatus [7]. They are composed of a cylindrical capsule body that elongates into a long tubule, which is coiled up in the capsule matrix. This basic structure varies between different cnidarian species, but there is a general tendency towards higher complexity in *medusozoa* compared to *anthozoa* [8]. Nematocyst production involves the coordinated secretion of proteins into the growing nematocyst vesicle, where these are assembled to form the collagenous capsule structure. Mature nematocysts are connected to a mechanosensory cnidocil apparatus that triggers their ultrafast discharge process [9].

In *Hydra*, four types of nematocysts have been described and several molecular capsule components have been extensively characterized. In particular, the large minicollagen family, which represents the major structural constituent of the organelle, has been the subject of numerous biochemical and structural studies [10,11,12,13].

Here, we present the first extensive description of the *Nematostella* cnidom and characterize the expression patterns and localization of several isolated minicollagens. Our work provides evidence for a basal nematocyst structure in the anthozoan-specific spirocysts and tools for further comparative studies on nematocyst development and evolution within the cnidarian clade.

Results

Morphological characterization of nematocyst types in *Nematostella*

Nematocysts of *Nematostella vectensis* were isolated by Percoll gradient centrifugation and characterized morphologically using light and scanning electron microscopy (SEM). We were able to distinguish three different capsule types according to the classification of Weill [14,15] (Figure 1): (i) the smallest and most common nematocyst type is the basitrichous haplonema (Figure 1A–E). It is about 12 µm long and 2 µm in width. The tubule has a diameter of 0.5 µm, with a total length of 90–110 µm (Figure 1B, C). Dense spines of 1–2 µm length are arranged in spirals along a stretch of 20–25 µm at the base of the tubule (Figure 1B–D). SEM analysis revealed smaller spines (~0.1 µm) (Figure 1E) covering up to 2/3 of the total tubule length; (ii) the larger microbasic mastigophores (Figure 1F–J) are 17–22 µm long and 3 µm in width. The clearly discernible tubule base (30–40 µm) is about 1.5 µm in diameter and covered with dense spirals of spines of 1–4 µm length (Figure G–I). The tubule has a total length of about 180 µm with a narrower and smooth distal part (Figure 1H, J); (iii) spirocysts are the characteristic cone-shaped nematocysts of anthozoans. In *Nematostella* they are about 25–30 µm long and thus represent the largest capsule type (Figure 1K–P). The spineless tubule (Figure 1P) is visible in typical large coils inside the capsule body and has an average diameter of 1 µm and

a length of about 180 µm (Figure 1K–M). Spirocysts are distinctive in exhibiting a less dense capsule wall than other nematocyst types. This apparent fragility is also reflected by the fact that most spirocysts are disrupted by the isolation procedure and quantification has to rely on a careful maceration procedure. SEM analysis revealed that spirocysts lack an opercular structure formed by the capsule wall (Figure 1N, O). Rather, capsule closure appears to be realized by folds at the base of the inverted tubule (Figure 1O) suggesting a continuous structure between tubule and capsule body for this nematocyst type.

Quantitative analysis of nematocysts at different developmental stages

To analyze whether the composition of nematocyst types changed during development we quantified nematocysts at different stages of *Nematostella* morphogenesis (Figure 2A, Table S1). In planula larvae basitrichous haplonemas clearly dominated, constituting 91% of all capsule types, while mastigophores and spirocysts were represented only to 5.3% and 3.7%, respectively. The percentage of basitrichous haplonemas was slightly reduced in primary (83.4%) and adult polyps (69.2%), whereas microbasic mastigophores were almost constant at 15% and 16.5%, respectively. Spirocysts stayed at a low level (1.6%) in primary polyps but were increased to 14.3% in adult animals. Considering the total tissue of the animal, nematocytes made up 4–5% of all cells at each developmental stage.

To analyze the distribution of nematocyst types along the different body parts of the animal we quantified capsules in head, body and foot regions of adult polyps (Figure 2B). Although mature nematocysts in *Nematostella* are distributed all along the body axis, the highest density of capsules is found in the tentacles, the tentacle base and the hypostomal area. In the head region, the majority of nematocysts (45.3%) are spirocysts, followed by basitrichous haplonemas (41.1%) and microbasic mastigophores (13.6%). Nematocysts in the body column and foot region are mainly basitrichous haplonemas (77% and 89.9%) and microbasic mastigophores (22.4% and 9.9%), suggesting that spirocysts and microbasic nematocysts are offensive capsule types used for prey capture, while basitrichous haplonemas mainly have a defensive function against predators.

Isolation of *Nematostella* minicollagen genes

Molecules of the minicollagen family are major structural constituents of nematocysts and have been identified in all cnidarian genomes analyzed so far [8]. Minicollagens are composed of a central collagen triple helix flanked by polyproline stretches and short cysteine-rich domains (CRDs) with a conserved cysteine pattern ($CX_3CX_3CX_3CX_3CC$) [12]. In *Hydra*, 17 members of this protein family have been isolated while in *Nematostella* only 5 could be identified in the genome database, reflecting the lower complexity of anthozoan nematocysts [8]. As minicollagens are important markers of nematocyst morphogen-

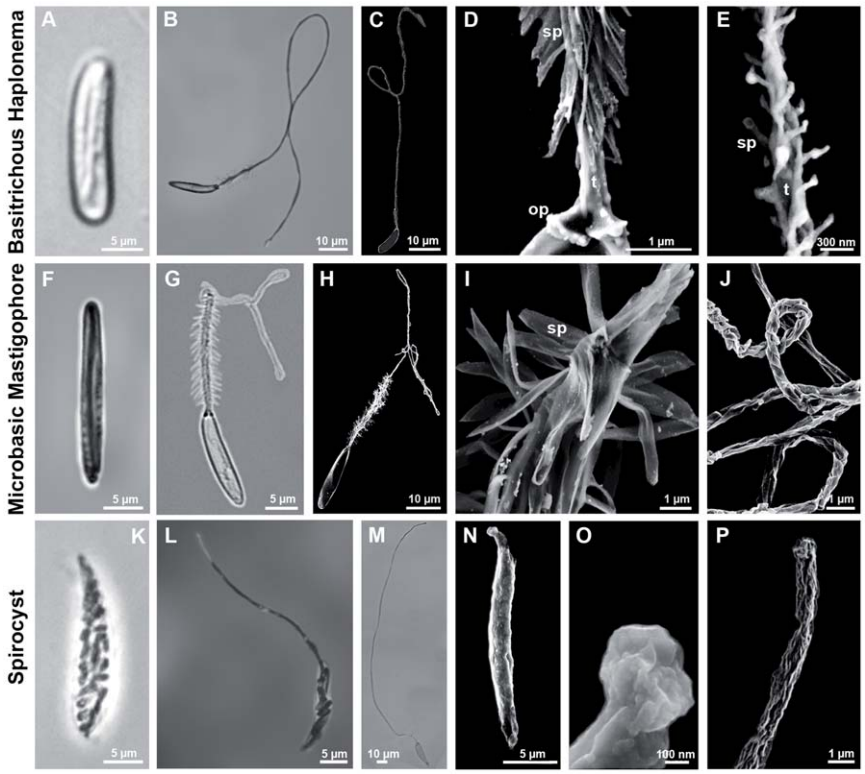

Figure 1. Capsule types in *Nematostella vectensis*. A–E. Basitrichous haplonemas. F–J. Microbasic mastigophores. K–P. Spirocysts. A, B. Light microscopic images of an undischarged (A) and a fully discharged (B) basitrichous haplonema. C–E. Scanning electron microscopic (SEM) images of haplonemas. C. Fully discharged haplonema. D. Detail of C, showing the basal spines (sp) and the opercular apparatus (op). E. Detail of the distal part of the tubule (t), revealing reduced spines (sp). F–J. Microbasic mastigophores. F, G. Undischarged (F) and fully discharged (G) capsule. H–J. SEM images of microbasic mastigophores. H. Fully discharged capsule. I. Detail of H showing the flexible spines (sp). J. Detail of the triangular tubule showing both the coiled and the distal uncoiled structure. K–P. Spirocysts. K–M. Light microscopic images of an undischarged (K), partly (L) and fully discharged spirocyst (M). N–P. SEM images of spirocysts. N. Undischarged spirocyst. O. Detail showing the closed opening of the capsule body. P. Distal end of discharged tubule. Scale bars are 10 µm (B, C, H, M), 5 µm (A, F, G, K, L, N), 1 µm (D, I, J, P), 300 nm (E), and 100 nm (O).
doi:10.1371/journal.pone.0022725.g001

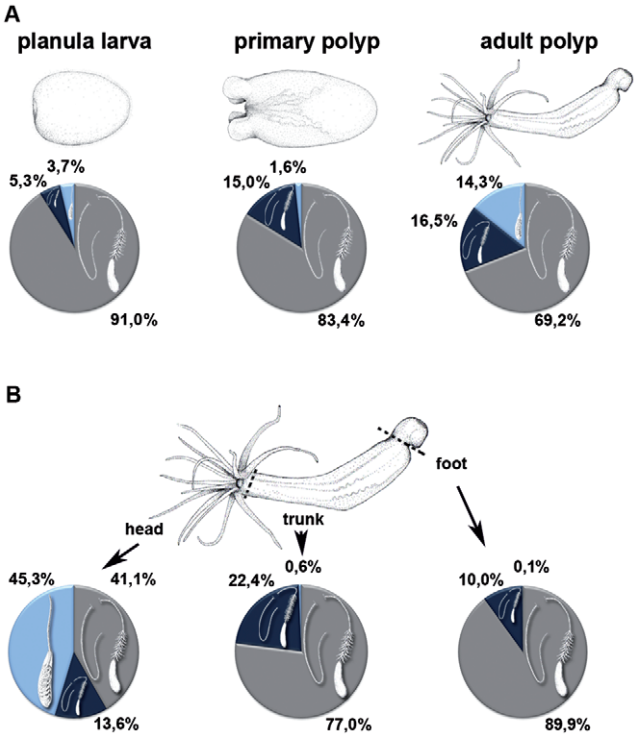

Figure 2. Quantitative distribution of nematocysts in *Nematostella* polyps. A. Distribution of nematocyst types in different developmental stages. B. Distribution of nematocyst types in different body parts of Nematostella vectensis.
doi:10.1371/journal.pone.0022725.g002

esis we isolated the *Nematostella* minicollagen genes by cloning from cDNA and raised peptide antibodies against their CRD peptides, which serve as signature domains. We succeeded in cloning minicollagens 1, 3, and 4 (NvNCol-1; NvNCol-3; NvNCol-4) while the predicted minicollagen gene sequences of NvNCol-5 and NvNCol-6 could not be amplified. This is probably due to highly homologous sequences between minicollagens and a lower abundance of the respective cDNAs.

The full-length minicollagen sequences are shown in Figure 3. NvNCol-1 has an open reading frame (ORF) of 516 nucleotides, coding for 172 amino acids. NvNCol-3 is slightly shorter with 429 nucleotides (143 amino acids) and NvNCol-4 comprises 570 nucleotides coding for 190 amino acids. All three identified NvNCols have individual signal peptides with 19–21 amino acids followed by a propeptide sequence terminating with the characteristic lysine-arginine (KR) cleavage site. Their domain composition includes a central collagen sequence comprising between 14–27 Gly-X-Y repeats flanked by variable polyproline stretches and terminal CRDs. NvNCol-3 and NvNCol-4 possess single canonical CRDs while NvNCol-1 shows a CRD duplication at the C-terminus with the second CRD lacking the first two cysteines of the conserved pattern as in *Hydra* NCol-15 [13]. In contrast to *Hydra*, the minicollagen genes in *Nematostella* are positioned on different scaffolds and do not occur in clusters of tandemly repeated genes sharing a common signal peptide [8].

Characterization of minicollagen expression patterns in different developmental stages

The expression patterns of the isolated minicollagen genes were assayed by *in situ* hybridization (ISH) of whole mounts from different developmental stages (Figure 4). All assayed *Nematostella*

NvNCol-1

MAFKITLLCVALYLATTQAKKVMQKRDANPCGMSCPMSCAPACTPMCCMAPPPPPPPPPV
MCCAPPPPPPAMIPGPPGPPGCMGPPGSPGCRGLPGCMGPMGPMGPPGSPGCPGSPGAPA
PPAPQCPPICIHHCMKICPMPCCSPPPPPPVVYYPPPPPPPMPVCMPSCAPACCK

NvNCol-3

MASKLILGVLALMVVSTYARSTYKRSAKACPPGCPNYCAPACQVSCCLPPPPPPPPPPPP
PPPPPEPARPGPPGPSGRQGPPGPVGPIGPMGEAGPPGPPGPQGPPGPPGEPAPPPPPPP
PCPAICAHTCVPSCPSGCCAGRR

NvNCol-4

MRNRVLLLLGCVLYTSTLTYGASMFKSSLHLKRSPNPCGGSCPASCAPLCASACCSFTPP
PPPPPPPYYPAPPPPPGPPGPDGPMGMPGPQGPDGPKGPPGLPGPPGPPGLPGLPGAPAG
IPGHDGPMGPPGPPGHMGPPGDMGPPGAPGLPGPPGPPAPATPYAAPCPQYCYRSCIPSC
PRGCCSRGK

Figure 3. Amino acid sequences of *Nematostella* minicollagens. Protein sequences of minicollagens NvNCol-1, NvNCol-3, and NvNCol-4. Signal peptides in grey; propeptide in green; poly-proline stretches in pink; cysteine-rich domains (CRDs) are indicated in underlines, cysteine residues are in red. The C terminal CRDs printed in italics were chosen for raising the polyclonal antibodies.
doi:10.1371/journal.pone.0022725.g003

minicollagens (NvNCol-1, NvNCol-3 and NvNCol-4) showed a comparable temporal and local expression. Initial signals in the late gastrula stage appeared spot-like and were evenly distributed (Figure 4A, E, I). In planula larvae the expression is significantly increased at the hypostomal area (Figure 4B, F, J). In primary polyps and adult animals minicollagen expression is mainly restricted to the tentacles and the hypostome (Figure 4C, G, K). NvNCol-3 showed additional weaker signals throughout the body column, which were not detectable for the other assayed minicollagens (Figure 4G). Minicollagen expressing cells were cuboidal-shaped epithelial cells and could be detected both, in the ectodermal and entodermal tissue layers (Figure 4D, H, L).

Localization of nematocyst minicollagens by immunocytochemistry

To analyze the distribution of the different minicollagens on the protein level, we raised polyclonal antibodies against their respective C terminal CRD domains (Figure 3). We have shown that the CRD domains in *Hydra* minicollagens can be used as discriminating antigens for antibody production and do not show cross-reactions with other minicollagen proteins [13]. All minicollagen antibodies used in our study specifically recognized developing nematocysts throughout the animal in adult polyps (Figure 5A, E, I). In contrast to *Hydra*, nematocytes in *Nematostella* do not migrate or form nests of multiple cells, which produce the same nematocyst type. As in the ISH experiment, the tentacles showed the highest density of minicollagen positive cells (Figure S1). Interestingly, the distribution of the different minicollagens among the various capsule types was inhomogeneous. NvNCol-1 could be detected in basitrichous haplonemas and microbasic mastigophores (Figure 5B–C). Spirocysts however, did not show any NvNCol-1 signal. This is demonstrated in Figure 5D by a co-staining with anti-NvNCol-4 antibody (green), which shows a developing spirocyst positive for NvNCol-4 but not for NvNCol-1. NvNCol-3 and NvNCol-4 were detected in all three capsule types with slight variations in their intensity (Figure 5E–L). While the NvNCol-3 antibody yielded strong signals in all capsule types (Figure 5F–H), the anti-NvNCol-4 staining was more pronounced in basitrichous haplonemas (Figure 5J) than in microbasic mastigophores and spirocysts (Figure 5K–L). The anti-NvNCol-1

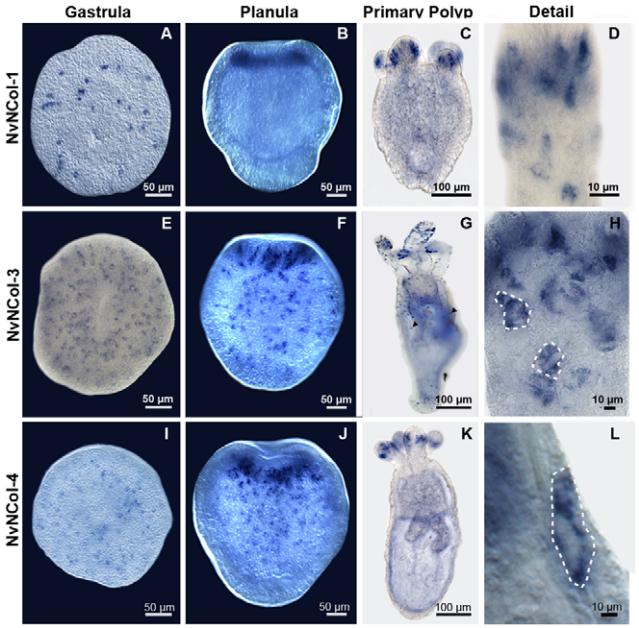

Figure 4. Whole mount *in situ* hybridization for minicollagen genes at different developmental stages of *Nematostella vectensis*. Gene expression patterns for *NvNCol-1* (A–D), *NvNCol-3* (E–H), and *NvNCol-4* (I–L). Arrows in G denote *NvNCol-3* positive signals distributed along the body column. Dotted lines in H and L mark the borders of nematocytes showing positive signals. Scale bars are 100 µm (C, G and K), 50 µm (A, B, E, F, I and J), and 10 µm (D, H and L).
doi:10.1371/journal.pone.0022725.g004

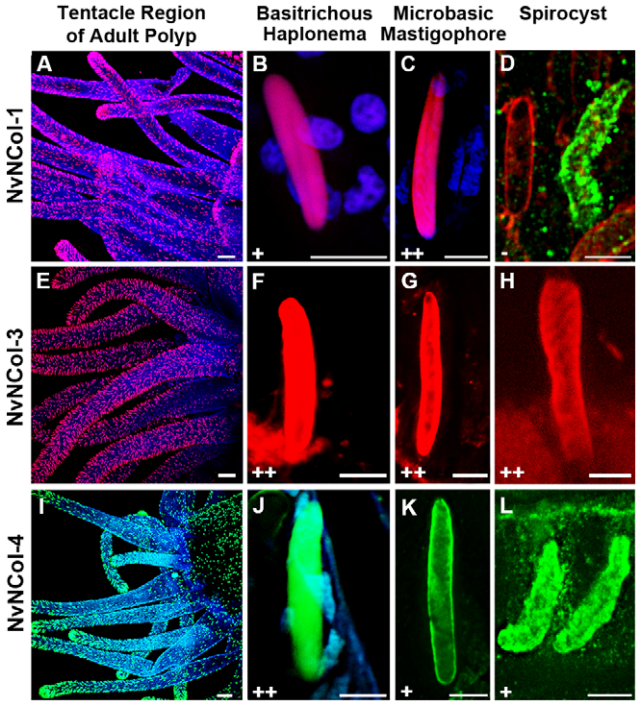

Figure 5. Detection of *Nematostella* minicollagens by immunocytochemistry. Adult polyps were stained with polyclonal minicollagen antibodies and DAPI. A–D. NvNCol-1 staining for different capsule types. D shows a co-staining with NvNCol-4 antibody (green) to demonstrate a lack of NvCol-1 staining in developing spirocysts. E–H. staining for nematocysts using anti-NvNCol-3 antibody. I–L. NvNCol-4 staining of different nematocysts. In A–C and E–H minicollagens were stained with Alexa-568 (red) and in I–L with Alexa-488 (green). + positive signal. ++ strong signal. − no signal. Scale bars are 100 µm (A, E, and I), 10 µm (L), and 5 µm (B, C, D, F, G, H, J, and K).
doi:10.1371/journal.pone.0022725.g005

antibody showed a stronger staining for microbasic mastigophores (Figure 5C) than for basitrichous haplonemas (Figure 5B). All signals detected by the minicollagen antibodies were restricted to the capsule body and did not show any tubule structures. A tubule staining had been expected for NvNCol-1 due to the homology of the cysteine pattern in its truncated C terminal CRD to the one in *Hydra* NCol-15 [13]. In summary, NvNCol-3 appeared to be a basic component of all capsule types, whereas the other minicollagens showed variations in their distribution among different capsule types.

As in *Hydra*, none of the minicollagen antibodies detected mature capsules, which is probably due to the densely polymerized wall structure. There was, however, a noticeable exception. Mature spirocysts were positive for both anti-NvNCol-3 and NvNCol-4, which might be due to the thinner wall structure of this capsule type (Figure S2). In contrast to *Hydra*, we were not able to detect minicollagen signals in Western Blots of isolated capsules under reducing conditions (Figure 6). *Hydra* nematocysts are extremely sensitive to reducing agents and minicollagens can be readily solubilized from the capsule wall by reduction [11]. *Nematostella* minicollagens were only detectable in tissue lysates containing developing nematocysts, indicating that after maturation minicollagen molecules were not only cross-linked by a disulfide-dependent process but by additional covalent bonds. The calculated molecular masses for the assayed minicollagens are 14.5 kDa for NvNCol-1, 11.2 kDa for NvNCol-3, and 14.7 kDa for NvNCol-4. The detected Western blot bands showed slightly higher apparent molecular masses for the minicollagen monomers (Figure 6), which is probably due to a retarded gel migration of the extended collagen molecules. All minicollagen antibodies detected additional bands at higher molecular masses, which might indicate posttranslational modification and cross-linking. This phenomenon was more pronounced for NvNCol-3 than for the other minicollagens.

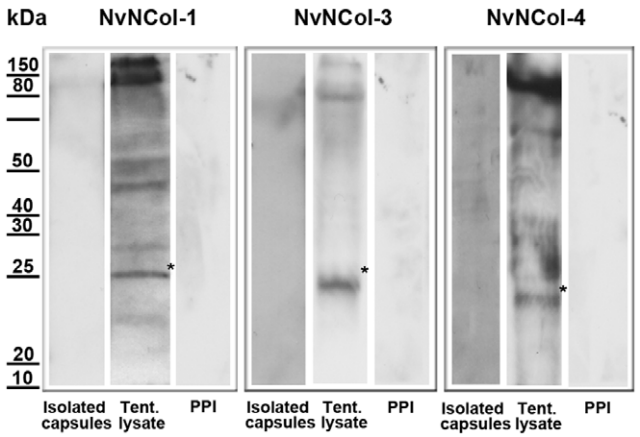

Figure 6. Detection of minicollagens by Western blot analysis. In each lane either isolated capsules or tentacle lysates of one adult head were applied. Preimmune serum (PPI) staining of tentacle lysates was used as negative control for each antibody. The asterisks mark the positions of the putative minicollagen monomer bands.
doi:10.1371/journal.pone.0022725.g006

Discussion

The characterization of the *Nematostella* cnidom opens an important evolutionary research perspective as it provides a basis for comparative molecular analyses on a complex organelle system, which probably contributed to the survival of the cnidarian clade since the Cambrian explosion. Furthermore, the reduced cnidocyst repertoire of Anthozoa compared to Medusozoa [16] is believed to reflect a basal state, which could allow insights into the evolutionary origin of nematocysts. Our study clearly defines three cnidocyst types in *Nematostella*, with varying distribution during the different developmental stages and along the body axis. The dominating nematocyst in early development and throughout the body column of all stages is the basitrichous haplonema, while spirocysts are clearly a feature of adult animals and most pronounced in the tentacle region, where they are probably used for prey capture (Figure 2). Spirocysts are often not classified as nematocysts due to their thin wall structure [16]. Our TEM and immunocytochemistry data confirm this notion and in addition demonstrate an apparent lack of a defined opercular structure in this capsule type. On the molecular level, though, our minicollagen stainings clearly demonstrate common protein components between spirocysts and other cnidocysts. Interestingly, spirocysts were the only capsule type, which was not positive for all three minicollagens tested. They lacked a staining for NvNCol-1 (Figure 5D), which is a derived minicollagen with altered CRD patterns. This indicates a simpler molecular architecture of spirocysts, which relies on fewer minicollagen molecules, in particular on NvNCol-3, which is the most conserved member of the protein family. Taken together, spirocysts may represent a primitive form of nematocysts, in which the thickening of the capsule wall and more elaborate structures like opercular flaps and tubule spines have not been realized. The evolutionary process leading to more sophisticated capsule types was apparently accompanied by a diversification of minicollagens. This is emphasized by the fact that the most simplified version of the minicollagen molecule, as in *Hydra* NCol-1 and *Nematostella* NCol-3, is conserved throughout all cnidarians analyzed so far, while minicollagens with more derived domain patterns show a restricted distribution [8].

An intriguing aspect of *Nematostella* minicollagens is the fact that their polymerization appears to involve additional cross-links different from intermolecular cysteine bonds. While minicollagens in *Hydra* can be readily solubilized from mature capsules by treatment with DTT, *Nematostella* minicollagens from mature capsules were resistant to reduction and could only be visualized biochemically in lysates of developing nematocytes. This behavior is reminiscent of fibrillar matrix collagens and might point to a closer relation of *Nematostella* minicollagens to ECM collagens. Such intermolecular cross-links were apparently lost in the more derived nematocysts of medusozoans in which the minicollagen repertoire got significantly expanded.

Materials and Methods

Nematostella culture

Nematostella polyps and embryos were kept in 1/3 seawater (Hand and Uhlinger 1992, Tropic Marine) at 18°C in the dark and fed once or two times a week with *Artemia nauplii*. Induction and gametogenesis were carried out as described before [17]. Oocytes were fertilized *in vitro* to synchronize development.

Isolation of Nematocysts

Intact, undischarged nematocysts were isolated from *Nematostella* tissue by centrifugation of frozen and thawed hypostomal tissue using isolation solution (50% Percoll, 10% sucrose, 0.003% Triton X-100) at 8200 rpm and 4°C. The isolated capsules were stored in PBS/10% sucrose at −20°C. To increase the yield of spirocysts several runs were done with decreasing Percoll concentration (50–30%).

Quantitative Nematocyst Analysis

For the quantitative analysis of nematocysts, 50 planula larvae, 50 primary polyps and three adult animals of equal size (sectioned into four parts, and evaluated individually) were dissolved in 2% SDS, spread on a slide and the nematocysts of 6 parallel lanes were counted using brightfield microscopy (Nikon Eclipse 80*i*). The experiment was repeated three times.

Microscopy. Fluorescence images, as well as phase contrast and interference contrast images were captured with the Nikon Eclipse 80*i*, confocal images with the Nikon A1R laser-scanning microscope.

SEM Analysis

Isolated nematocysts were applied to Poly-L-lysine coated cover slides (Sigma-Aldrich Chemie GmbH) and incubated for 10 min in 0.2% glutaraldehyde/2% formaldehyde. After several washes in PBS the procedure was repeated with 2.5% glutaraldehyde/PBS. For dehydration the slides were washed with increasing concentrations of ethanol in PBS before transferring to 100% acetone.

DNA Sequence Analysis

Commonly used recombinant techniques such as gel electrophoresis, sub-cloning, growth of plasmids, and restriction nuclease digestions were carried out as described by Maniatis et al. (1982). For DNA sequence determination fragments were cloned into a pGEM-T vector (Promega). DNA sequencing was done by Eurofins MWG Operon's sequencing service. Sequence data were analyzed with the sequence analysis software Chromas lite (Technelysium Pty Ltd).

In Situ Hybridization

For fixation, relaxed adult polyps were paralyzed with 3.57% $MgCl_2$ in *Nematostella* medium and fixed for 1 h with 4% paraformaldehyde. The polyps were then washed in PBT (PBS and 0.1% Tween20) and incubated for 1 h in MeOH followed by several washes in PBT with decreasing concentrations of MeOH. Polyps were afterwards treated for 5 min with PBT containing 10 µg/ml Proteinase K. Proteinase K digestion was stopped by incubation in 4 mg/ml glycine in PBT for 10 min. Afterwards the adult polyps were incubated for 10 min in 100 mM Triethanolamine (TEA) and 10 min in 100 mM TEA/0.25% acetic anhydride. After two washes in PBT (10 min) the polyps were fixed in 4% paraformaldehyde for 20 min, then washed five times 5 min in PBT and pre-hybridized in a solution containing 50% formamide, 5× SSC, 200 µg/ml yeast-RNA, 0.1% Chaps, 1× Denhardt's, 100 µg/ml heparin, and 0.1% Tween20) for 2 h at 60°C. After adding the heat-denatured, digoxigenin-labeled probe (0.1 ng/µl), samples were hybridized for two days at 60°C followed by several washes in PBT with decreasing concentrations of hybridization solution. The polyps were then incubated for 2 h in blocking solution (1% blocking reagent (Roche) in PBT, 0.02% sodium acid). The hybridized probe was detected using anti-DIG/AP (Roche) at 1/3000 in blocking solution and incubated over night at 4°C. After incubating for 5 min in both NTMT (100 mM NaCl, 100 mM Tris pH 9.5, 50 mM $MgCl_2$, 0.1% Tween20) and 1 mM Levamisol/NTMT the staining reaction was performed using NBT/BCIP (Roche ×50 solution) for 45–60 min at 37°C. After staining, the polyps were mounted with PBS/Glycerol and

analyzed using the Nikon Eclipse 80*i* microscope with 4×, 20×, 40× and 60× interference contrast optics.

Immunoblotting

For western blot analysis the capsules were solubilized by heating (95°C, 10 min) in sample buffer (200 mM Tris-HCl pH 6.8, 8% SDS, 0.4% bromphenol blue, 40% glycerin, 1 M β-Mercaptoethanol) The samples were separated by SDS-PAGE using 12% gels, transferred to PVDF membranes and incubated with specific antibodies after blocking for 1 h with 5% skim milk powder in PBS/0.1% Tween 20. The primary antibody was detected using an antibody coupled to horseradish peroxidase (1:10.000) and the ECL chemoluminescence system (Amersham Biosciences).

Immunofluorescence

Relaxed animals were paralyzed with 3.57% $MgCl_2$ for several minutes and then fixed in Lavdovski's fixative (ethanol:formaldehyde:acetic acid:H_2O bidest; 50:10:4:36) over night. After several washing steps using PBT (0.1% Triton X-100 in PBS), the polyps were incubated over night at 4°C with NvNCol-1, NvNCol-3 or NvNCol-4 antibodies in PBS/0.1% BSA. Thereafter the polyps were washed several times in PBS and incubated for 2 h with anti-guinea pig (NvNCol-1, NvNCol-3) or anti-rabbit (NvNCol-4) antibody coupled to ALEXA Fluor 568/488 (Molecular Probes) at a 1/400 in PBS/0.1% BSA. The animals were washed again several times in PBS before mounting in PBS/Glycerol. Fluorescence image analysis was performed using the Nikon A1R laser-scanning microscope.

Supporting Information

Figure S1 Minicollagen-3 staining of *Nematostella* whole mounts. Overview; B. Hypostomal area; C. Body column; D. Foot region. Scale bars are 100 μm.
(TIF)

Figure S2 Anti-NvNCol-3 staining of mature nematocysts. A. Mature basitrichous haplonema. B. Mature microbasic mastigophore. C. Mature spirocyst. Scale bars are 5 μm.
(TIF)

Table S1 Quantitative analysis of capsules at different developmental stages.
(DOC)

Acknowledgments

We thank Thomas Holstein for critical reading of the manuscript, Prakash Balasubramanian for assistance with genomic data analysis, and Charles N. David for open peer review.

Author Contributions

Conceived and designed the experiments: SÖ. Performed the experiments: CZ MOD TT. Analyzed the data: SÖ CZ. Contributed reagents/materials/analysis tools: TT. Wrote the paper: SÖ CZ.

References

1. Steele RE, David CN, Technau U (2011) A genomic view of 500 million years of cnidarian evolution. Trends Genet 27: 7–13.
2. Chapman JA, Kirkness EF, Simakov O, Hampson SE, Mitros T, et al. (2010) The dynamic genome of Hydra. Nature 464: 592–6.
3. Putnam NH, Srivastava M, Hellsten U, Dirks B, Chapman J, et al. (2007) Sea anemone genome reveals ancestral eumetazoan gene repertoire and genomic organization. Science 317: 86–94.
4. Wittlieb J, Khalturin K, Lohmann JU, Anton-Erxleben F, Bosch TC (2006) Transgenic Hydra allow in vivo tracking of individual stem cells during morphogenesis. Proc Natl Acad Sci U S A 103: 6208–6211.
5. Renfer E, Amon-Hassenzahl A, Steinmetz PR, Technau U (2010) A muscle-specific transgenic reporter line of the sea anemone, Nematostella vectensis. Proc Natl Acad Sci U S A 107: 104–108.
6. Özbek S (2010) The cnidarian nematocyst: a miniature extracellular matrix within a secretory vesicle. Protoplasma. pp 1–6.
7. Özbek S, Balasubramanian PG, Holstein TW (2009) Cnidocyst structure and the biomechanics of discharge. Toxicon 54: 1038–1045.
8. David CN, Özbek S, Adamczyk P, Meier S, Pauly B, et al. (2008) Evolution of complex structures: minicollagens shape the cnidarian nematocyst. Trends Genet 24: 431–438.
9. Nuchter T, Benoit M, Engel U, Özbek S, Holstein TW (2006) Nanosecond-scale kinetics of nematocyst discharge. Curr Biol 16: R316–318.
10. Holstein TW, Benoit GM, Herder Gv, Wanner G, David CN, et al. (1994) Fibrous Mini-Collagens in Hydra Nematocysts. Science 265: 402–404.
11. Özbek S, Pertz O, Schwager M, Lustig A, Holstein T, et al. (2002) Structure/function relationships in the minicollagen of Hydra nematocysts. J Biol Chem 277: 49200–49204.
12. Meier S, Jensen PR, David CN, Chapman J, Holstein TW, et al. (2007) Continuous molecular evolution of protein-domain structures by single amino acid changes. Curr Biol 17: 173–178.
13. Adamczyk P, Meier S, Gross T, Hobmayer B, Grzesiek S, et al. (2008) Minicollagen-15, a novel minicollagen isolated from Hydra, forms tubule structures in nematocysts. J Mol Biol 376: 1008–1020.
14. Weill R (1934) Contribution a l'etude des cnidaires et de leurs nematocystes, I. Recherehes sur les nematocystes (Morphologie, Physiologie Developpement). Trav. pp 1–347.
15. Weill R (1934) Contribution a l'etude des cnidaires et de leurs nematocystes. II. Valeur taxonomique du cnidome. Trav. pp 351–701.
16. Kass-Simon G, Scappaticci JAA (2002) The behavioral and developmental physiology of nematocysts. Can J Zool 80: 1772–1794.
17. Fritzenwanker JH, Technau U (2002) Induction of gametogenesis in the basal cnidarian Nematostella vectensis (Anthozoa). Dev Genes Evol 212: 99–103.

PROCEEDINGS OF THE ROYAL SOCIETY B BIOLOGICAL SCIENCES

Neurotoxin localization to ectodermal gland cells uncovers an alternative mechanism of venom delivery in sea anemones

Yehu Moran, Grigory Genikhovich, Dalia Gordon, Stefanie Wienkoop, Claudia Zenkert, Suat Özbek, Ulrich Technau and Michael Gurevitz

Proc. R. Soc. B published online 2 November 2011
doi: 10.1098/rspb.2011.1731

PROCEEDINGS OF THE ROYAL SOCIETY B

FirstCite® e-publishing

Proc. R. Soc. B
doi:10.1098/rspb.2011.1731
Published online

Neurotoxin localization to ectodermal gland cells uncovers an alternative mechanism of venom delivery in sea anemones

Yehu Moran[1,2,*], Grigory Genikhovich[2], Dalia Gordon[1], Stefanie Wienkoop[3], Claudia Zenkert[4], Suat Özbek[4], Ulrich Technau[2] and Michael Gurevitz[1]

[1]*Department of Molecular Biology and Ecology of Plants, George S. Wise Faculty of Life Sciences, Tel Aviv University, Ramat Aviv, 69978 Tel Aviv, Israel*
[2]*Department of Molecular Evolution and Development, and* [3]*Department of Molecular Systems Biology, Faculty of Life Sciences, University of Vienna, Althanstrasse 14, 1090 Vienna, Austria*
[4]*Department of Molecular Evolution and Genomics, Centre of Organismal Studies, Heidelberg University, Im Neuenheimer Feld 230, 69120 Heidelberg, Germany*

Jellyfish, hydras, corals and sea anemones (phylum Cnidaria) are known for their venomous stinging cells, nematocytes, used for prey and defence. Here we show, however, that the potent Type I neurotoxin of the sea anemone *Nematostella vectensis*, Nv1, is confined to ectodermal gland cells rather than nematocytes. We demonstrate massive Nv1 secretion upon encounter with a crustacean prey. Concomitant discharge of nematocysts probably pierces the prey, expediting toxin penetration. Toxin efficiency in sea water is further demonstrated by the rapid paralysis of fish or crustacean larvae upon application of recombinant Nv1 into their medium. Analysis of other anemone species reveals that in *Anthopleura elegantissima*, Type I neurotoxins also appear in gland cells, whereas in the common species *Anemonia viridis*, Type I toxins are localized to both nematocytes and ectodermal gland cells. The nematocyte-based and gland cell-based envenomation mechanisms may reflect substantial differences in the ecology and feeding habits of sea anemone species. Overall, the immunolocalization of neurotoxins to gland cells changes the common view in the literature that sea anemone neurotoxins are produced and delivered only by stinging nematocytes, and raises the possibility that this toxin-secretion mechanism is an ancestral evolutionary state of the venom delivery machinery in sea anemones.

Keywords: sea anemone; neurotoxin; nematocyst; venom

1. INTRODUCTION

The phylum Cnidaria consists of venomous carnivores such as hydras, jellyfish, corals and sea anemones [1], of which some comprise risks to human health [2]. Despite unusual morphological and genetic diversity, all cnidarians bear specialized cells named nematocytes that contain miniature stinging devices, nematocysts, used for hunting and defence [3,4]. Nematocysts are highly complex intracellular proteinaceous structures and their release is considered to be among the fastest biological processes in nature [5]. It is widely assumed that the venom of cnidarians is produced in the nematocytes and is injected via the nematocysts upon encounter [1,3]. Direct proof for this assumption relies mostly on chromatographic fractionation of nematocysts from several species [6–8], and on immunolocalization of phospholipases and pore-forming toxins to the nematocysts of a single jellyfish and a single sea anemone species, respectively [9,10]. Intriguingly, the nematocyst-derived fractions were often less toxic than whole tentacle extracts, raising the possibility that toxins may also reside in non-nematocyst compartments [11,12]. Among the better studied cnidarian venom components are the potent sea anemone Type I neurotoxins. These are peptides of 46–51 amino acids that inhibit the inactivation of voltage-gated sodium channels, thus inducing paralysis of prey or predator (reviewed in [13,14]).

The starlet sea anemone *Nematostella vectensis* of the northwest Atlantic serves as a model organism in the study of cnidarians owing to the easily inducible spawning, fast embryogenesis and its completely sequenced genome [15–17]. While studying the evolution and expression patterns of sea anemone neurotoxins, we found that *N. vectensis* produces a single Type I neurotoxin, Nv1, which is encoded by multiple genes [18]. Moreover, the Nv1 transcript in young life stages of *N. vectensis* is unspliced, introducing a pre-mature stop codon and raising the possibility that the neurotoxin is expressed solely in adult anemones [19]. This finding is surprising since nematocytes in *N. vectensis* appear as soon as 24 h after fertilization [20]. Therefore, we examined immunochemically at which developmental stage the toxin can be detected. This analysis revealed an unexpected cellular localization of Nv1, raising the question as to its mechanism of delivery.

2. MATERIAL AND METHODS

(a) *Animal culture*

Nematostella vectensis polyps were raised in the laboratory and spawning was induced as previously described [15].

* Author for correspondence (yehum79@yahoo.com).

Electronic supplementary material is available at http://dx.doi.org/10.1098/rspb.2011.1731 or via http://rspb.royalsocietypublishing.org.

Received 17 August 2011
Accepted 12 October 2011

Anemonia viridis polyps were collected at Michmoret, Israel, and kept in artificial sea water at 28°C in order to minimize the number of symbiotic zooxanthellae. *Anthopleura elegantissima* polyps were kindly provided by Dr D. Abed-Navandi (Haus des Meeres, Vienna, Austria). The polyps were fed twice a week with freshly hatched *Artemia salina* nauplii. Zebrafish larvae were kindly provided by Dr Y. Gothilf (Tel Aviv University) and were handled according to standard procedures [21].

(b) *Antibody production and enzyme-linked immunosorbent assay (ELISA)*

Nv1 was produced in recombinant form using a method previously described for the *A. viridis* toxin Av3 [22]. Toxin purity was assessed by mass spectrometry. Purified toxin was used to immunize New Zealand white rabbits (performed by Adar Biotech, Israel; the detailed immunization protocol is available upon request from the authors). Specificity of the antiserum was assayed by ELISA according to a protocol detailed in electronic supplementary material, figure S1.

(c) *Immunohistochemistry and imaging*

For whole-mount immunostaining, *Nematostella* and *Anemonia* samples were fixed for 1 h in 4 per cent paraformaldehyde in 0.1 per cent Tween-20 in phosphate buffered saline (PBS) (1.86 mM NaH_2PO_4, 8.4 mM Na_2HPO_4, 175 mM NaCl, pH 7.4). After fixation, the samples were washed in 0.1 per cent Tween-20 in PBS and stored in absolute methanol at −20°C until use. After stepwise rehydration, the samples were blocked for 2 h with 20 per cent sheep serum (Sigma) and 1 per cent bovine serum albumin (BSA) (fraction V) in PBS containing 0.2 per cent Triton X-100. Primary antibodies were added at various dilutions for optimal results (electronic supplementary material, table S1). After overnight incubation at 4°C, the samples were washed five times with 0.2 per cent Triton X-100 in PBS, blocked again, and then incubated with secondary antibodies (electronic supplementary material, table S1). The samples were then washed five times with 0.2 per cent Triton X-100 in PBS and mounted on microscope slides in SlowFade (Invitrogen, USA) or VectaShield (Reactolab SA, Switzerland). Maceration was performed as described for *Hydra* [23]. The immunostaining procedure thereafter was similar to that of the whole-mount. The samples were visualized using a Zeiss LSM 510 META scanning confocal microscope (Carl Zeiss, Germany), a Leica TCS SP5 X scanning confocal microscope (Leica, Germany) or a Nikon Eclipse 80i fluorescent microscope.

(d) *Protein extraction from tentacles*

Tentacles of sea anemones starved for at least 4 days were removed and frozen at −80°C. After 1 h, the tentacles were thawed on ice and cold non-denaturing extraction buffer (20 mM Tris HCl pH 8, 137 mM NaCl, 10% glycerol, 1% Nonidet P-40 (NP-40), 2 mM ethylenediaminetetraacetic acid (EDTA)) with protease inhibitor cocktail (Roche, Germany) was added. The tentacles were incubated at 4°C under slow rotation for 3 h and then centrifuged at 20 000*g* for 10 min. The supernatant was centrifuged through an Amicon Ultra centrifugal filter (Millipore, USA) with a 10 kDa cutoff according to the manufacturer's instructions. The filtrate was then applied to an Amicon Ultra centrifugal filter (Millipore) with a 3 kDa cutoff and concentrated to a minimal volume. The buffer was then exchanged with 50 mM Tris HCl. Samples were kept at −20°C until use.

(e) *Mass spectrometry*

Peptides were separated with an ultraHPLC Eksigent system (Axel Semrau G, bH and CoKG, Germany) using a C_{18} reversed-phase column (150 mm, 100 μm internal dimensions, Chromolith, Merck, Germany) directly coupled to an Orbitrap XL mass spectrometer (Thermo Scientific, Germany). The peptides were eluted with a 40 min gradient of 0–60% acetonitrile. The Orbitrap was run in Fourier transform full scan positive mode with a resolution of 100 000. The *m*/*z* range was set from 600 to 1800 for expected three to five times charged peptide masses.

(f) *Nv1 ectopic expression*

Primers bearing *Pac*I and *Asc*I (New England Biolabs, USA) restriction sites were used to amplify by PCR one of the Nv1 genes together with the 1.8 kb region upstream of the transcription start site. The PCR product was cloned at the corresponding restriction sites of a *Nematostella* expression vector bearing the mCherry reporter gene [24]. To ensure the expression of an Nv1-mCherry chimera, the TAA stop codon of Nv1 and the ATG translation start site of mCherry were removed. A $(Gly\text{-}Gly\text{-}Ser)_2$ linker between Nv1 and mCherry was introduced by the PCR primer in order to improve folding. Injections into fertilized *Nematostella* oocytes were performed as previously described [24].

(g) *Toxicity assays*

Recombinant toxins were dissolved to a concentration of 0.5 mg ml^{-1} in filtrated artificial sea water or E3 medium [21] for assays with 1-day-old *Artemia salina* and 3-day-old *Danio rerio*, respectively. The assays were performed in 24-well plates (Thermo-Fisher Scientific). Paralysis and lethality were assessed by microscopic observation and responsiveness to contact with a plastic tip. BSA of 5 mg ml^{-1} or mutant toxin 0.5 mg ml^{-1} were used in control experiments.

3. RESULTS AND DISCUSSION

(a) *The Nv1 neurotoxin of* Nematostella vectensis *is localized to non-nematocyte cells*

In order to localize Nv1 expression in *N. vectensis*, we used the anti-Nv1 serum raised in rabbits. Whole-mount immunohistochemistry revealed no staining at early life stages such as the 3–6 day-old planula larvae (figure 1), which was in accordance with our previous observation at the RNA level [19]. In 9 day-old primary polyps, which settle and begin to hunt, a few cells containing Nv1-positive vesicles were observed in the four primary tentacles (figure 1), whereas numerous cells were stained in the tentacles of the adult polyp (figures 1 and 2*a*, and electronic supplementary material, movie S1). The staining did not co-localize with the numerous nematocytes easily observed by light microscopy owing to their dense nematocysts (figure 1*c*). Interestingly, some toxin appeared in clumps outside of the ectodermal layer (figure 2*a* and electronic supplementary material, movie S1).

While tentacle nematocytes in *N. vectensis* are thin and long like in other sea anemone species (electronic supplementary material, figure S2), the anti-Nv1-stained cells are thick, slightly round and filled with vesicles positive for the antibody (figures 1 and 2*b*), strongly suggesting that the Nv1-positive cells are gland cells. To validate these results, we co-stained *Nematostella* tentacles with anti-Nv1 and antibodies against the tubule component chondroitin and the capsule component Nv-Ncol 3, two

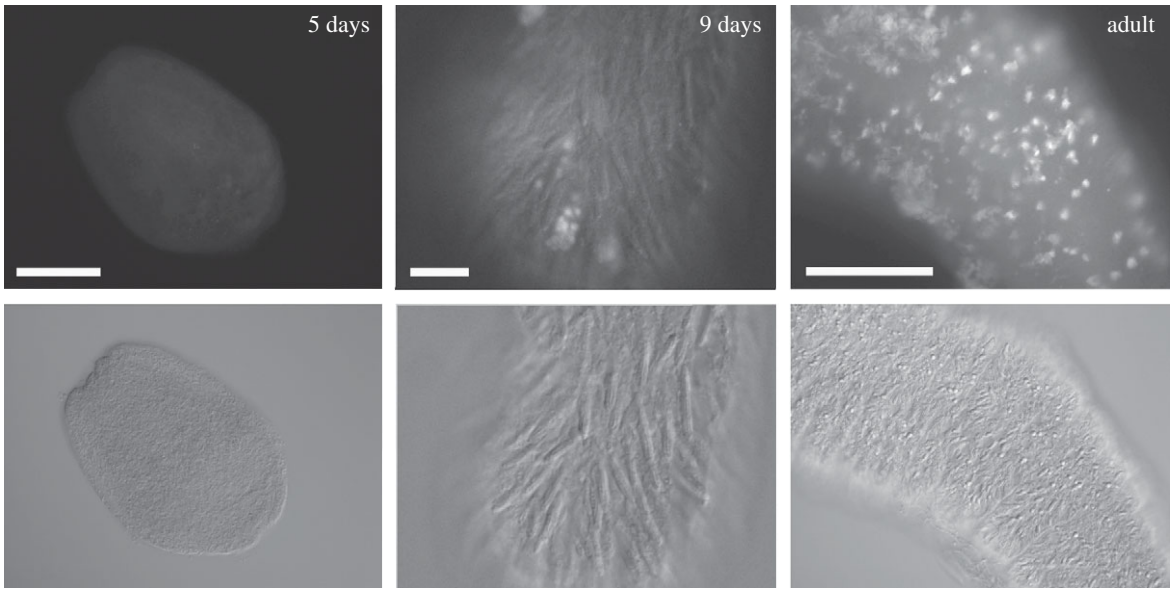

Figure 1. Nv1 expression in various life stages of *N. vectensis*. Nv1 antibody and an Alexa Fluor-conjugated secondary antibody were used to localize Nv1 in whole-mounts of three *N. vectensis* developmental stages: 5 day-old planula, 9 day-old primary polyp and an adult. Scale bars: 100, 50 and 200 μm.

molecular components detectable at early developmental stages of nematocysts [25–27]. No co-localization was observed and each antibody stained distinct structures in the tentacle, precluding the possibility that the anti-Nv1-stained cells are developing nematocytes that contain vesicles (figure 2*b*,*c*). To verify the observations made on the whole-mounts, we immunostained tentacle macerates. As shown in figure 2*d* and electronic supplementary material, figure S3, the cells containing the Nv1 toxin indeed differ substantially from nematocytes in shape, and they lack nematocysts. Granule-rich gland cells that highly resemble the immunostained cells are common in the *Nematostella* tentacle ectoderm ([28]; electronic supplementary material, figure S2) and were also described in tentacles of other sea anemone species [29–31]. Although accessibility of nematocysts for antibody staining is highly increased upon maceration with acetic acid that leads to their discharge, not a single nematocyst stained with anti-Nv1 was observed in the macerated *Nematostella* tissues.

(b) *Localization of Type I neurotoxins in other sea anemone species*

Anemonia viridis (previously named *Anemonia sulcata*) is a common Mediterranean sea anemone species distantly related to *N. vectensis* [32]. It produces several Type I neurotoxins with moderate sequence similarity (approx. 50%) to Nv1 [14]. Nevertheless, the structure of Av2, the most abundant *A. viridis* neurotoxin, resembles that of Nv1 [19] and the anti-Nv1 antibody recognizes recombinant Av2 in ELISA (electronic supplementary material, figure S1).

Whole-mount anti-Nv1 staining of *A. viridis* tentacles revealed structures resembling the Nv1-containing gland cells described for *N. vectensis* (figures 3*a* and electronic supplementary material, figure S3). However, these cells were less abundant in *A. viridis*. In addition to the gland cells, numerous long threads were stained in the tentacle. Induced discharge of nematocysts by acetic acid substantially increased the number of the stained threads (figure 3*b*). Maceration of tentacles enabled a better examination of the gland cell structure (figure 3*c*) and also revealed that the stained threads are tubules of discharged nematocysts (figure 3*d*). Although the Nv1 antibody stained mostly the discharged nematocysts, several charged nematocytes were still accessible to the antibody (figure 3*e*), possibly owing to fractures in the capsule wall during maceration. Indeed, nematocytes in 10 μm thick tentacle cryosections were stained (figure 3*f*). The staining pattern in these stinging cells suggests that the toxin is associated with the tubule prior to discharge (figure 3*e*). The coiled tubule and the nematocyst structure indicate that the stained capsules are microbasic b-mastigophores, the nematocyte type previously identified in *A. viridis* tentacles (figure 3*e*) [33]. Toxin staining in these cells is restricted to the tubule and is not observed in the barbed shaft at the base of the tubule (figure 3*d*). This staining pattern supports the suggestion by Klug *et al.* [34]; that the venom is distributed along the tubule. It is important to note that various antibodies were reported to adhere non-specifically to capsules and threads (e.g. [35]), but in our experiments, the pre-immune serum and secondary antibodies did not stain nematocyst threads without anti-Nv1, indicating specific staining of Type I toxins (electronic supplementary material, figure S4).

The common pacific species *A. elegantissima* is much closer to *Anemonia* than to *Nematostella* based on morphological traits and molecular phylogeny (figure 4*a*) [32]. It produces several Type I neurotoxins with remarkable homology to Av2 (up to 96% identity and 98% similarity) [36]. We macerated *A. elegantissima* tentacles and stained them with the anti-Nv1 serum. Surprisingly, no stained nematocyst threads were observed, whereas clear staining was found in vesicle-containing cells, resembling the staining of the *N. vectensis* Type I toxin (figure 4*b*).

(c) *Further verification of toxin localization to gland cells*

The localization of Type I toxins to ectodermal gland cells rather than nematocytes was also analysed using fractionation and mass spectrometry. The tentacle protein was extracted without disruption of nematocyst capsules,

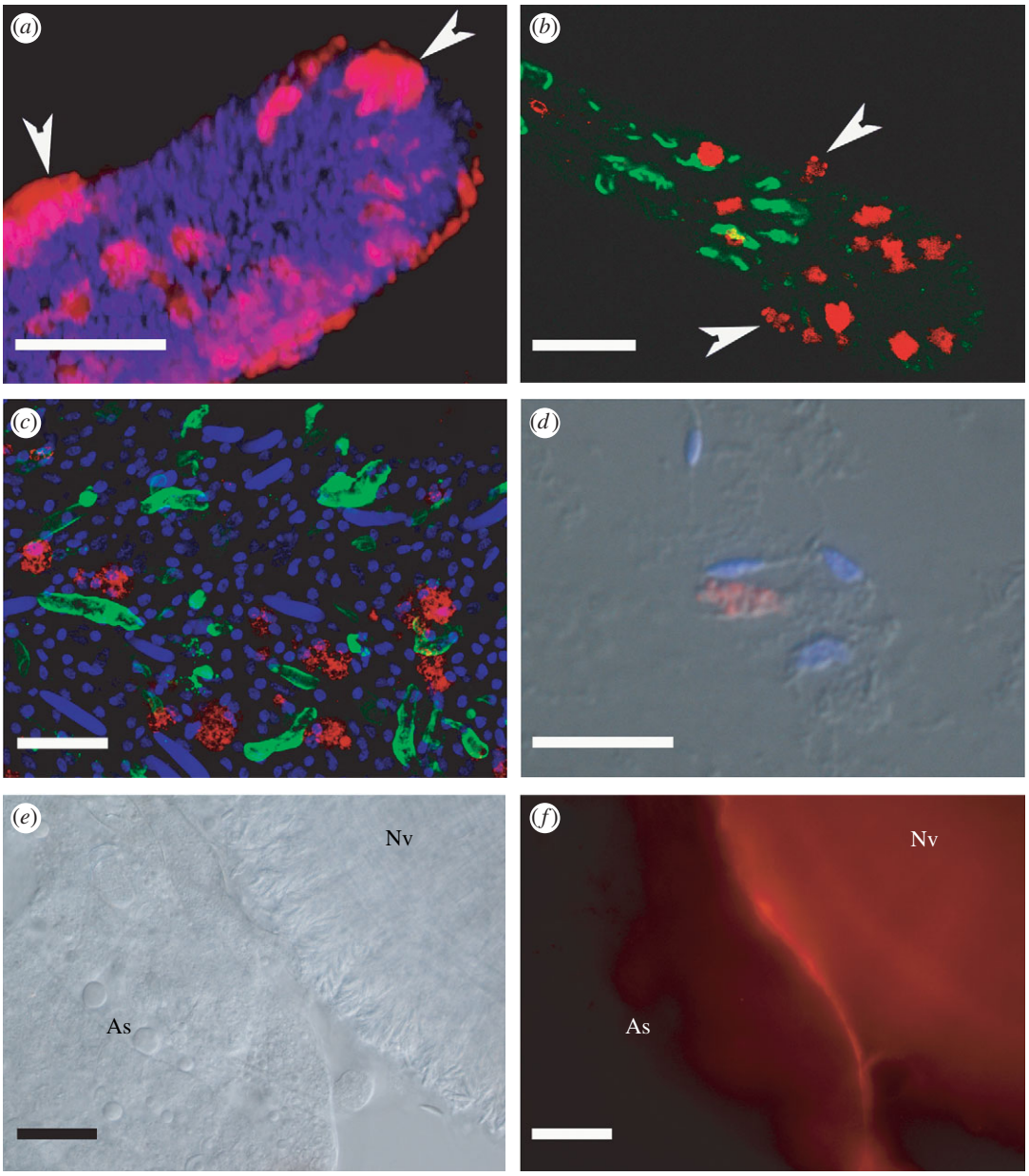

Figure 2. Nv1 is accumulated in gland cells of *N. vectensis* and is released to the water during preying. Nv1 antibody and an Alexa Fluor-conjugated secondary antibody were used to localize Nv1 (appear in red). Nuclei were stained with 4′,6-diamidino-2-phenylindole dihydrochloride (DAPI) (blue). (*a*) Nv1 is localized to thick gland cells inside the tentacle and to clumped structures at the tentacle surface (indicated by arrowheads). (*b*) Double immunostaining of Nv1 (red) and chondroitin (green; a proteoglycan involved in nematocyst tubule formation) shows that these molecules are also localized to different cells. Cells with Nv1-positive vesicles are designated by arrowheads. (*c*) Double immunostaining of Nv1 (red) and Nv-Ncol 3 (green; a minicollagen component of the nematocyst capsule) clearly shows that these peptides are localized to different cells. (*d*) An Nv1-containing gland cell in *N. vectensis* tentacle macerate. The vesicular structures suggest toxin accumulation in vesicles. (*e*,*f*) Nomarski and fluorescent images localize Nv1 to the surface of interaction between *N. vectensis* tentacles (shown as Nv) and *Artemia salina* (shown as As) during feeding. Scale bars: (*a*) 100 µm; (*b*) 25 µm; (*c*) 10 µm; (*d*) 20 µm and (*e*,*f*) 50 µm.

and following size-selection was analysed by mass spectrometry. Mass to charge ratios (*m*/*z*) identical or similar to those of the known Type I toxins of *N. vectensis*, *A. viridis* and *A. elegantissima* were detected in each of the corresponding samples (figure 4*c* and electronic supplementary material, figure S5). To further verify the specificity of the anti-Nv1 antibody staining, we performed a transgenesis assay. A measure of 1.8 kb of the sequence upstream of the *Nv1* transcription start site was used to drive the expression of the *Nv1::mCherry* fusion (electronic supplementary material, figure S6). Injection of this construct into fertilized *N. vectensis* eggs [24] resulted in transient expression of mCherry in random patches 24 h after fertilization, which did not resemble the native expression pattern of Nv1 (electronic supplementary material, figure S6). A similar phenomenon was also observed for sequences upstream of several other *Nematostella* genes and may result from the absence of other regulatory elements (U. Technau 2011, unpublished results). Nevertheless, these embryos were fixed and double-stained with anti-mCherry and anti-Nv1 antibodies (electronic supplementary material, figure S6). Since the earliest endogenous expression of Nv1 protein is observed in the primary polyp (figure 1), it is clear that all Nv1 protein at the gastrula stage can only have transgenic origin. The signals of anti-Nv1 and

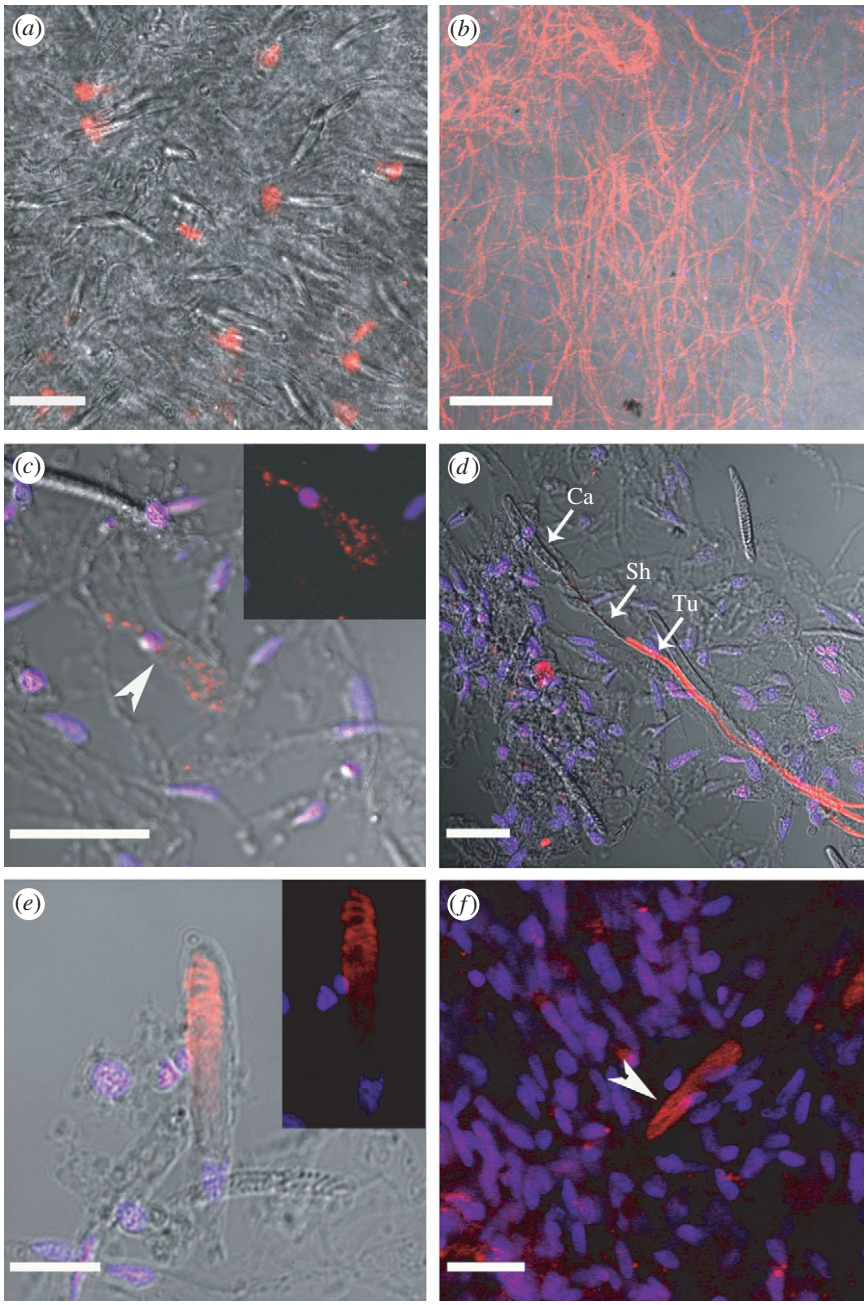

Figure 3. *Anemonia viridis* Type I neurotoxins are localized to both gland cells and nematocytes. Nv1 antibody and an Alexa Fluor 568-conjugated secondary antibody were used to localize Nv1 homologues in *A. viridis* (appear in red). Nuclei were stained with DAPI (blue). (*a*) In whole-mount tentacles, anti-Nv1 staining is observed in thick gland cells. (*b*) After treatment with acetic acid, numerous thread-like structures are stained in whole-mount tentacles. (*c*) Maceration of *A. viridis* tentacles reveals the structure of the gland cells (indicated by an arrowhead) and suggests that the neurotoxin is packed in vesicles (a non-merged image is provided as an inset). (*d*) Maceration reveals that the thread-like stained structures are tubules of *A. viridis* nematocysts (shown as Tu). Unlike the tubule, the capsule and the barbed shaft (indicated as Ca and Sh, respectively) are not stained. (*e*) The Nv1 immunostaining in charged nematocytes indicates that the tubule is coiled, and that the neurotoxin is probably packed on or inside the tubule prior to discharge (a non-merged image is provided as inset). (*f*) Cryosectioning of the tentacle enables anti-Nv1 immunostaining of a charged nematocyte (indicated by an arrowhead) without maceration. Scale bars: (*a*,*b*,*d*,*f*) 20 μm; (*c*) 50 μm and (*e*) 10 μm.

anti-mCherry clearly co-localized in the transgenic embryos and supplied sound evidence for the specificity of the Nv1 antibody for the toxin in the immunolocalization experiments (electronic supplementary material, figure S6).

(**d**) *Delivery of sea anemone neurotoxins*

To gain further insight on neurotoxin delivery in *N. vectensis*, tentacles were fixed during and after predation of *A. salina* nauplii. The tentacles that *a priori* were charged with toxin were nearly depleted of stained gland cells upon contact with the crustacean, and in some preparations, the surface of the tentacle was rich in stained large granules located outside of the cellular layer (electronic supplementary material, figure S7). The intense staining observed at the tentacle surface and in the narrow space between the tentacle and the prey suggested toxin secretion during predation (figure 2*e*,*f*; electronic supplementary material, movie S2 and figure S7).

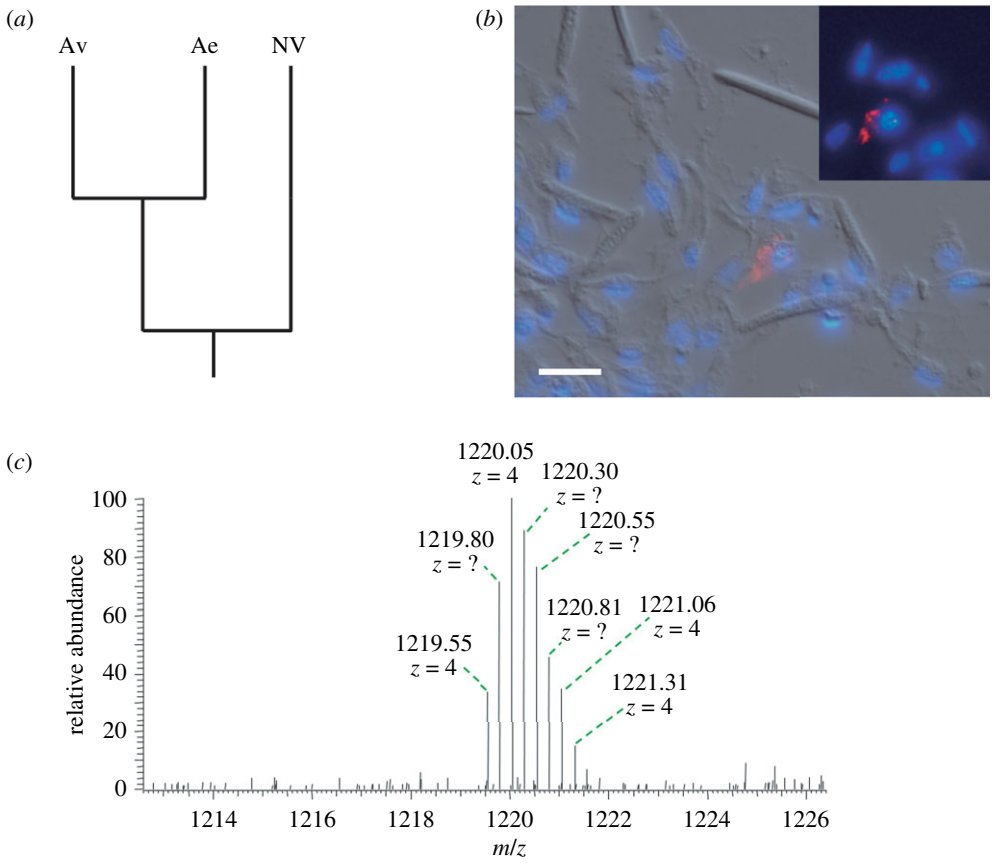

Figure 4. *Anthopleura elegantissima* Type I neurotoxins are localized to gland cells. (*a*) Phylogeny of *A. elegantissima*, *A. viridis* and *N. vectensis* based on previous analysis [32]. (*b*) Nv1 antibody staining of *A. elegantissima* tentacles localizes the toxin to granule-rich gland cells and suggests that the neurotoxin is packed in vesicles (a non-merged image is provided as an inset). Scale bar, 10 µm. (*c*) Mass spectrometry analysis of extracts from *A. elegantissima* tentacle soft tissue reveals mass to charge ratios (*m*/*z*) identical (approx. 8 ppm) to those of the APE 2-1 Type I neurotoxin (expected *m*/*z* of 1219.56 Da when $z = 4$).

To examine the possibility that the toxin released into the medium affects the prey, we exposed intact *Artemia* nauplii to recombinant neurotoxin (0.5 mg ml^{-1} Nv1 or Av2). Notably, impaired swimming, paralysis and death were observed within several hours, while 5 mg ml^{-1} BSA had no effect on control animals (electronic supplementary material, movie S3). Intoxication of zebrafish (*D. rerio*) larvae by Av2 was much faster than *Artemia* nauplii, and 10 min after exposure to 0.5 mg ml^{-1} toxin, all fish were either paralysed or exhibited strong convulsions and impaired swimming (electronic supplementary material, movie S4). Identical doses of Nv1 caused tail twitching accompanied by impaired swimming after 20 min and complete paralysis within 45 min. By contrast, fish exposed to 5 mg ml^{-1} BSA (control) were active during the entire experiment and did not exhibit any of the symptoms induced by the toxins. Moreover, application of the weakly active mutant toxin Av2^{L5A} slightly affected the fish only after several hours [37]. Thus, Type I neurotoxins can penetrate into prey even without nematocysts and reach their sodium channel targets. However, the fast paralysis of prey within seconds of interaction with the tentacle, compared with the slower paralysis observed in our experiments using recombinant toxins, suggests that piercing by the numerous discharging nematocysts expedites toxin delivery during capture of prey.

In the light of their phylogeny and living habitat, the differences in toxin localization and mechanism of venom delivery between *Nematostella* and *Anthopleura* to *Anemonia* despite contrasting phylogeny (figure 4*a*) suggest that the ecology of these species might have played a major role in the development of the venom apparatus. It is likely that nematocytes loaded with toxins are more efficient in envenomation compared with the gland cell secretion mechanism. Both *N. vectensis* and *A. elegantissima* feed on a limited variety of small animals [38–40], whereas *A. viridis* exhibits a more active feeding behaviour and preys on a wider variety, including larger animals [41]. Moreover, while *N. vectensis* and *A. elegantissima* avoid other species by contraction and *Nematostella* can burrow in the substrate, *A. viridis* is unable to contract and is exposed in its rocky environment and attacked by nudibranch molluscs [42]. The different ecologies of *N. vectensis* and *A. viridis* are also reflected by their different neurotoxin content, with a much greater arsenal in *Anemonia* [14,18]. Previous studies have already shown that diet and ecology probably affected the evolution of the venom arsenal and delivery devices in reptiles [43,44]. Since the complex venom production and delivery mechanisms require considerable energetic resources, but are crucial for survival, ecological shifts might have imposed a strong selective pressure on these systems to either evolve or atrophy. Whether the production of neurotoxins in gland cells of *A. viridis* is an additional mechanism of venom delivery or a remainder of an ancestral delivery system is still unknown. In a previous study, chromatographic analysis of *Stichodactyla gigantea* fractions suggested that a major fraction of the

neurotoxins, including a Type I toxin are located in an unknown tentacle compartment other than the nematocyte [45]. Thus, it is possible that neurotoxin-producing gland cells are common in most actiniarian species. Moreover, neurotoxins have been isolated from tentacles of cubozoan and scyphozoan cnidarians and although their cellular origin was unclear, they were not derived from nematocytes as was shown chromatographically [11,12,46]. This may suggest that an alternative venom delivery system also exists in non-actiniarian cnidarians. Yet, such an assumption requires the study of toxin localization in other cnidrarian classes, including non-actiniarian anthozoans.

It has been shown that both gland cells and nematocytes in Hydrozoa are derived from interstitial stem cells (for review see Bode [47]). Although the common cellular origin of gland cells and nematocytes has not been shown in Anthozoa, the fact that Golgi vesicles are involved in both secretion from gland cells and also in nematocyst morphogenesis raises a possibility for a common evolutionary ancestry of these two seemingly distinct venom-containing cells. Secretion of neurotoxins by gland cells is a slower delivery mechanism in comparison with nematocyst discharge and therefore it is hard to imagine that cnidarians would give up on the fast mechanism in favour of a slow delivery mechanism. On the other hand, secretion by gland cells may allow for delivery of larger amounts of the toxin and a recovery of the toxin-synthesizing cell, whereas nematocytes are single-use cells. Thus, whether venom-secreting ectodermal gland cells are an adaptation to the environment and the food regime in some anemones, or whether they actually represent the ancestral venom-secreting cell type, remains to be shown by the investigation of more anthozoan species.

We are indebted to A. Barbul, D. Frenkel, H. Levy and N. Ohad (Tel Aviv University) for their invaluable technical assistance and advice. We thank A. Gilles, S. Jahnel and M. Walzl (University of Vienna) for advice and for providing us with the paraffin sections shown in the electronic supplementary material. Y.M. was supported during this work by a short-term fellowship from EMBO (ASTF 269-2008). M.G. and D.G. were supported by the United States–Israel Binational Agricultural Research and Development grants IS-3928-06 and IS-4066-07, and by the Israeli Science Foundation grants 1008/05 and 107/08. U.T. was supported by the Austrian Research Council FWF and the Norwegian Reseach Council NFR.

REFERENCES

1 Ruppert, E. E. & Barnes, R. D. 1994 The cnidarians. In *Invertebrate zoology*, pp. 103–154, 6th edn. Philadelphia, PA: Saunders College Publishing.
2 Tibballs, J. 2006 Australian venomous jellyfish, envenomation syndromes, toxins and therapy. *Toxicon* **48**, 830–859. (doi:10.1016/j.toxicon.2006.07.020)
3 Kass-Simon, G. & Scappaticci Jr, A. A. 2002 The behavioral and developmental physiology of nematocysts. *Can. J. Zool.* **80**, 1772–1794. (doi:10.1139/z02-135)
4 Özbek, S., Balasubramanian, P. G. & Holstein, T. W. 2009 Cnidocyst structure and the biomechanics of discharge. *Toxicon* **54**, 1038–1045. (doi:10.1016/j.toxicon.2009.03.006)
5 Nüchter, T., Benoit, M., Engel, U., Ozbek, S. & Holstein, T. W. 2006 Nanosecond-scale kinetics of nematocyst discharge. *Curr. Biol.* **16**, R316–R318. (doi:10.1016/j.cub.2006.03.089)
6 Grotendorst, G. R. & Hessinger, D. A. 1999 Purification and partial characterization of the phospholipase A2 and co-lytic factor from sea anemone (*Aiptasia pallida*) nematocyst venom. *Toxicon* **37**, 1779–1796. (doi:10.1016/S0041-0101(99)00120-8)
7 Carrette, T. & Seymour, J. 2004 A rapid and repeatable method for venom extraction from cubozoan nematocysts. *Toxicon* **44**, 135–139. (doi:10.1016/j.toxicon.2004.04.008)
8 Schlesinger, A., Zlotkin, E., Kramarsky-Winter, E. & Loya, Y. 2009 Cnidarian internal stinging mechanism. *Proc. R. Soc. B* **276**, 1063–1067. (doi:10.1098/rspb.2008.1586)
9 Lotan, A., Fishman, L., Loya, Y. & Zlotkin, E. 1995 Delivery of a nematocyst toxin. *Nature* **375**, 456. (doi:10.1038/375456a0)
10 Basulto, A., Perez, V. M., Noa, Y., Varela, C., Otero, A. J. & Pico, M. C. 2006 Immunohistochemical targeting of sea anemone cytolysins on tentacles, mesenteric filaments and isolated nematocysts of *Stichodactyla helianthus*. *J. Exp. Zool. A Comp. Exp. Biol.* **305**, 253–258. (doi:10.1002/jez.a.256)
11 Ramasamy, S., Isbister, G. K., Seymour, J. E. & Hodgson, W. C. 2005 Pharmacologically distinct cardiovascular effects of box jellyfish (*Chironex fleckeri*) venom and a tentacle-only extract in rats. *Toxicol. Lett.* **155**, 219–226. (doi:10.1016/j.toxlet.2004.09.018)
12 Xiao, L., He, Q., Guo, Y., Zhang, J., Nie, F., Li, Y., Ye, X. & Zhang, L. 2009 *Cyanea capillata* tentacle-only extract as a potential alternative of nematocyst venom: its cardiovascular toxicity and tolerance to isolation and purification procedures. *Toxicon* **53**, 146–152. (doi:10.1016/j.toxicon.2008.10.023)
13 Wanke, E., Zaharenko, A. J., Redaelli, E. & Schiavon, E. 2009 Actions of sea anemone type 1 neurotoxins on voltage-gated sodium channel isoforms. *Toxicon* **54**, 1102–1111. (doi:10.1016/j.toxicon.2009.04.018)
14 Moran, Y., Gordon, D. & Gurevitz, M. 2009 Sea anemone toxins affecting voltage-gated sodium channels: molecular and evolutionary features. *Toxicon* **54**, 1089–1101. (doi:10.1016/j.toxicon.2009.02.028)
15 Fritzenwanker, J. H. & Technau, U. 2002 Induction of gametogenesis in the basal cnidarian *Nematostella vectensis* (Anthozoa). *Dev. Genes Evol.* **212**, 99–103. (doi:10.1007/s00427-002-0214-7)
16 Darling, J. A., Reitzel, A. R., Burton, P. M., Mazza, M. E., Ryan, J. F., Sullivan, J. C. & Finnerty, J. R. 2005 Rising starlet: the starlet sea anemone, *Nematostella vectensis*. *Bioessays* **27**, 211–221. (doi:10.1002/bies.20181)
17 Putnam, N. H. *et al.* 2007 Sea anemone genome reveals ancestral eumetazoan gene repertoire and genomic organization. *Science* **317**, 86–94. (doi:10.1126/science.1139158)
18 Moran, Y., Weinberger, H., Sullivan, J. C., Reitzel, A. M., Finnerty, J. R. & Gurevitz, M. 2008 Concerted evolution of sea anemone neurotoxin genes is revealed through analysis of the *Nematostella vectensis* genome. *Mol. Biol. Evol.* **25**, 737–747. (doi:10.1093/molbev/msn021)
19 Moran, Y., Weinberger, H., Reitzel, A. M., Sullivan, J. C., Kahn, R., Gordon, D., Finnerty, J. R. & Gurevitz, M. 2008 Intron retention as a posttranscriptional regulatory mechanism of neurotoxin expression at early life stages of the starlet anemone *Nematostella vectensis*. *J. Mol. Biol.* **380**, 437–443. (doi:10.1016/j.jmb.2008.05.011)
20 Marlow, H. Q., Srivastava, M., Matus, D. Q., Rokhsar, D. & Martindale, M. Q. 2009 Anatomy and development of the nervous system of *Nematostella vectensis*, an anthozoan cnidarian. *Dev. Neurobiol.* **69**, 235–254. (doi:10.1002/dneu.20698)
21 Westerfield, M. 1994 *The zebrafish book: a guide for the laboratory use of zebrafish*. Eugene, OR: University of Oregon Press.

22 Moran, Y., Kahn, R., Cohen, L., Gur, M., Karbat, I., Gordon, D. & Gurevitz, M. 2007 Molecular analysis of the sea anemone toxin Av3 reveals selectivity to insects and demonstrates the heterogeneity of receptor site-3 on voltage-gated Na-channels. *Biochem. J.* **406**, 41–48. (doi:10.1042/BJ20070233)

23 David, C. N. 1972 Quantitative method for maceration of hydra tissue. *Wilhelm Roux's Arch. Dev. Biol.* **171**, 259–263.

24 Renfer, E., Amon-Hassenzahl, A., Steinmetz, P. R. & Technau, U. 2010 A muscle-specific transgenic reporter line of the sea anemone, *Nematostella vectensis*. *Proc. Natl Acad. Sci. USA* **107**, 104–108. (doi:10.1073/pnas.0909148107)

25 Adamczyk, P. *et al.* 2010 A non-sulfated chondroitin stabilizes membrane tubulation in cnidarian organelles. *J. Biol. Chem.* **285**, 25 613–25 623. (doi:10.1074/jbc.M110.107904)

26 David, C. N., Ozbek, S., Adamczyk, P., Meier, S., Pauly, B., Chapman, J., Hwang, J. S., Gojobori, T. & Holstein, T. W. 2008 Evolution of complex structures: minicollagens shape the cnidarian nematocyst. *Trends Genet.* **24**, 431–438. (doi:10.1016/j.tig.2008.07.001)

27 Zenkert, C., Takahashi, T., Diesner, M. O. & Özbek, S. 2011 Morphological and molecular analysis of the *Nematostella vectensis* cnidom. *PLoS ONE* **6**, e22725. (doi:10.1371/journal.pone.0022725)

28 Frank, P. G. & Bleakney, J. S. 1976 Histology and sexual reproduction of the anemone *Nematostella vectensis* Stephenson. *J. Nat. Hist.* **10**, 441–449. (doi:10.1080/00222937600770331)

29 Watson, G. M. & Mariscal, R. N. 1983 Comparative ultrastructure of catch tentacles and feeding tentacles in the sea anemone *Haliplanella*. *Tissue Cell* **15**, 939–953. (doi:10.1016/0040-8166(83)90059-9)

30 Westfall, J. A. & Sayyar, K. L. 1997 Ultrastructure of neurons and synapses in the tentacle epidermis of the sea anemone *Calliactis parasitica*. *J. Morphol.* **232**, 207–216. (doi:10.1002/(SICI)1097-4687(199705)232:2<207::AID-JMOR5>3.0.CO;2-6)

31 Delgado, L. M., Couve, E. & Schmachtenberg, O. 2010 GABA and glutamate immunoreactivity in tentacles of the sea anemone *Phymactis papillosa* (Lesson 1830). *J. Morphol.* **271**, 845–852. (doi:10.1002/jmor.10838)

32 Daly, M., Chaudhuri, A., Gusmão, L. & Rodríguez, E. 2008 Phylogenetic relationships among sea anemones (Cnidaria: Anthozoa: Actiniaria). *Mol. Phylogenet. Evol.* **48**, 292–301. (doi:10.1016/j.ympev.2008.02.022)

33 Thomason, J. C. 1991 Cnida discharge and mechanism of venom delivery in *Anemonia viridis* (Cnidaria, Actiniaria). *Hydrobiologia* **216/217**, 649–654. (doi:10.1007/BF00026526)

34 Klug, M., Weber, J. & Tardent, P. 1989 Hemolytic and toxic properties of *Hydra attenuata* nematocysts. *Toxicon* **27**, 325–339. (doi:10.1016/0041-0101(89)90180-3)

35 Krayesky, S. L., Mahoney, J. L., Kinler, K. M., Peltier, S., Calais, W., Allaire, K. & Watson, G. M. 2010 Regulation of spirocyst discharge in the model sea anemone, *Nematostella vectensis*. *Mar. Biol.* **8**, 183–193. (doi:10.1007/s00227-009-1384-x)

36 Bruhn, T. *et al.* 2001 Isolation and characterisation of five neurotoxic and cardiotoxic polypeptides from the sea anemone *Anthopleura elegantissima*. *Toxicon* **39**, 693–702. (doi:10.1016/S0041-0101(00)00199-9)

37 Moran, Y., Cohen, L., Kahn, R., Karbat, I., Gordon, D. & Gurevitz, M. 2006 Expression and mutagenesis of the sea anemone toxin Av2 reveals key amino acid residues important for activity on insect voltage-gated sodium channels. *Biochemistry* **45**, 8864–8873. (doi:10.1021/bi060386b)

38 Frank, P. G. & Bleakney, J. S. 1978 Asexual reproduction, diet, and anomalies of the anemone *Nematostella vectensis* in Nova Scotia. *Can. Field Nat.* **92**, 259–263.

39 Sebens, K. P. 1981 The allometry of feeding, energetics, and body size in three sea anemone species. *Biol. Bull.* **161**, 152–171. (doi:10.2307/1541115)

40 Van-Praët, M. 1985 Nutrition of sea anemones. *Adv. Mar. Biol.* **22**, 65–99. (doi:10.1016/S0065-2881(08)60050-4)

41 Chintiroglou, C. & Koukouras, A. 1992 The feeding habits of three Mediterranean sea anemone species, *Anemonia viridis* (Forskal), *Actinia equina* (Linnaeus) and *Cereus pedunculatus* (Pennant). *Helgolander. Meeresunters* **46**, 53–68. (doi:10.1007/BF02366212)

42 Edmunds, M., Potts, G. W., Swinfen, R. C. & Waters, V. L. 1974 The feeding preferences of *Aeolidia papillosa* (L.) (Mollusca, Nudibranchia). *J. Mar. Biol. Assoc. UK* **54**, 939–947. (doi:10.1017/S0025315400057660)

43 Barlow, A., Pook, C. E., Harrison, R. A. & Wüster, W. 2009 Coevolution of diet and prey-specific venom activity supports the role of selection in snake venom evolution. *Proc. R. Soc. B* **276**, 2443–2449. (doi:10.1098/rspb.2009.0048)

44 Fry, B. G., Vidal, N., Van der Weerd, L., Kochva, E. & Renjifo, C. 2009 Evolution and diversification of the toxicofera reptile venom system. *J. Proteomics* **72**, 127–136. (doi:10.1016/j.jprot.2009.01.009)

45 Honma, T., Nagai, H., Nagashima, Y. & Shiomi, K. 2003 Molecular cloning of an epidermal growth factor-like toxin and two sodium channel toxins from the sea anemone *Stichodactyla gigantea*. *Biochim. Biophys. Acta* **1652**, 103–106. (doi:10.1016/j.bbapap.2003.08.007)

46 Nagai, H., Takuwa, K., Nakao, M., Sakamoto, B., Crow, G. L. & Nakajima, T. 2000 Isolation and characterization of a novel protein toxin from the Hawaiian box jellyfish (sea wasp) *Carybdea alata*. *Biochem. Biophys. Res. Commun.* **275**, 589–594. (doi:10.1006/bbrc.2000.3352)

47 Bode, H. R. 1996 The interstitial cell lineage of hydra: a stem cell system that arose early in evolution. *J. Cell. Sci.* **109**, 1155–1164.

Nematocyte Identity in *Nematostella vectensis*

Claudia Zenkert[1], Kathrin Keller[1], Thomas W. Holstein[1] and Suat Özbek[1]

[1]Department for Molecular Evolution and Genomics, Centre for Organismal Studies, University of Heidelberg, Heidelberg, Germany

Abstract

Nematocysts, or stinging organelles, are the hallmark of cnidarians. They are synthesized as secretory products in specialized cells called nematocytes. In *Hydra*, the interstitial stem cell lineage gives rise to neurons, germ cells and nematocytes. A similar stem cell lineage has not been reported for the starlet sea anemone *Nematostella vectensis*, which belongs to the anthozoan clade. We have recently presented a characterization of the *Nematostella* cnidom and proposed an epithelial origin of nematocytes in this model organism. Here, by performing a cell type analysis and using minicollagens as molecular markers, we have identified cuboidal-shaped epithelial cells as the origin of nematocytes in *Nematostella*. We present evidence that nematocyte specification takes place in both epithelial cell layers and is initiated shortly after fertilization.

Introduction

Results

Cell type analysis *in Nematostella vectensis*

To identify the cellular origin of nematocysts in *Nematostella* we have performed a qualitative cell type analysis using primary polyps. The animals were macerated and cell nuclei were visualized by Dapi staining. As shown in Fig. 1 we were able to distinguish seven different cell types. Epithelial cells range from cuboidal to columnar in shape They generally contain a few vacuoles and a visible nucleolus or densely dotted chromatin. Considering the variation in morphological appearance we have classified three different types of epithelial cells (Fig. 1 A- C): (i) the columnar epithelial cell with a length of 20- 25 µm and a width ranging from 2- 9 µm. The nucleus is round to elliptic and occupies up to 45 % of the cell body (Fig. 1 A). (ii) cuboidal epithelial cells vary from 18- 25 µm in length and 15-25 µm in width. The nucleus is centered, less dense than the ones in columnar epithelial cells, but with a visible nucleolus (Fig. 1 B). (iii) entodermal epithelial cells, which are 12- 15 µm in length and 10- 14 µm in width and vary greatly in shape, ranging from columnar to elliptical. The nucleus is generally located at base of the cell (Fig. 1 C). The Nematostella tissue also contains numerous gland cells that are cylindrical in shape, 20- 25 µm long and 5- 10 µm wide, and densely packed with granulae (Fig. 1 E). Gland cells were easiest to rupture during maceration. We have identified two different types of neurons (Fig. 1 F- G). Their nuclei range from 8- 10 µm, the chromatin is dense and granular, and lacks a nucleolus. According to morphology we distinguished sensory neurons (Fig. 1 F), and multipolar (mainly tripolar) ganglions (Fig. 1 G). There is no interstitial stem cell lineage reported for *Nematostella vectensis*. Nevertheless, we were able to identify two types of small and seemingly undifferentiated cells. Fig. 1 I shows an undifferentiated cell with elliptic shape ranging from 5- 7 µm in size. Most of the

cell body is taken up by the nucleus, which is dense and lacks a nucleolus. The second type ranged from 10- 14 µm in length and is characterized by an elongated, bent shape of the nucleus taking up most of the cell body (Fig. 1 H). Nematocyte-containing cells were found frequently in macerates and represented cuboidal epithelial cells (Fig. 1 D, J). The cnidom of *Nematostella vectensis* contains 3 different nematocyst types, basitrichous haplonemas, microbasic mastigophores and spirocysts (Zenkert et al., 2011). Mature nematocysts take up most of the cell body, the nucleus being tightly set against the capsule body.

Nematocyte synthesis in cuboidal epithelial cells

To verify the cellular identity of nematocyst-synthesizing cells we stained macerates with a minicollagen antibody. Minicollagens are major structural constituents of nematocytes and have been shown to be present in all capsule types in *Nematostella* {Zenkert, #773}. Minicollagen signal could be detected already at early stages of nematocyst morphogenesis in the form of vesicles that bud off from the Golgi apparatus to generate the capsule primordium.

To check the nematocyst distribution in the endoderm, cryocuts of Nematostella polyps were stained with minicollagen 3 (NvNcol-3) and analyzed using confocal and phase contrast microscopy (Nikon 80i and Nikon A1R) (Fig.2). The cross section revealed that the tissue framing the distal parts of the mesenteries contains plenty of nematocysts (Fig. 2 A, B). Of the three different types of nematocysts we could locate two in the endoderm, microbasic mastigophores and basitrichous haplonema (Fig. 2 C, D), both in mature and immature states.

Quantitative cell type analysis

To analyze whether the composition of tissue changed during development we quantified the different cell types during Nematostella morphogenesis (Fig. 3, Table S1). The *Nematostella*

tissue has a throughout epithelial character (85.4 % in planula, 74.9 % in primary polyps and 86.5 % in adult animals). In planula larvae columnar epithelial cells clearly dominated, constituting 72.5 % of all epithelial cells, while cuboidal epithelial cells and endodermal epithelial cells were represented only by 15.6 % and 11.9 %, respectively. Gland cells make up 10.6 % of the planula tissue. Neurons are only represented by 1.0 %, same as pinnochio cells. The undifferentiated cells make up 2.0 % of the tissue. The composition of epithelial cells changes in primary polyps, for columnar cells provide 40.1 % while the cuboidal type makes up 49.2 % of the tissue. The percentage of endodermal epithelial cells is the same as in planula larvae (10.7 %). Gland cells make up 8.6 %, while undifferentiated cells (6.1 %) and pinnochios (6.0 %) are equally contributed. The level of neurons rises to 4.4 %. In adult polyps the columnar epithelial cells are most common with 45.4 %, followed by the cuboidal type with 34.1 % and endodermal cells with 20.5 %. Gland cells make up 6.7 % of the adult Nematostella tissue, a little lower than in primary polyps. Neurons keep level with 4.5 %. Undifferentiated cells make up 0.9 % of the tissue, while pinnochios provide 1.4 % respectively.

Cell cycle kinetics in Nematostella vectensis

To evaluate the cell cycle kinetics of *Nematostella vectensis*, proliferating cells were labeled with 1 µM EdU (5 ethynyl-2’ deoxyuridine) and stained with Alexa 488. Afterwards macerated tissue as well as whole mounts (SFig. 1) were analyzed using light and confocal microscopy (Nikon 80i and the Nikon A1R confocal microscope). A labeling index was determined after one hour of EdU incubation (t0). For cuboidal epithelial cells the labeling index was 18%. Within 48 h the percentage of proliferating cells went up 21.9 % to 39.9 %. After 72 h of EdU incubation, 61.0 % were EdU positive. At t120, 77.2 % and after 240 h, 93.6 % of all cuboidal epithelial cells were Alexa 488 positive (Fig. 2 A). Mature

nematotcysts had a labeling index of 26.9 % (t0). After 48 h of EdU incubation 35.6 % of the nematocysts were EdU positive. The proliferation rate was up to 68.3 % after 72 h respectively. 120 h of labeling resulted in 76.6 % stained nuclei and after 240 h, 96.7 % of all mature nematocysts were labeled. Hence, nematocysts are synthesized by cuboidal epithelial cells, we expected a similar proliferation rate (Fig. 4 A). Figure 4 B depicts the cell cycle kinetics of columnar and endodermal epithelial cells, pinnochios and undifferentiated cells.

Columnar epithelial cells have a labeling index (t0) of 13.1 %. Within 48 h, 33.2 % were labeled. Within the next 24 h the proliferation rate increased to 55.4 % respectively. This tendency continues to 70.0 % after 120 h of EdU incubation. After 240 h of labeling, 95.7 % of all columnar epithelial cells were Alexa 488 positive. A similar proliferation kinetics can be found in pinnochio cells, that pose a labeling index of 13.1 %. In the next 48 h the percentage rises up to 33.4 %. This ratio of about 14 % increase per 48 h continues up to t120, when 62.5 % of all pinnochios are Alexa 488 positive. At the end (t240 h), 90.1 % of the pinnochios were EdU positive. Both cell types have elongated nuclei and an almost synonymous proliferation pattern, hence pinnochios could be precursor cells to columnar epithelial cells.

Endodermal epithelial cells have a labeling index of 32.1 % and the level of proliferating cells rises to 46.0% within 48 h. After 72 h of EdU treatment 50.1 % of endodermal epithelial cells are labeled. At t120 the proliferation rate has reached 81.7 %. After 24h h 98.3 % of the endodermal epithelial cells are Alexa 488 positive. Eventhough there is no stem cell lineage reported in *Nematostella vectensis*, there are still undifferentiated cells to be acknowledged. They have a labeling index of 0.0 %, but increase to 15.9 % within 48 h. At t72 17.4 % and after 120h 50.5 % of the cells were EdU positive. After 240 h of labeling, 79.4 % of all undifferentiated cells were labeled. The pattern of cell proliferation is shifted but other than

that synonymus of the one in endodermal epithelial cells, therefore they could be endodermal precursor cells (Fig. 4 B).

The cell cycle kinetics of gland cells and neurons are shown in Fig. 4 C. The labeling index of gland cells is 33.9 %. After 48 h the proliferation rate is 52.1 % and at t72 the proliferation rate is up 55.7 %. At t120 72.2 % of the cells and after 240 h of labeling 83.5 % of the gland cell are EdU positive. Gland cells are most fragile to the maceration process. Neurons have a labeling index of 0.0 % and the proliferation rate slowly rises within 48 h to 4.7 %. After 72 h neurons have a proliferation rate of 8.6 %, which rises to 22.1 % after 120 h of EdU labeling. 240 h of labeling resulted in a proliferation rate of 45.9 %.

Capsule synthesis in cuboidal epithelial cells

In *Nematostella vectensis* morphological analysis proved cuboidal epithelial cells to be responsible for nematocyst production. To analyze capsule synthesis we fixed and stained embryos at different time points (6 h intervals) with anti-minicollagen3 (NvNcol 3). The first random protein vesicles appear in the nematocytes 30 h post fertilization (Fig. 5A). After 42 h the protein filled vesicles start to organize (Fig. 5B). The capsule body fills up with NvNcol-3 protein by 48 h (Fig. 5C). At 54 h post fertilization the tubule starts to elongate (Fig. 5D). The nematocyst is ready with the tubule coiled up inside 60 h post fertilization (Fig. 5E, F). At this the antibody signal weakens, for the minicollagen is linked to other nematocyst components.

Discussion

Materials and Methods

5-ethynyl-2’-deoxyuridine labeling. Long term EdU (5-ethynyl-2’-deoxyuridine) labeling was performed using the Click-iT™ EdU Alexa Fluor® Imaging Demonstration Kit

(Invitrogen) as adviced by manufacturer. The labeling period was 240 hours and primary polyps were incubated with 1 µM EdU in Nematostella medium. At given time points 25 polyps of equal size and nourishment were taken for maceration (described below), while some were separately fixed as whole mounts. EdU was detected and stained with Alexa 488 as described in the kit. The animals were fed daily with sonified *Artemia salina* tissue and the medium was exchanged about four hours after the feeding. The results were examined using phase contrast (Nikon 80i) and confocal microscopy (Nikon A1R). For the analysis of mature nematocysts only intact nematocytes were considered (nucleus attached).

Cryocuts in Nematostella vectensis. Nematostella polyps were paralyzed with 7.14 % of MgCl2 and afterwards fixed over night with 4 % Paraformaldehyde in Nematostella medium. The fixed polyps were kept in 15 % Sucrose solution for at least two hours at 4 °C. The animals were then transferred into 30 % Sucrose solution and incubated over night at 4 °C. Afterwards the animals are frozen in liquid nitrogen embedded in tissue freezing medium (Jung, Tissue Freezing Medium, Leica instruments GmbH). The animals were cut using the …..

***Nematostella* culture.** *Nematostella* polyps and embryos were kept in 1/3 seawater (Hand and Uhlinger 1992, Tropic Marine) at 18 °C in the dark and fed once or two times a week with Artemia nauplii. Induction and gametogenesis was carried out as described before {Fritzenwanker, 2002 #758}. Oocytes were fertilized in vitro to fairly synchronize development.

Maceration of *Nematostella vectensis* tissue. For morphological cell type analysis primary polyps were macerated (maceration solution: 1 acetic acid: 1 glycerin: 13 dd water) for 1.5 h

at 39 °C, then fixed with 4 % formaldehyde, spread on 1 % gelatine coated slides (1-2 drops of 10% Tween 20 added previously) and completely dried off. Dapi staining was performed for better contrast.

Microscopy. Fluorescence images, as well as phase contrast and interference contrast images were captured with the Nikon Eclipse 80*i,* confocal images with the Nikon A1R laser scanning microscope.

Immunofluorescence. Relaxed animals were paralyzed with 3.57% $MgCl_2$ for several minutes and then fixed in Lavdovski's fixative (ethanol:formaldehyde:acetic acid:H_2O bidest; 50:10:4:36) over night. After several washing steps using PBT (0.1% Triton X100 in PBS), the polyps were incubated over night at 4 °C with NvNcol-3 or NvNcol-4 antibodies in PBS/0.1% BSA. Thereafter the polyps were washed several times in PBS and incubated for 2 h with anti-guinea (NvNcol-3) or anti-rabbit (NvNcol-4) antibody coupled to ALEXA Fluor 568/488 (Molecular Probes) at a 1/400 in PBS/0.1% BSA. The animals were washed again several times in PBS before mounting in PBS/Glycerol. Fluorescence image analysis was performed using the Nikon A1R laser-scanning microscope.

Quantitative Analysis. For the quantitative analysis of cell types, 50 planula larvae, 50 primary polyps and three adult animals of equal size (sectioned into four parts, and evaluated individually) were macerated as above, spread on a slide and the different cells were counted using brightfield microscopy (Nikon Eclipse 80*i*). The experiment was repeated three times.

Figure Legends and Tables

Figure 1: Different Cell types in *Nematostella vectensis*. A Columnar epithelial cell. B Cuboidal epithelial cell. C Entodermal epithelial cell with food vacuoles. D Nematocyte with growing microbasic mastigophore. Asterisk points at the stilette apparatus inside the capsule body. E Gland cell with granules. F- G Neurons. F Sensory neuron. G Tripolar neuron. H Pinnochio. I Undifferentiated cells. J Cuboidal epithelial cell with growing basitrichous haplonema. Scale bars 5 µm (A, B, C, D, E and J) and 2 µm (F, G, H and I).

Figure 2: Quantitative Distribution of Cell types in Nematostella polyps among different developmental stages.

Figure 3: Overview of cell cycle kinetics in *Nematostella vectensis*. Long term labeling with 1 µM EdU over a time period of 240 hours. At defined time points 25 animals were taken, macerated, stained and the different cell types were quantitatively evaluated using light microscopy (Nikon 80*i*). A Cell proliferation in cuboidal epithelial cells and mature nematocysts. B Cell cycle kinetics of columnar- and entodermal epithelial cells including their precursor cells, namely columnar epithelial precursor cells and undifferentiated cells. C Cell proliferation in gland cells and neurons.

Figure 4: Detection of minicollagen 4 (NvNcol-4) and chondroitin along the endoderm and the mesenteries by immunocytochemistry. Anti-minicollagen 4 staining in red (Alexa 568) and chondroitin in green (Alexa 488) show developing nematocysts. A 60 µm thick section through an adult *Nematostella vectensis*. Mesenteries (m) branch deep into the gastro vascular cavity. B Detail of single mesentery. The inner rim is densely set with nematocysts, both immature (NvNcol-4 in red and chondroitin in green) and mature. Discharged tubules are marked by asterisks. C-D Close up on nematocysts. C Antibody staining overlayed with a

phase contrast image. Discharged capsules never show antibody signals, for the signal is lost when nematocyst components link. Discharged tubules are marked by asterisks. D Same as C without phase contrast but with Dapi staining (in blue), pointing out the nuclei. The chondroitin signal grows weaker as the tube is coiled into the capsule (marked by two asterisks). Ectoderm (ect), endoderm (end), mesogleoa (mes), microbasic mastigophores (mm) and basitrichous haplonema (bh) are labeled. Scale bars 100 µm (A), 50 µm (B) and 10 µm (C, D).

Figure 5: Antibody staining of minicollagen 3 (NvNcol-3) showing nematocyst synthesis during development. A 30 h post fertilization, first protein vesicles can be detected. B 42 h post fertilization. Vesicles begin to organize. C 48 h post fertilization. NvNcol-3 vesicles take part in producing the capsule body. D 54 h post fertilization. Once the capsule body takes shape, the tubule elongates (marked by an asterisk). E- F 60 h post fertilization. The tubule is coiling up inside the capsule and the signal weakens caused by linkage to other components. At this time point we can find functioning mature nematocysts. Scale bar 5 µm.

Supplemental Figure 1: Overview of cell cycle kinetics in Nematostella vectensis primary polyps. Proliferating cells stained with Alexa 488 (green) using the EdU Click it kit (Invitrogen). Nuclei are stained with Dapi (blue). A Cell labeling index after 1 h (0) of 1 µM EdU incubation. B Proliferating cells after 48 h of EdU incubation. C Primary polyp after 72 h of EdU labeling. E Primary polyp after 240 h of EdU labeling. Scale bar is 50 µm.

Supplemental Table 1: Absolute number of cells among the different developmental stages: average value (±) standard degression cell types in the tissue. Evaluated were 100 planula larvae, 50 primary polyps and one adult animals (dissected into 4 parts, which were analyzed

separately). The number of cells was ascertained using macerated probes. 50 µl of macerated animals were put on a slide, the cells of six lanes per slide were counted. The experiments were repeated four times. Asterisk indicates the distortion of counted cell numbers due to cell rupture of gland cells.

Figure 1

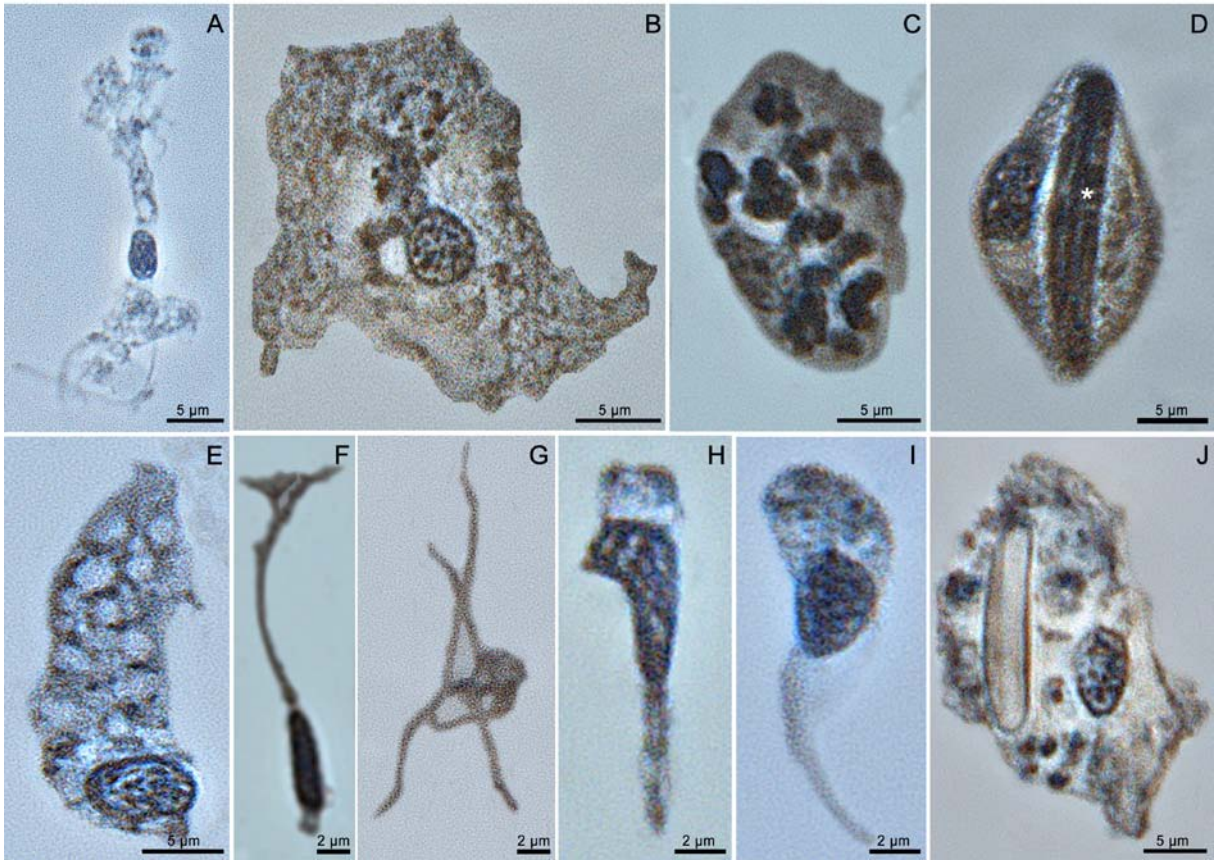

Figure 2

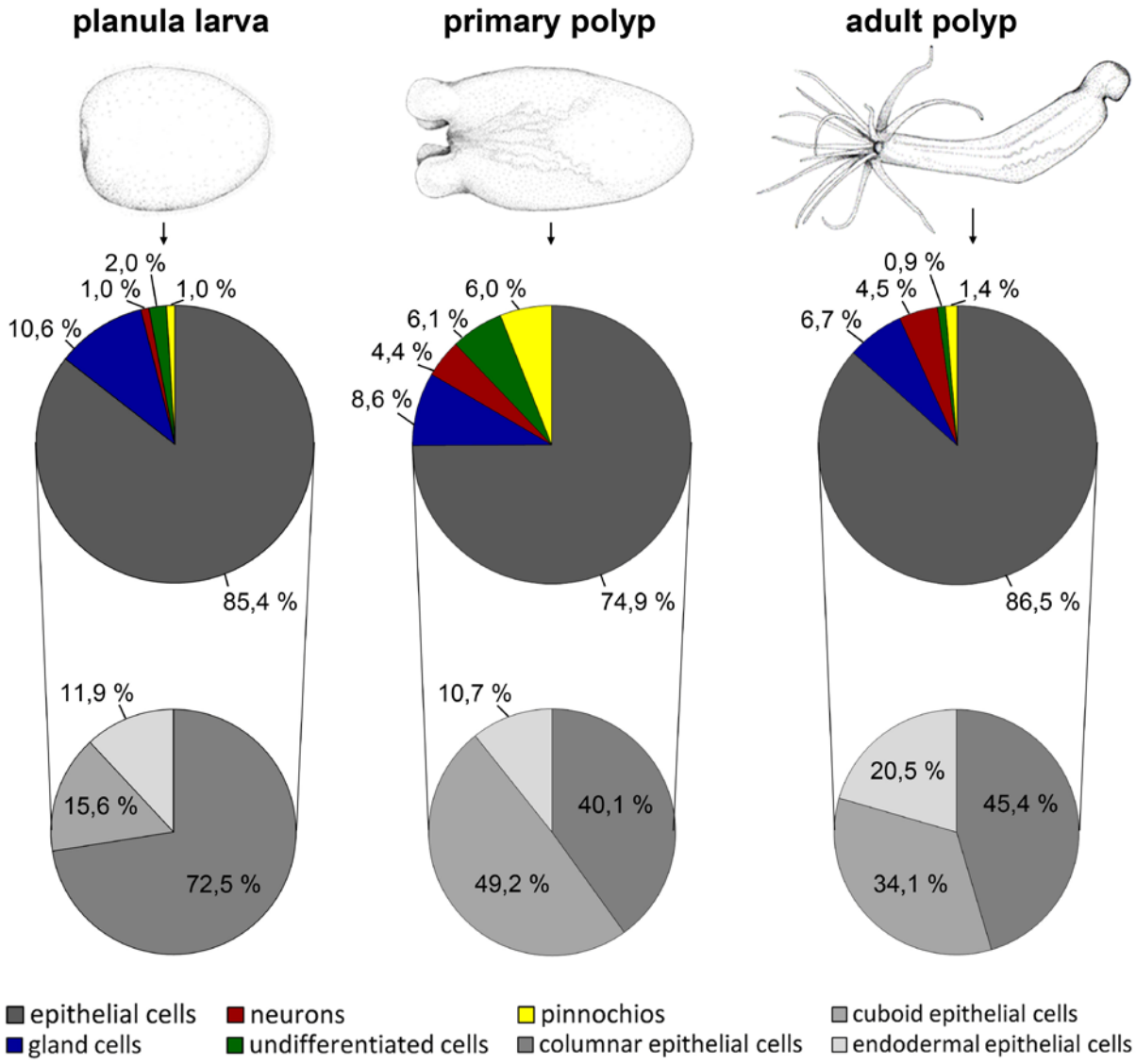
planula larva
primary polyp
adult polyp
2,0 %
1,0 %
1,0 %
10,6 %
85,4 %
11,9 %
15,6 %
72,5 %
6,0 %
6,1 %
4,4 %
8,6 %
74,9 %
10,7 %
40,1 %
49,2 %
0,9 %
4,5 %
1,4 %
6,7 %
86,5 %
20,5 %
45,4 %
34,1 %
epithelial cells
neurons
pinnochios
cuboid epithelial cells
gland cells
undifferentiated cells
columnar epithelial cells
endodermal epithelial cells

Figure 3

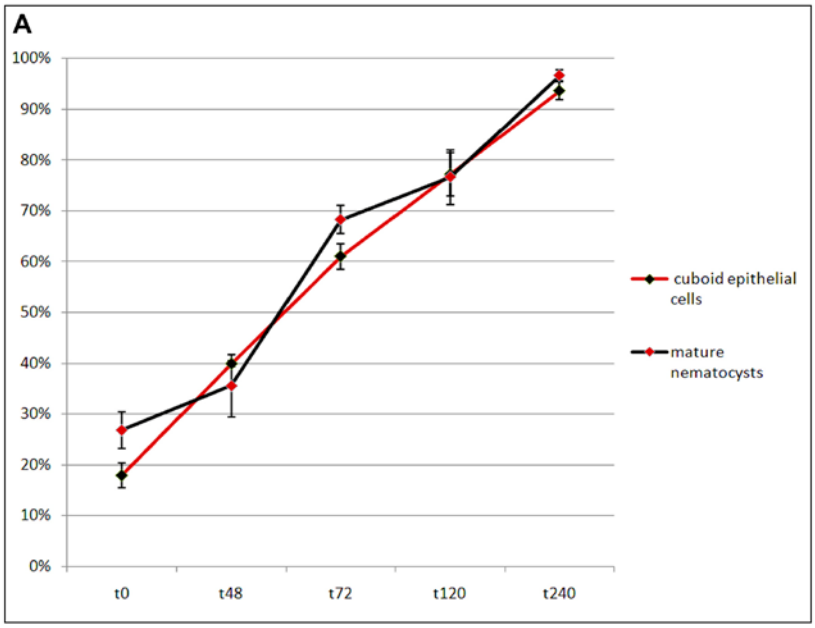
A
100%
90%
80%
70%
60%
50%
40%
30%
20%
10%
0%
t0
t48
t72
t120
t240
cuboid epithelial cells
mature nematocysts

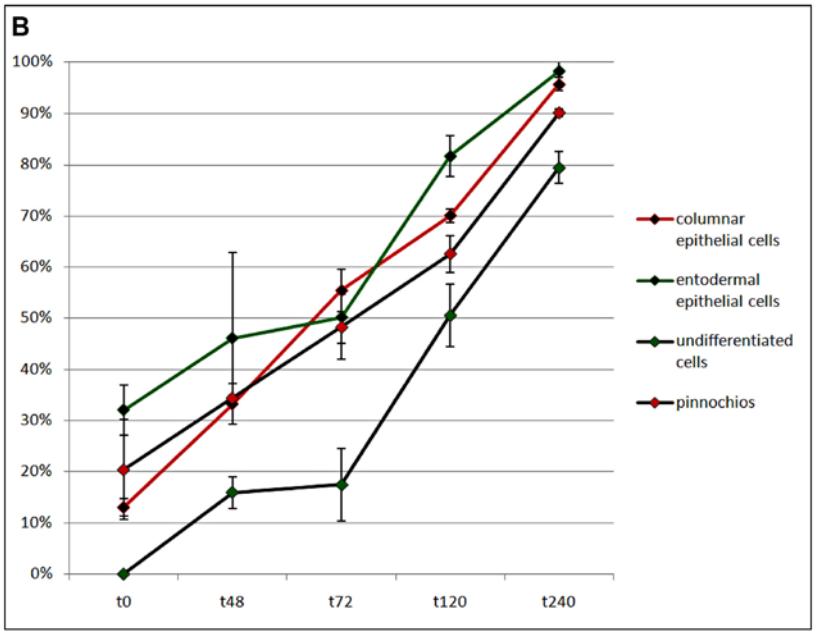
B
100%
90%
80%
70%
60%
50%
40%
30%
20%
10%
0%
t0
t48
t72
t120
t240
columnar epithelial cells
entodermal epithelial cells
undifferentiated cells
pinnochios

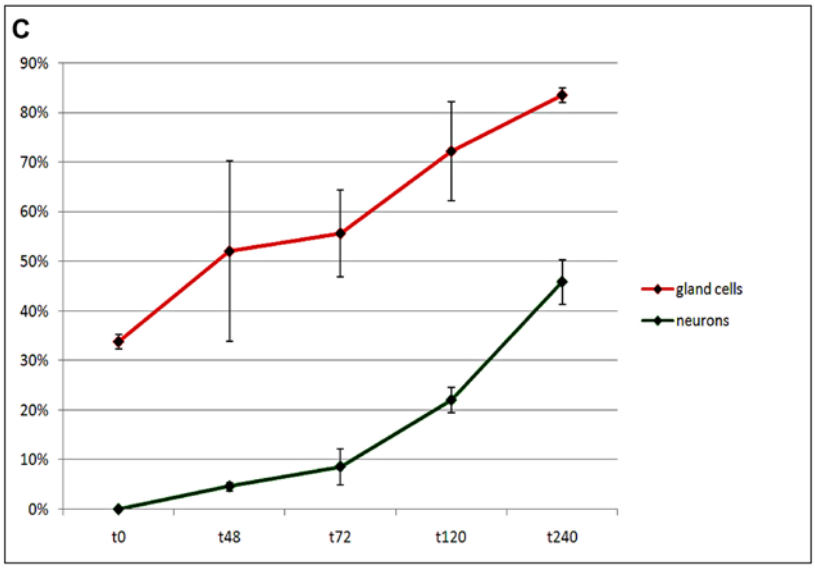
C
90%
80%
70%
60%
50%
40%
30%
20%
10%
0%
t0
t48
t72
t120
t240
gland cells
neurons

Figure 4

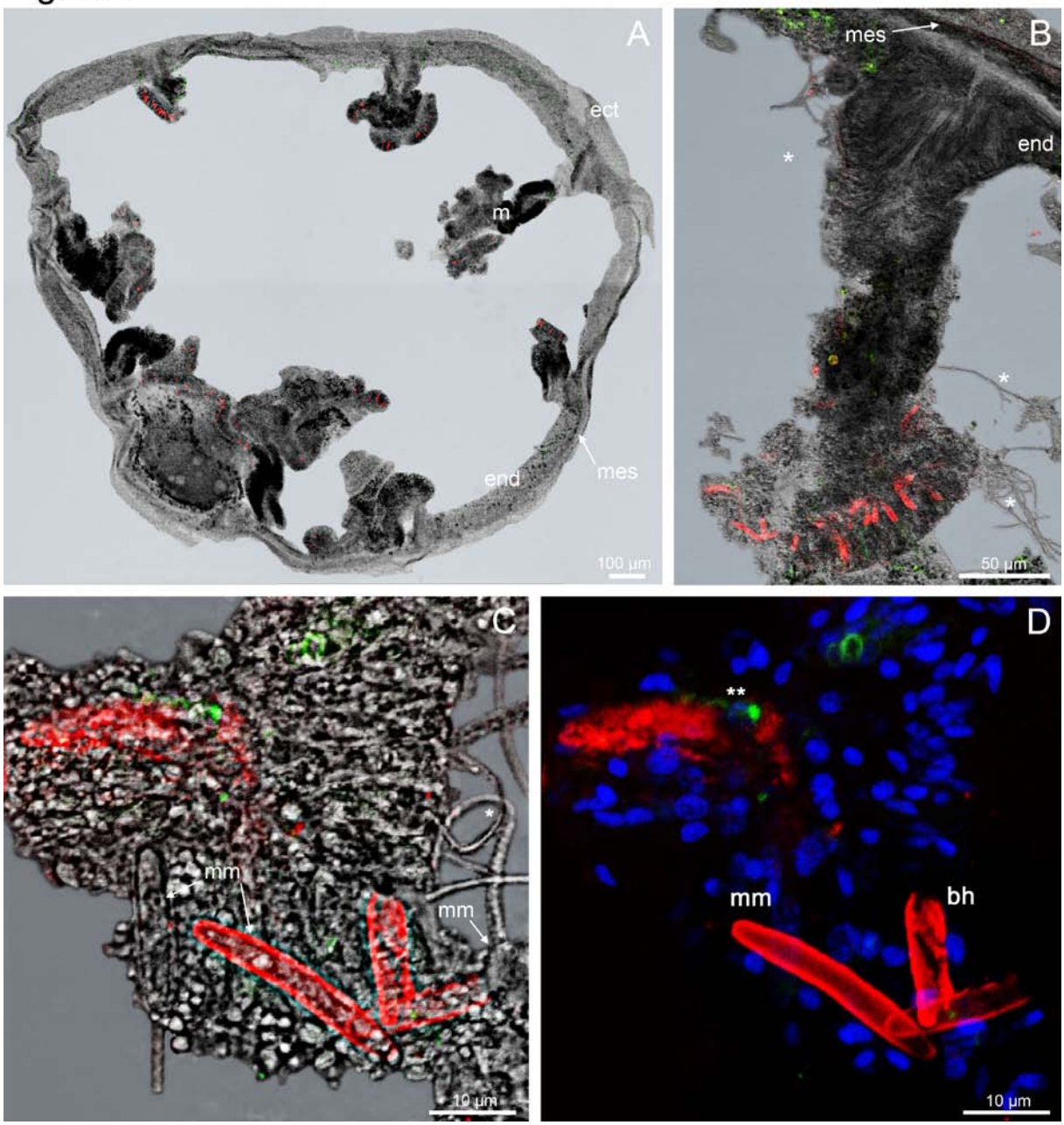

Figure 5

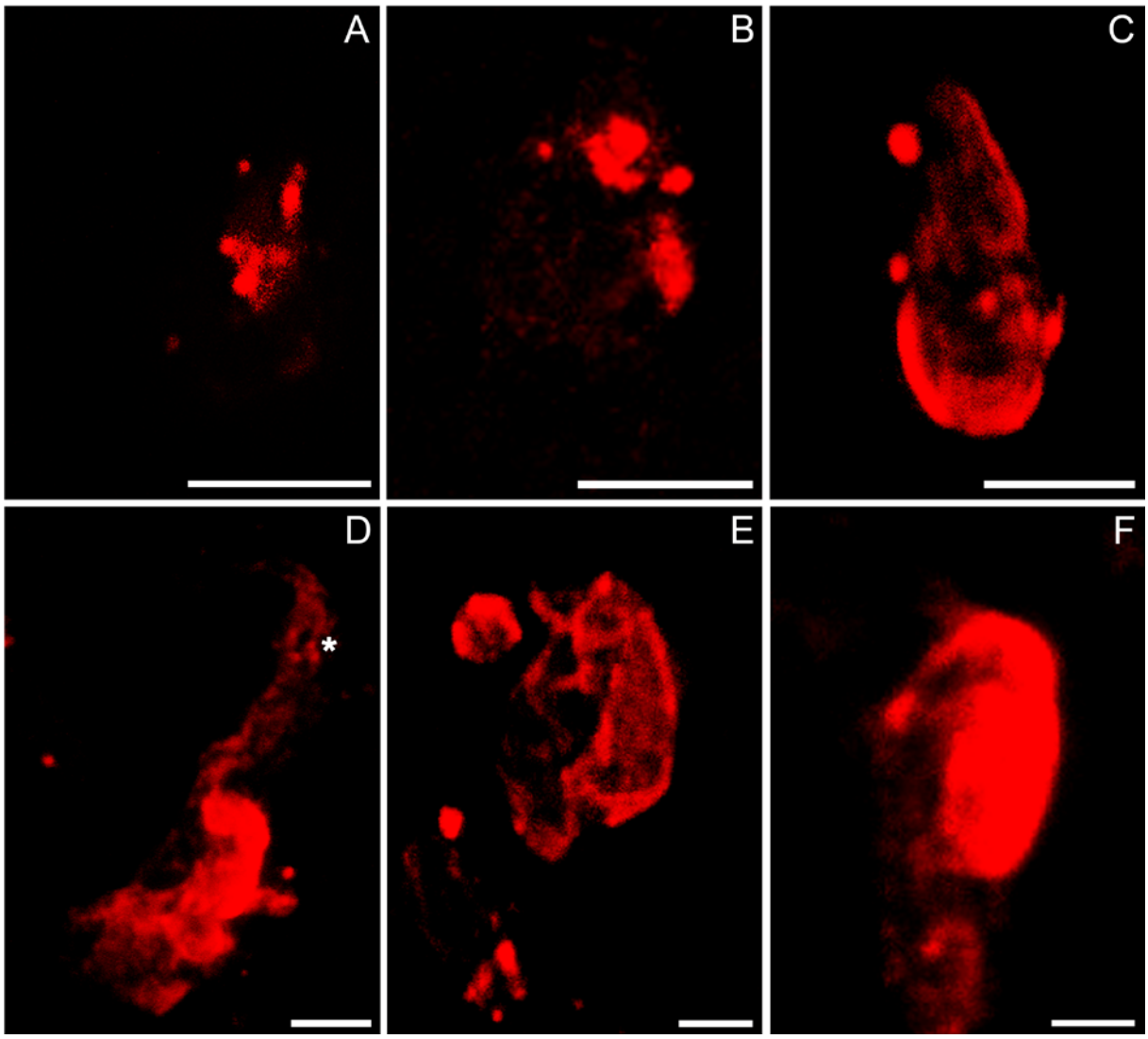

Supplemental Figure 1

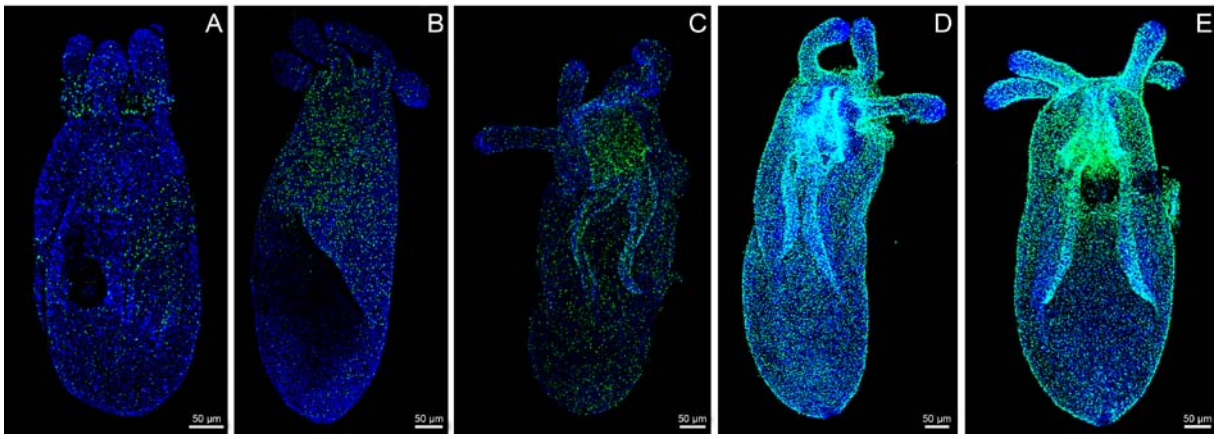

Supplemental Table 1

Cell type	Total number of cells in planula larvae	Total number of cells in primary polyps	Total number of cells in adult polyps
Columnar epithelial cells	13711 ± 1433	8865 ± 964	5745152 ± 800245
Cuboid epithelial cells	2949 ± 510	8603 ± 948	4315136 ± 717294
Endodermal epithelial cells	2260 ± 396	2368 ± 176	2595413 ± 396356
Gland cells*	2324 ± 1194	2527 ± 185	971861 ± 137323
Pinnochios	214 ± 70	1774 ± 135	200704 ± 10242
Neurons	210 ± 90	1305 ± 46	658261 ± 52701
Undifferentiated cells	449 ± 51	1804 ± 193	134798 ± 42566
= Σ	22117 ± 6083	27246 ± 2647	14621325 ±2156727

Acknowledgement

I want to thank all the people who contributed directly or indirectly to this work, particularly Suat Özbek for his scientific guidance, supervision and never ending patience, and Angela Oberthür for financial and mental support, without whom, I could have never accomplished this work. I learned so much from you!

This work was performed in an inspiring and friendly atmosphere with colleagues and friends. Therefore I would like to thank the whole group, especially Prof. Thomas Holstein for giving me the opportunity to do my PhD in the laboratories of the Department of Molecular Evolution and Genomics at the Centre for Organismal Studies at the University Heidelberg.

For their willingness to serve as referee for my thesis, I would like to thank Prof. Dr. Ursula Kummer and Dr. Alexis Maizel.

And I will always be grateful to Toshitaka and Chiemi Fujisawa for opening this path of science and taking me in their lab for an entire year. Because of you, I fell in love with Japan.

Special thanks go to my dear colleagues and friends: Patricia Adamczyk, Anna Beckmann, Benjamin Trageser, Melanie Mikosch, Jennifer Strompen and Hendrik Petersen, for a great time in the lab (my second home) always welcome scientific advices and minds to my mouth.

Finally, I am most grateful to my Mom and Dad who made me become the person I am today and to Borsti and his family (who took over caring for me) for all their encouragement and support. And where would I be without all of you – Kathi, Feliks, Simi, Franzi, Nikola, Anita, Lia, Martin, Alex, San San, Marion, Holger, Bonnie and Fred?! You were always there, and it is because of you, that I am still standing and still smiling. I couldn't imagine a world without you!